



**NTNU – Trondheim**  
Norwegian University of  
Science and Technology

# Development of heat pipes with potassium as working fluid: Performance limitations and test rig development

**Dan Adrian Odden**

Master of Science in Product Design and Manufacturing

Submission date: June 2012

Supervisor: Erling Næss, EPT

Co-supervisor: Geir Hansen, EPT

Norwegian University of Science and Technology  
Department of Energy and Process Engineering



EPT-M-2012- 70

## MASTEROPPGAVE

for

Stud.techn. Dan Adrian Odden

Våren 2012

### Utvikling av varmerør med kalium som arbeidsmedium: Ytelsesbegrensninger og utvikling av testrigg

*Development of heat pipes with potassium as working fluid: Performance limitations and test rig development*

#### Bakgrunn og målsetting

Bruk av varmerør (engelsk: "heat pipes") har vist seg å være en meget effektiv metode for varmetransport, og finner stadig nye anvendelsesområder. Institutt for Energi- og Prosessteknikk er involvert i forskning og utvikling av varmerør for høytemperatur prosesskjøling og varmegjenvinning. Varmerøret benytter kalium som arbeidsmedium. Internt i varmerøret foregår varmetransporten ved fordampning og kondensasjon av kalium. Varmerøret har en veke (porøs struktur) i fordampersesjonen. Fordampningen av arbeidsmediet skjer da fra vekens overflate. Koking i veken i varmerøret vil være ødeleggende for vekens funksjon, og er derfor uønsket. Vekens maksimale ytelse i et varmerør kalles kapillærbegrensningen, og denne kan være begrensende for hvor stort areal varmerøret kan kjøle. Operasjonsområdet for varmerøret er satt til 400-650°C, med varmefflukser opp til 300 kW/m<sup>2</sup>. Utsatt for store varmefflukser vil vekens løftehøyde være meget begrenset.

Målet for oppgaven er å analysere to viktige ytelsesbegrensninger for varmerør, og å foreslå løsninger for å omgå dem. I tillegg ønskes utført en energianalyse av en testrigg for varmerør.

#### Oppgaven bearbeides ut fra følgende punkter

1. Det skal gjennomføres et litteraturstudium innen kokestart ved vertikale vekebelagte flater, hvor det skjer fordampning fra vekeoverflaten. Betingelsene for kokestart med arbeidsmediene vann og kalium beregnes, sammenlignes og drøftes.
2. Kapillærtrykksbegrensningen for et vertikalt flatt varmerør skal beregnes for tilgjengelige veker. Det skal etableres løsninger med tilhørende modeller som viser hvordan en større vertikal flate kan kjøles med ett eller flere flate varmerør.
3. Det gjøres beregninger ved ulike driftssituasjoner for modellene i punkt 2. Forutsetningene diskuteres. Resultatene skal presenteres og vurderes.
4. Uttesting av kjølekrets for varmerør: Kjølekretsen er en lukket sirkulasjonskrets med nitrogengass, utstyrt med en massestrømsmåler og et antall temperaturmålinger. Det skal utføres varmebalansemålinger for alle komponentene i testriggen. Varmetap fra kretsen

skal estimeres og det skal utarbeides et totalt energiregnskap for kretsen. Det skal gjennomføres tester av kjølekretsen ved ulike driftsforhold. Temperaturer under forskjellige driftsforhold beregnes og sammenlignes med målte temperaturer der de foreligger.

5. Det skal utarbeides forslag til videre arbeid.

Senest 14 dager etter utlevering av oppgaven skal kandidaten levere/sende instituttet en detaljert fremdrift- og eventuelt forsøksplan for oppgaven til evaluering og eventuelt diskusjon med faglig ansvarlig/veiledere. Detaljer ved eventuell utførelse av dataprogrammer skal avtales nærmere i samråd med faglig ansvarlig.

Besvarelsen redigeres mest mulig som en forskningsrapport med et sammendrag både på norsk og engelsk, konklusjon, litteraturliste, innholdsfortegnelse etc. Ved utarbeidelsen av teksten skal kandidaten legge vekt på å gjøre teksten oversiktlig og velskrevet. Med henblikk på lesning av besvarelsen er det viktig at de nødvendige henvisninger for korresponderende steder i tekst, tabeller og figurer anføres på begge steder. Ved bedømmelsen legges det stor vekt på at resultatene er grundig bearbeidet, at de oppstilles tabellarisk og/eller grafisk på en oversiktlig måte, og at de er diskutert utførlig.

Alle benyttede kilder, også muntlige opplysninger, skal oppgis på fullstendig måte. For tidsskrifter og bøker oppgis forfatter, tittel, årgang, sidetall og eventuelt figurnummer.

Det forutsettes at kandidaten tar initiativ til og holder nødvendig kontakt med faglærer og veileder(e). Kandidaten skal rette seg etter de reglementer og retningslinjer som gjelder ved alle (andre) fagmiljøer som kandidaten har kontakt med gjennom sin utførelse av oppgaven, samt etter eventuelle pålegg fra Institutt for energi- og prosessteknikk.

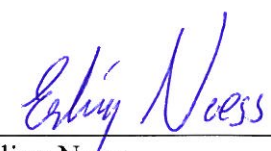
Risikovurdering av kandidatens arbeid skal gjennomføres i henhold til instituttets prosedyrer. Risikovurderingen skal dokumenteres og inngå som del av besvarelsen. Hendelser relatert til kandidatens arbeid med uheldig innvirkning på helse, miljø eller sikkerhet, skal dokumenteres og inngå som en del av besvarelsen.

I henhold til "Utfyllende regler til studieforskriften for teknologistudiet/sivilingeniørstudiet" ved NTNU § 20, forbeholder instituttet seg retten til å benytte alle resultater og data til undervisnings- og forskningsformål, samt til fremtidige publikasjoner.

Besvarelsen leveres digitalt i DAIM. Et faglig sammendrag med oppgavens tittel, kandidatens navn, veileders navn, årstall, instituttnavn, og NTNUs logo og navn, leveres til instituttet som en separat pdf-fil. Etter avtale leveres besvarelse og evt. annet materiale til veileder i digitalt format.

NTNU, Institutt for energi- og prosessteknikk, 16. januar 2012

  
Olav Bolland  
Instituttleder

  
Erling Næss  
Faglig ansvarlig/veileder

Medveileder(e)  
Ph.d.-kandidat Geir Hansen, EPT



---

## Preface and acknowledgments

This master thesis is a part of my master's degree at NTNU at the department of energy and process engineering. During this semester I have become highly interested in heat transfer and flow conditions, and I have developed a solid understanding of heat pipes and heat transfer phenomena in general.

I would like to give special thanks to my supervisor, Professor Erling Næss, who has been very helpful, and have provided guidance and shared his knowledge throughout this master thesis. I would also like to thank assistant supervisor, Ph.D. candidate Geir Hansen, who has always taken the time to discuss and answer my questions.

Trondheim, June 9, 2012

Dan Adrian Odden



---

## Abstract

The incentive to reduce energy consumption in the industry is big, especially in high temperature systems. Heat pipes are of great interest for this purpose due to their favorable thermomechanical properties. This master thesis is a part of the ongoing study of Ph.D. candidate Geir Hansen, who is currently developing a rectangular heat pipe with potassium as working fluid at NTNU. The rectangular heat pipe is intended to be implemented in the walls of electrolysis cells as a part of a heat recovery system.

The present work reports results of theoretical calculations of two important heat transfer limitations, the incipience of boiling and the capillary limitation for two types of nickel foam wicks. Results of experimental tests carried out on the cooling circuit for the proposed rectangular heat pipe are also reported. The foam porosity, permeability and effective pore radius for wick 1 is 0.797,  $31 \cdot 10^{-12} \text{m}^2$  and  $62 \cdot 10^{-6} \text{m}$ , respectively, and for wick 2; 0.886,  $205 \cdot 10^{-12} \text{m}^2$  and  $126 \cdot 10^{-6} \text{m}$ .

A literature survey showed that porous coated surfaces improves the heat transfer and requires less superheat for boiling to commence. Calculations performed showed no danger of homogeneous nucleation in the proposed heat pipe. Boiling inside the nickel foam wick(s) were found to only be of concern for wick 2 at high heat fluxes and a operating temperature of  $600^\circ\text{C}$ .

Calculations of the capillary limit showed that wick 2 is the best choice for sustaining high heat fluxes. Increasing the wick length to 20cm made wick 2 not suitable for usage, and wick 1 was the best choice for increased wick length. Combination of the two wick types showed to be very effective and significantly (factor of almost 4) improved the performance. An uneven heat flux distribution where a lower heat flux is at the bottom region of the evaporator is found to lower the performance, while a higher heat flux at the bottom region increases the performance.

Early tests revealed that the PID controller was marginally stable, so the controller was tuned and stable operating conditions were achieved. Experiments showed that in order to get an accurate heat balance for the test rig, knowledge about the exact position of the thermocouples is needed.



---

## Sammendrag

Drivkraften for å redusere energiforbruket i industrien er stor, spesielt i høytemperatursystemer. Varmerør er av stor interesse for dette bruksområdet grunnet dets gode termomekaniske egenskaper. Denne masteroppgaven er en del av en pågående studie av dr.philos. kandidat Geir Hansen, som utvikler et rektangulært varmerør med kalium som arbeidsmedium for NTNU. Dette er planlagt å bli implementert i veggene på elektrolyse celler som en del av et varmegjenvinningssystem.

Det foreliggende arbeidet rapporterer resultater fra teoretiske beregninger av to viktige ytelsesbegrensninger, kokestart og kapillærtrykksbegrensningen for to typer nikkelskum veke. Resultater fra eksperimentelle tester utført på en kjølekrets for det foreslåtte rektangulære varmerøret er også dokumentert. Nikkelskummets porøsitet, permeabilitet og effektiv poreradius for veke 1 er henholdsvis  $0.797$ ,  $31 \cdot 10^{-12} \text{ m}^2$  og  $62 \cdot 10^{-6} \text{ m}$ , og for veke 2;  $0.886$ ,  $205 \cdot 10^{-12} \text{ m}^2$  og  $126 \cdot 10^{-6} \text{ m}$ .

Et litteraturstudium viste at overflater dekket av porøse strukturer forbedrer varmeoverføringen og krever mindre overoppheting før koking inntreffer. Beregninger utført viste at det er ingen fare for homogen koking i det aktuelle varmerøret. Koking inni nikkelskumveken(e) ble funnet å bare være mulig for veke 2 ved høye varmefflukser og en driftstemperatur på  $600^\circ\text{C}$ .

Beregninger av kapillærtrykksbegrensningen viste at veke 2 er det beste valget for å oppnå høyest mulig varmefflukser. Ved å øke vekelengden til  $20\text{cm}$ , ble veke 2 funnet uegnet for bruk, og veke 1 viste seg å være det beste valget når vekelengden økes. Kombinasjon av de to veketyperne viste seg å være svært effektiv og ytelsen ble forbedret betraktelig (faktor på nesten 4). En ujevn varmeffluksfordeling der en lavere varmeffluks inntreffer i den nedre delen av fordampere reduserer ytelsen, mens en høyere varmeffluks i den nedre regionen øker ytelsen.

Tidlige tester viste at PID-regulatoren var marginalt stabil, derfor ble regulatoren tunet til stabile driftsforhold ble oppnådd. Eksperimenter viste at for å utføre en korrekt varmebalanse av testtriggen, er kunnskap om den nøyaktige plasseringen av termoelementene nødvendig.





# Table of Contents

<b>Preface and acknowledgments</b>	<b>i</b>
<b>Abstract</b>	<b>iii</b>
<b>Sammendrag</b>	<b>v</b>
<b>Table of Contents</b>	<b>vii</b>
<b>List of Figures</b>	<b>ix</b>
<b>List of Tables</b>	<b>xi</b>
<b>Nomenclature</b>	<b>xii</b>
<b>1 Introduction</b>	<b>1</b>
1.1 Project aim and limitations . . . . .	2
1.2 Structure of the report . . . . .	3
1.3 Principle of a heat pipe . . . . .	3
1.4 Applications and temperature ranges . . . . .	4
1.5 Limitations . . . . .	4
1.5.1 Capillary limit . . . . .	4
1.5.2 Boiling limit . . . . .	5
1.5.3 Entrainment limit . . . . .	5
1.5.4 Sonic limit . . . . .	5
1.5.5 Viscous limit . . . . .	6
1.5.6 Frozen startup limit . . . . .	6
1.5.7 Condenser limit . . . . .	6
1.5.8 Continuum flow limit . . . . .	6
<b>2 Boiling</b>	<b>7</b>
2.1 Bubble formation . . . . .	7
2.2 Homogeneous nucleation . . . . .	8
2.3 Bubble formation at surfaces . . . . .	8
2.3.1 Model 1 . . . . .	11
2.3.2 Model 2 . . . . .	11
2.3.3 Model 3 . . . . .	11
2.3.4 Model 4 . . . . .	12
2.4 Literature survey - Heat transfer and the incipience of boiling from porous surfaces . . . . .	12
2.5 Pressure distribution in the wick . . . . .	13
2.6 Results and discussion . . . . .	14
2.7 Chapters conclusions . . . . .	26

---

<b>3</b>	<b>Capillary limit</b>	<b>27</b>
3.1	Results and discussion . . . . .	28
3.1.1	Combination of wicks . . . . .	35
3.1.2	Different operating conditions . . . . .	37
3.2	Chapters conclusions . . . . .	40
<b>4</b>	<b>Energy balance of test rig</b>	<b>41</b>
4.1	Heat transfer theory . . . . .	41
4.1.1	Conduction . . . . .	42
4.1.2	Convection . . . . .	42
4.1.3	Free Convection . . . . .	46
4.1.4	Heat exchanger . . . . .	47
4.1.5	Side channel blower . . . . .	47
4.2	Geometry and dimensions . . . . .	48
4.3	Controller - Tracing . . . . .	50
4.4	Instrumentation . . . . .	52
4.5	Uncertainty analysis . . . . .	53
4.6	Experimental procedure . . . . .	53
4.7	Results and discussion . . . . .	54
4.8	Chapter conclusions . . . . .	65
<b>5</b>	<b>Conclusions</b>	<b>67</b>
<b>6</b>	<b>Further work</b>	<b>69</b>
	<b>References</b>	<b>71</b>
	<b>Appendices</b>	
	<b>Appendix A</b>	<b>I</b>
	<b>Appendix B</b>	<b>VIII</b>
	<b>Appendix C</b>	<b>XI</b>
	<b>Appendix D</b>	<b>XXII</b>

## List of Figures

1.1	Schematic of the proposed system taken from [1] . . . . .	1
1.2	Schematic of the proposed system evaporator (left) and condenser (right) taken from [1] . . . . .	2
1.3	Schematic of a cylindrical heat pipe taken from [6] . . . . .	4
1.4	Limitations in a heat pipe taken from Faghri [5]. . . . .	5
2.1	Force balance of a bubble . . . . .	8
2.2	Illustration of the contact angle between the vapor/liquid. . . . .	9
2.3	Different cavities at surfaces. . . . .	9
2.4	Illustration of the critical radius . . . . .	10
2.5	Heat transfer and vapor formation in wicks. . . . .	11
2.6	Variation of the liquid mass flow as a function of the height $z$ . . . . .	14
2.7	Pressure distribution inside a 8 layer thick wick 1 for different heat fluxes. . . . .	16
2.8	Pressure distribution inside a 12 layer thick wick 1 for different heat fluxes. . . . .	17
2.9	Pressure distribution inside a 8 layer thick wick 2 for different heat fluxes. . . . .	18
2.10	Pressure distribution inside a 12 layer thick wick 2 for different heat fluxes. . . . .	19
2.11	Clausius-Clapyerons equation / saturation curve. . . . .	20
2.12	Critical radius as a function of heat flux with wick 1 at an operating temperature of 450°C. . . . .	21
2.13	Critical radius as a function of heat flux with wick 2 at an operating temperature of 450°C. . . . .	22
2.14	Critical radius as a function of heat flux with wick 1 at an operating temperature of 100°C. . . . .	23
2.15	Critical radius as a function of heat flux with wick 2 at an operating temperature of 100°C. . . . .	23
2.16	Critical radius as a function of heat flux with wick 1 at an operating temperature of 600°C. . . . .	24
2.17	Critical radius as a function of heat flux with wick 2 at an operating temperature of 600°C. . . . .	24
2.18	Critical radius as a function of heat flux with wick 1 at an operating temperature of 250°C. . . . .	25
2.19	Critical radius as a function of heat flux with wick 2 at an operating temperature of 250°C. . . . .	25
3.1	Pressure loss inside a 8 layer wick 2 as a function of $z$ . . . . .	28
3.2	Pressure loss inside a 15 layer wick 2 as a function of $z$ . . . . .	29
3.3	Pressure loss inside a 8 layer wick 1 as a function of $z$ . . . . .	29
3.4	Pressure loss inside a 15 layer wick 1 as a function of $z$ . . . . .	30
3.5	Pressure loss inside a 8 layer wick 2 as a function of $z$ . . . . .	31
3.6	Pressure loss inside a 15 layer wick 2 as a function of $z$ . . . . .	31
3.7	Pressure loss inside a 8 layer wick 1 as a function of $z$ . . . . .	32
3.8	Pressure loss inside a 8 layer wick 1 as a function of $z$ . . . . .	32
3.9	Compression method for the wick. . . . .	33

3.10	Pressure loss inside a 8 layer wick 1 as a function of z. . . . .	34
3.11	Pressure loss inside a 8 layer wick 1 as a function of z. . . . .	34
3.12	Pressure loss inside a 8 layer wick 1 as a function of z. . . . .	35
3.13	Combined wick. . . . .	35
3.14	Liquid mass flow with different operating conditions. . . . .	38
3.15	Uneven heat flux distribution with wick 1 . . . . .	39
3.16	Uneven heat flux distribution with wick 2 . . . . .	39
4.1	Process and instrumentation diagram for the test rig . . . . .	41
4.2	Control volume for internal flow in a tube based on figure from [4]. . . . .	43
4.3	Temperature variation for internal pipe flow. (a) Constant heat flux. (b) Constant surface temperature. Based on figure from [4]. . . . .	44
4.4	Temperature distribution in a counterflow heat exchanger based on figure from [4]. . . . .	47
4.5	Bypass tube dimensions. . . . .	48
4.6	Horizontal insulated tube main dimensions. . . . .	48
4.7	Vertical insulated tube. . . . .	49
4.8	Resistance network for the heat transfer from the inside of the tube to the surroundings. . . . .	49
4.9	Stability properties for a system. . . . .	51
4.10	Good gain method. . . . .	52
4.11	Temperature at heat pipe inlet for different controller parameters. . . . .	55
4.12	Marginal stable PID controller. . . . .	56
4.13	Unstable PID controller. . . . .	56
4.14	Stable PID controller. . . . .	57
4.15	Stable PID controller. . . . .	57
4.16	Time difference due to heating of steel in cooling circuit. . . . .	58
4.17	Outlet temperature of side channel blower as a function of rpm. . . . .	61
4.18	Temperature sequence throughout cooling circuit. . . . .	62
4.19	Calibration of the water mass flow . . . . .	63



## List of Tables

1	Wick properties . . . . .	15
2	Pressure within a 8 layer wick 1 at z=0.15m. . . . .	15
3	Pressure within a 12 layer wick 1 at z=0.15m. . . . .	16
4	Pressure within a 8 layer wick 2 at z=0.15m. . . . .	18
5	Pressure within a 12 layer wick 2 at z=0.15m. . . . .	19
6	Necessary superheat for homogeneous nucleation. . . . .	19
7	Performance of a 15cm 8 layer combined wick . . . . .	36
8	Performance of a 20cm 8 layer combined wick . . . . .	37
9	Performance of a 25cm 8 layer combined wick . . . . .	37
10	Performance of a 30cm 8 layer combined wick . . . . .	37
11	PID controller parameters . . . . .	54
12	LabView logging parameters . . . . .	59
13	Horizontal insulated tube calculations . . . . .	59
14	Bypass tube calculations . . . . .	60
15	Vertical insulated tube calculations . . . . .	61
16	Heat added by tracing . . . . .	62
17	Side channel blower calculations . . . . .	64
18	Performance of a 20cm 10 layer combined wick . . . . .	IX
19	Performance of a 25cm 10 layer combined wick . . . . .	IX
20	Performance of a 30cm 10 layer combined wick . . . . .	IX
21	Performance of a 20cm 12 layer combined wick . . . . .	IX
22	Performance of a 25cm 12 layer combined wick . . . . .	IX
23	Performance of a 30cm 12 layer combined wick . . . . .	X
24	Performance of a 20cm 15 layer combined wick . . . . .	X
25	Performance of a 25cm 15 layer combined wick . . . . .	X
26	Performance of a 30cm 15 layer combined wick . . . . .	X

# Nomenclature

## Symbols

$\bar{h}$	average heat transfer coefficient, W/m <sup>2</sup> ,
$\dot{m}$	mass flow, kg/s
$\dot{V}$	Volumetric flow rate, m <sup>3</sup> /h
$A$	wick area, m <sup>2</sup>
$A_c$	wick cross sectional area, m <sup>2</sup>
$c_p$	specific heat capacity, J/kg K
$f$	friction factor
$G$	free energy of formation
$g$	gravity, m/s <sup>2</sup>
$Gr$	Grashof number
$h$	heat transfer coefficient, W/m <sup>2</sup> K, height in chapter 3, m
$h_{fg}$	latent heat of vaporization, J/kg
$K$	permeability, m <sup>2</sup>
$k$	Boltzmann constant
$k$	thermal conductivity in chapter 2.6 and 4, W/mK
$k_l$	liquid thermal conductivity, W/mK
$L$	length
$N$	number of nuclei
$Nu$	Nusselt number
$P$	wetted perimeter, m
$p$	pressure, N/m <sup>2</sup>
$p_l$	liquid pressure, N/m <sup>2</sup>
$p_v$	vapor pressure, N/m <sup>2</sup>
$p_{loss}$	pressure loss, N/m <sup>2</sup>
$Pr$	Prandtl number
$Q$	heat, W
$q$	heat flux, W/m <sup>2</sup>
$q_r$	radial heat flux, W/m <sup>2</sup>
$q_s''$	heat flux, W/m <sup>2</sup>
$R$	resistance
$R$	universal gas constant, J/kgK
$r$	bubble radius, m

---

$r$	coordinate
$r_{eff}$	effective pore radius, m
$Ra$	Rayleigh number
$Re$	Reynolds number
$s$	entropy, J/kgK
$T$	temperature, K
$t$	time
$T_{sat}$	saturation temperature, K
$v_l$	specific liquid volume, m <sup>3</sup> /kg
$v_v$	specific vapor volume, m <sup>3</sup> /kg
$x$	coordinate
$y$	coordinate
$z$	coordinate

**Greek letters**

$\beta$	volumetric expansion coefficient, $K^{-1}$
$\Delta p$	pressure difference
$\Delta p_{drop}$	pressure drop, N/m <sup>2</sup>
$\Delta$	increment
$\gamma$	specific heat ratio
$\lambda$	collision frequency, s <sup>-1</sup>
$\mu$	dynamic viscosity, kg/m s
$\mu_l$	liquid dynamic viscosity, kg/m s
$\nu$	kinematic viscosity, m <sup>2</sup> /s
$\phi$	coordinate
$\rho_l$	liquid density, kg/m <sup>3</sup>
$\rho_v$	vapor density, kg/m <sup>3</sup>
$\sigma$	surface tension, N/m

**Superscripts**

'	per unit length
"	per area

**Subscripts**

o	outer in chapter 4
o	reference
$\delta$	liquid-vapor interface

---

<i>air</i>	surrounding air
<i>bp</i>	bypass
<i>c</i>	cold in chapter 4
<i>c</i>	condenser
<i>calc</i>	calculated
<i>cap</i>	capillary
<i>conv</i>	convective
<i>D</i>	diameter
<i>drop</i>	drop
<i>e</i>	evaporator
<i>eff</i>	effective
<i>exp</i>	experimental
<i>fd</i>	fully developed
<i>g</i>	gravity
<i>H</i>	horizontal
<i>h</i>	hot
<i>h</i>	hydrodynamic in chapter 4
<i>i</i>	inner
<i>l</i>	liquid
<i>lm</i>	log mean
<i>loss</i>	loss
<i>m</i>	mean
<i>max</i>	maximum
<i>r</i>	reduced quantity
<i>RW</i>	rockwool
<i>s</i>	surface
<i>sat</i>	saturation
<i>steel</i>	steel material
<i>t</i>	thermal
<i>tot</i>	total
<i>trac</i>	tracing
<i>V</i>	vertical
<i>v</i>	vapor
<i>w</i>	wall
<i>wick</i>	wick
<i>y</i>	outer

# 1 Introduction

In an effort to reduce energy consumption in aluminum production, a rectangular heat pipe, or thermosyphon, is being developed at NTNU. The heat pipe is to be used in a heat recovery system, where the goal is to utilize the waste heat from electrolysis cells to produce electrical power. The proposed heat pipe is shown in figure 1.1 and 1.2.

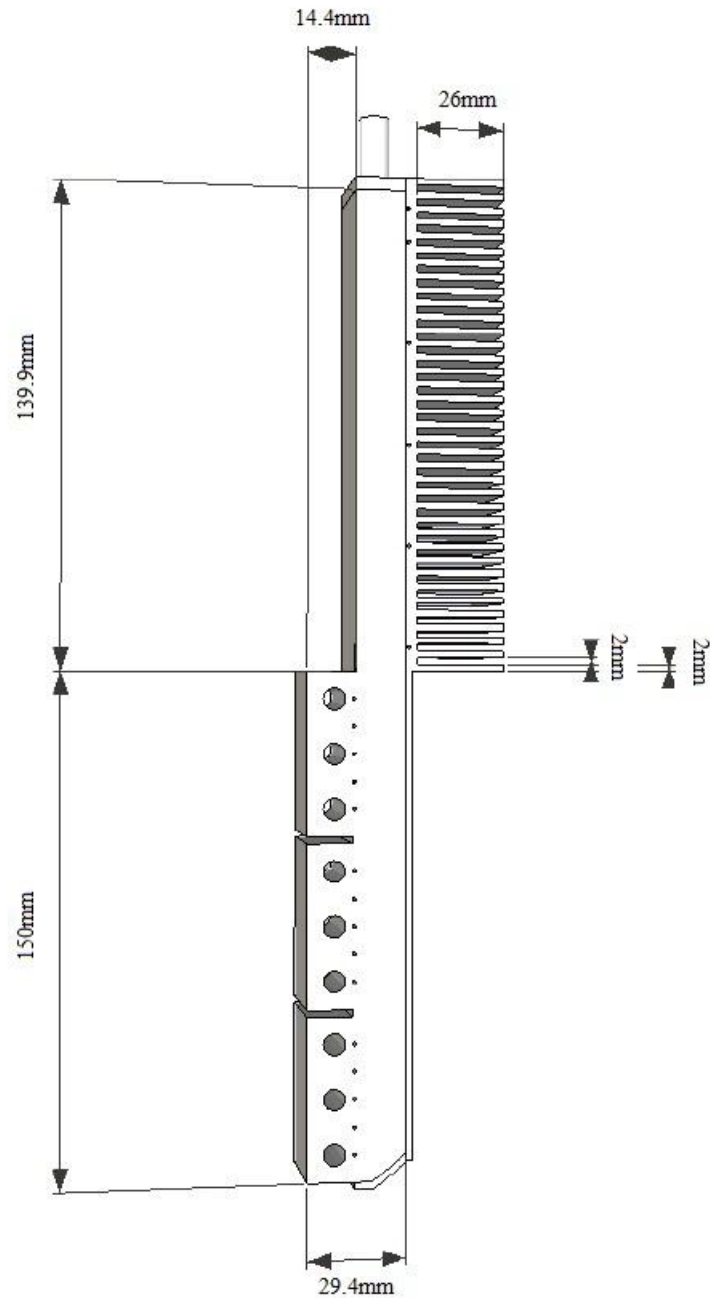
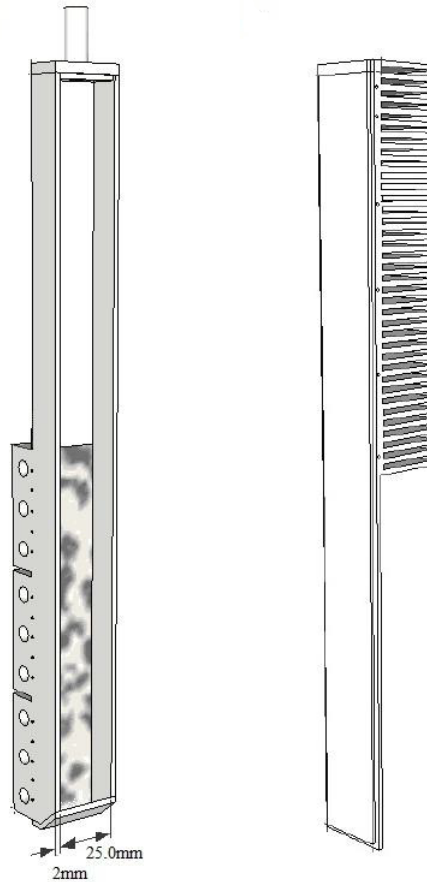


Figure 1.1: Schematic of the proposed system taken from [1]





**Figure 1.2: Schematic of the proposed system evaporator (left) and condenser (right) taken from [1]**

In figure 1.1 the design and main dimensions are shown. These dimensions will be used in the calculations throughout this master thesis. The shaded area on the figure to the left in figure 1.2 represents the wick of the thermosyphon. The wick material consist of a nickel foam, and the casing is made of nickel [2]. The holes in the evaporator section illustrated in figure 1.2 are for heat cartridges which will be used for applying heat flux to the proposed heat pipe. It should be noted that the proposed system do not have an adiabatic section which is common in normal heat pipes.

## 1.1 Project aim and limitations

One of the aims of this master thesis is to analyze two important heat transfer limitations for the proposed heat pipe, the boiling limit and the capillary limit, and suggest solutions to avoid encountering these. A literature survey for the incipience of boiling on porous coated surfaces shall also be performed. In addition to investigating two heat transfer limitations, experimental testing and a total energy balance for the heat pipe cooling circuit is to be performed.

The flow of liquid in the wick is modeled by Darcy's law in one dimen-

sion, and the incipience of boiling is limited to surfaces coated with a porous structure. The heat pipe test rig was not designed for making an energy balance, which will make some important parameters (e.g. heat input from tracing) impossible to determine from the experiments. Whenever there are quantities that are not possible to measure, assumptions or explanation will be given. In agreement with supervisor Erling Næss and the department, it has been decided that tuning of the PID controller is to be performed, as well as testing the response time of the system. The operating temperature region for the proposed system is 400-650°C, and the thermophysical properties of potassium are taken from Vargaftik et al. [3]. Vargaftik et al. was recommended by Annette Hultin after a literature survey performed in 2011 [1]. The nitrogen and air properties are taken from Incropera et al. [4]. All property data used can be found in appendix A.

## 1.2 Structure of the report

This master's thesis will first present a short overview of a heat pipe and its applications and limitations. Chapter 2 presents theory of bubble formation and boiling, as well as a literature review of boiling heat transfer from porous coated surfaces. Calculations and discussions of the incipience of boiling for the proposed system are also presented in chapter 2.

In chapter 3 the capillary limit is discussed and calculated for two wick types. A solution for achieving better performance (i.e. that the wick can sustain higher heat fluxes), and a discussion of uneven heat flux distribution is also presented.

Laboratory experiments of the cooling circuit for the proposed heat pipe are presented in chapter 4. Heat transfer theory, PID controller tuning theory and calculations of the heat loss in the cooling circuit are also given. Conclusions and further work is presented in chapter 5 and 6, respectively.

## 1.3 Principle of a heat pipe

The heat pipe is a closed container that consists of three different sections, evaporator, adiabatic and condenser section. It can best be understood by looking at figure 1.3 where each section is illustrated. In the evaporator section heat is supplied and the working fluid starts to evaporate. The vapor is driven by the higher vapor pressure in the evaporator, and mass is added throughout the evaporator until the vapor enters the adiabatic section where there is no addition of heat/mass. In the condenser section, heat is removed, the latent heat of vaporization is released, and the vapor mass flow decreases due to condensation. As is shown in Figure 1.3, a wick structure is surrounding the inside of the heat pipe. This structure pumps the condensed fluid back to the evaporator section, where it is evaporated again and starts to flow in the direction of the condenser. This process is continuous and will proceed as long as there is sufficient capillary pressure to drive the condensate back to the evaporator. This gives a system that is very reliable, has high thermal conductivity and requires zero maintenance.

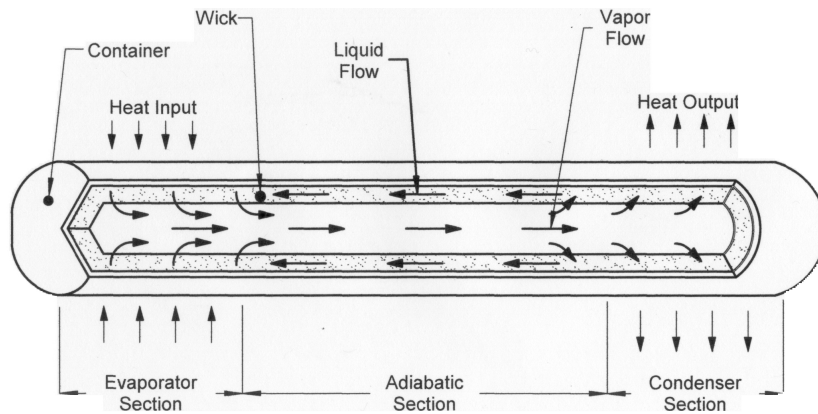


Figure 1.3: Schematic of a cylindrical heat pipe taken from [6]

## 1.4 Applications and temperature ranges

Heat pipes can operate over a wide range of temperatures, from cryogenic temperatures down to 4 Kelvin, to high temperature heat pipes operating at temperatures above 1300 Kelvin. The wide range of temperatures combined with the various ways of constructing the heat pipe, results in many different applications. Aerospace, heat exchangers, electronics and permafrost stabilization are just some of its applications. The main applications are separation of heat source and sink, temperature equalization, and temperature control [5]. A waste heat recovery system is one application where the heat pipe can effectively be used. The proposed heat pipe of Ph.D. candidate Geir Hansen, is to be used in a heat recovery system for an aluminum cell [2].

## 1.5 Limitations

During the operation of a heat pipe there are a number of physical phenomena that can be encountered, which may cause operating limits to the heat pipe. In Figure 1.4 the most important heat transfer limitations are shown as a function of heat rate and temperature.

### 1.5.1 Capillary limit

For the heat pipe to operate, the maximum capillary pressure must be greater than the total pressure drop in the pipe [7]. The total pressure drop in the pipe consists of five components; liquid pressure drop from returning the liquid from the condenser to the evaporator, the vapor pressure drop necessary to drive the vapor from the evaporator to the condenser, the gravitational pressure drop that comes from the inclination of the heat pipe, and pressure drops due to the evaporation and condensation at the liquid-vapor interface. In order for the heat pipe to operate the following condition must then always be maintained,

$$\Delta p_{cap,max} \geq \Delta p_l + \Delta p_v + \Delta p_{e,\delta} + \Delta p_{c,\delta} + \Delta p_g. \quad (1.1)$$

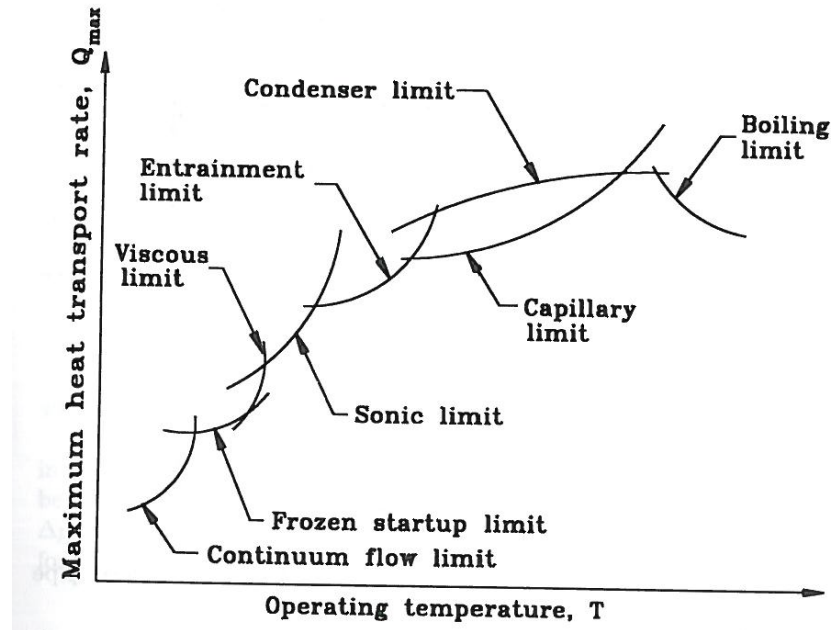


Figure 1.4: Limitations in a heat pipe taken from Faghri [5].

If the condition above is not satisfied, and the right hand side of equation (1.1) exceeds the maximum capillary pressure the wick can sustain, it will cause dry out of the wick and the heat pipe will fail to operate.

### 1.5.2 Boiling limit

The boiling limit is related to the radial heat flux in the evaporator. If this becomes too high, vapor bubbles form in the wick and prevent wetting of the wall. The hot spots occurring from the vapor bubbles formed, cause an excessive temperature difference that could dry out the wick. This is defined as the boiling limit.

### 1.5.3 Entrainment limit

At the interface between the vapor and liquid flow, the vapor will exert a shear force on the liquid flowing. If this force is too big compared with the resisting surface tension in the liquid, droplets are entrained in the vapor stream, and depending on the amount of liquid entrained, the entrainment limit is reached. If too much liquid is entrained, causing the liquid flow to stop, flooding occurs. The flooding limit will represent a failure limit because it will cause dry out of the wick.

### 1.5.4 Sonic limit

Some heat pipes, in particular those with liquid metals as working fluids can reach high vapor flow velocities. If the vapor flow becomes sonic or supersonic, a choked condition occurs and the sonic limitation is reached.

This is usually encountered during startup, and as mentioned, with liquid-metal heat pipes where the vapor velocities are high and the densities are low.

#### **1.5.5 Viscous limit**

With liquid-metals as working fluids, the viscous forces dominate the vapor flow during startup due to the very low vapor pressure inside the heat pipe. Given the very low vapor pressure, the pressure difference from the condenser to the evaporator could be too small to overcome the viscous forces, thus restricting the vapor flow. As heat is applied in the evaporator the temperature, and also the pressure will increase, leading to a pressure difference which is large enough to overcome the viscous forces.

#### **1.5.6 Frozen startup limit**

At startup the fluid is at a frozen state, and during the startup process the vapor from the evaporator section could be frozen again in the adiabatic or condenser section. If this happens, eventually there will no longer be any working fluid left in the evaporator section, and this leads to dry out of the evaporator.

#### **1.5.7 Condenser limit**

If the condenser is not capable of providing sufficient cooling, the maximum heat rate transported by the heat pipe may be limited. Also, If inert gases are present, the cooling capacity of the condenser can be reduced.

#### **1.5.8 Continuum flow limit**

A vapor free molecular or rarefied vapor flow condition can occur in small heat pipes, or in heat pipes operating at very low temperatures. The heat transport will then be limited because the continuum vapor state has not been reached [5].

## 2 Boiling

Formation of bubbles within the wick or at the wick-wall surface is undesirable because this will prevent the circulating liquid from wetting the surface. Failing to wet the surface will cause dry-spots at the wall, leading to a sudden increase of the wall temperature, which in turn can lead to dry-out of the wick. In order to incipience nucleate boiling, a superheat of the liquid is necessary. The needed superheat depends on fluid properties, surface conditions and the ability of wetting of the surface [8]. Bulk boiling of pure degassed liquids requires a very high superheat, water for example, could be superheated to 300°C in experiments at atmospheric pressure before boiling occurred [9]. However, the presence of a porous structure at the heated surface, like the nickel foam in the proposed system could trap vapor bubbles inside the wick, thus lowering the required superheat to incipience boiling. In the literature the boiling limit is referred to as when there is a continuous vapor film at the heated wall (Figure 2.5, model 4), which prevents the liquid from wetting the wall, causing burn out of the heat pipe. This heat transfer limit is similar to film boiling in pool boiling heat transfer, and must be avoided at all time. With potassium as working fluid, or liquid metals in general, Faghri [5] reports that the boiling limit is rarely encountered due to their favorable physical properties. Nevertheless, due to the very low operating pressure of the proposed heat pipe, the possibility of nucleation inside the wick or at the wall could be of concern. Figures 2.1-2.4 are all based on figures from the compendium "Industrial Heat Engineering" by Erling Næss and Martin Løvland [10].

### 2.1 Bubble formation

The formation of bubbles is closely linked to boiling. For a vapor bubble to exist, mechanical equilibrium has to be fulfilled, and it has to be in thermodynamic equilibrium with the surrounding liquid[10]. Figure 2.1 illustrates the force balance between a vapor bubble and the surrounding liquid. The mechanical equilibrium for this bubble yields,

$$p_v \pi r^2 = p_l \pi r^2 + 2\pi r \sigma \Rightarrow p_v - p_l = \frac{2\sigma}{r}. \quad (2.1)$$

In order to relate the pressure difference to the superheat, the Clausius-Clapeyron equation,

$$\left( \frac{dp}{dT} \right)_{sat} = \frac{h_{fg}}{T_{sat}(v_v - v_l)}, \quad (2.2)$$

together with equation (2.1) and assuming that  $\rho_v \ll \rho_l$  the following equation is obtained,

$$T_v - T_{sat,l} = \frac{2\sigma T_{sat,l}}{\rho_v h_{fg} r}. \quad (2.3)$$

As can be seen from equation (2.3), the degree of superheat is inversely proportional to the bubble radius, that is, big vapor bubbles needs less superheat than small vapor bubbles to exist in a liquid pool.

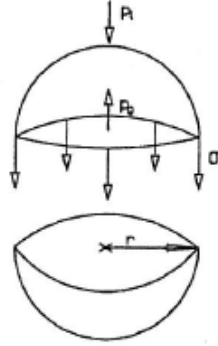


Figure 2.1: Force balance of a bubble

## 2.2 Homogeneous nucleation

Homogeneous nucleation will represent an upper limit for the possibility of boiling, meaning if there is any danger of homogeneous nucleation, changes to the proposed system must be done. *"In a metastable liquid thermal fluctuations occur, and there is a small but finite probability of a cluster of molecules with vapor-like energies coming together to form a vapor embryo of the size of the equilibrium nucleus"* [11]. This process of vapor formation in a metastable liquid is referred to as "homogeneous nucleation" [11]. The theory of homogeneous nucleation is rather complicated, and the derivation of equation (2.4), which gives the rate of nucleation in a metastable liquid, will not be presented here. The derivations can be found in Collier and Thome [11].

$$\frac{dn}{dt} = \lambda N(r) = \lambda N e^{-\Delta G(r)/kT_v}, \quad (2.4)$$

where  $N(r)$  is the number of nuclei of radius  $r$ ,  $\Delta G(r)$  is the free energy of formation of a nucleus of radius  $r$  and  $k$  is the Boltzmann constant. It is rather awkward to use equation (2.4) to evaluate  $T_v$ , and the much simpler expression produced by Lienhard [12] is sufficiently accurate for most purposes [11],

$$(T_{rv} - T_{rSAT}) = 0.905 - T_{rSAT} + 0.095T_{rSAT}^8. \quad (2.5)$$

The subscript 'r' refers to a reduced quantity, i.e., an absolute temperature divided by the critical temperature.

## 2.3 Bubble formation at surfaces

The required wall superheat for nucleation at surfaces is much lower than for nucleation in the bulk of the liquid. As mentioned earlier, a superheat

of 300°K was reported in the bulk of water to incipience boiling, while only a 5°K superheat is sufficient to incipience boiling at the wall [10]. Even the smoothest surfaces have small cavities where inert gases or vapor can be trapped, and these cavities act as nucleation sites. Whether or not a cavity will contain gas depends on the shape of the cavity and the wetting properties of the fluid. The wetting properties is described by the contact angle  $\beta$  in the liquid between the vapor/liquid interface and the surface of the material. Figure 2.2 shows how the contact angle is measured for vapor bubbles and liquid droplets. A liquid is said to be wetting when  $\beta < 90^\circ$ , and non-wetting when  $\beta > 90^\circ$ . The cavities have a highly irregular shape, and figure 2.3 illustrates different types of possible cavities at the surface.

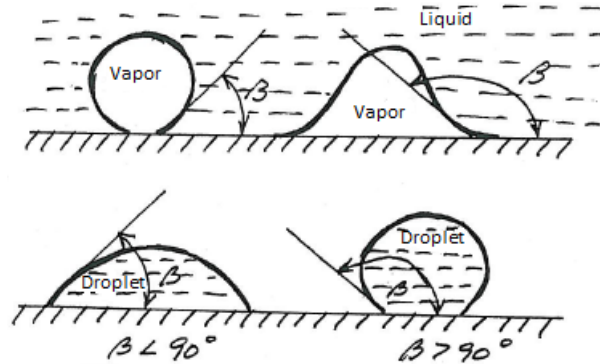


**Figure 2.2:** Illustration of the contact angle between the vapor/liquid.

Another important criteria for a cavity to produce a vapor bubble is the critical radius ( $r_c$ ). The critical radius is equal to the estuary radius of the cavity, and for a cavity to produce vapor bubbles the superheat in the growing bubble must be sufficient at  $r_c$ . Figure 2.4 shows a growing bubble at different time intervals and the critical radius  $r_c$ . By assuming that the temperature inside the bubble ( $T_v$ ) equals the wall temperature ( $T_w$ ), equation (2.3) takes the form,

$$T_w - T_{sat,l} = \frac{2\sigma T_{sat,l}}{\rho_v h_{fg} r_c}. \quad (2.6)$$

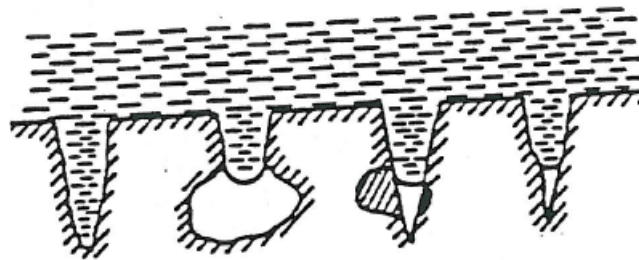


**Figure 2.3:** Different cavities at surfaces.



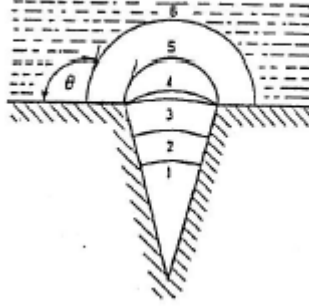


**Figure 2.4: Illustration of the critical radius**

For the bubble to exist, the equilibrium condition in equation (2.6) must be satisfied. At the heated wall, the bubble will grow in a superheated boundary layer with thickness  $\delta$ . By assuming that the temperature profile in the boundary layer is linear, the temperature profile can be described as,

$$T = T_w - \frac{qr_c}{k_l}. \quad (2.7)$$

Combining equation (2.6) and (2.7), the onset of nucleate boiling can be calculated,

$$T_w - T_{sat,l} = \frac{2\sigma T_{sat,l}}{r_c h_{fg} \rho_v} + \frac{qr_c}{k_l}. \quad (2.8)$$

By taking the derivative of equation (2.8) with respect to  $r_c$ , an expression for the critical radius yields,

$$r_c = \min \left[ r_{c,max}, \sqrt{\frac{2\sigma T_{sat,l} k_l}{qh_{fg} \rho_v}} \right]. \quad (2.9)$$

$r_{c,max}$  is the maximum estuary radius for a cavity that can contain vapor, which varies depending on the working fluid. This parameter is  $5\mu\text{m}$  for water, but for potassium there is no literature on  $r_{c,max}$ .  $\sqrt{\frac{2\sigma T_{sat,l} k_l}{qh_{fg} \rho_v}}$  is the calculated maximum estuary radius that can contain vapor based on the assumptions above. Potassium which is to be used as working fluid in the proposed system, and other alkali metals generally wet their containers very well. They also wet the larger cavities and render them inactive [13]. This combined with the fact that alkali metals have less steep vapor pressure curves in practical temperature ranges, and their capacity to dissolve inert gases increases with an increase in temperature, tend to give higher incipient-boiling wall superheat compared with ordinary liquids [13].

Heat transfer in heat pipe wicks is more complicated than at a plane surface due to the capillary structure of the wick. Properties of the working fluid and wick play an important role in how the heat distributes inside the

wick. Both Faghri [5] and Invanovskii et al. [9] presents four different models of heat transfer in wicks, and these are shown in figure 2.5.

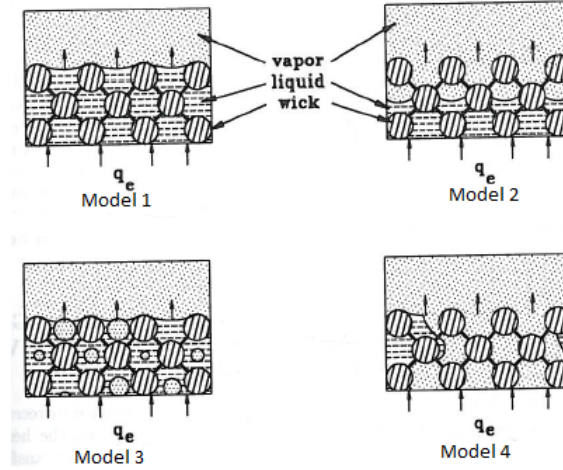


**Figure 2.5: Heat transfer and vapor formation in wicks.**

### 2.3.1 Model 1

The whole wick is saturated with liquid and evaporation takes place from its surface. Heat is transported by conduction through the liquid filled wick, and no boiling occurs within the wick. This is a common working condition for non-metallic working fluids under a low heat flux, and metallic working fluids under a low to moderate heat flux.

### 2.3.2 Model 2

The liquid-vapor interface has receded into the wick because of an increase in the heat flux. If the heat flux is reduced, the receding of the liquid will stop, and the wick will be saturated again. However, if the heat flux is not reduced it may cause the entire wick to be depleted, thus causing burn out of the wick. This is actually the capillary limit and not the boiling limit. The vaporization will still take place at the liquid-vapor interface, and no boiling occurs in the wick.

### 2.3.3 Model 3

If the temperature difference across the wick is large, nucleate boiling may take place within the wick. The bubbles grow and escape through the wick before they bursts at the surface of the liquid-vapor interface. This could disrupt the established menisci and reduce, or even eliminate the capillary forces for pumping the liquid in the evaporator.

### 2.3.4 Model 4

The heat flux is increased and more bubbles are formed, they coalesce and form a layer of vapor adjacent to the heated wall. This layer prevents wetting of the heated surface, leading to a sudden increase of temperature which could burn out the heat pipe. This is referred to the boiling limit of the heat pipe.

## 2.4 Literature survey - Heat transfer and the incipience of boiling from porous surfaces

The models presented above represents four different ways of describing the heat transfer in the wick of a heat pipe. As mentioned before, there are several factors that play a role in how the heat transfer can best be modeled, like fluid properties and surface conditions for example. Several authors [13][14][15] have pointed out the difference of heat transfer in porous coatings between liquid metals and non-metallic fluids (water for instance). Winston et al. [15] studied wicks which were fabricated from beds of packed beads or planar slabs of sintered metal fibers and powders. They used liquid potassium at a saturation temperature of 866K and water at atmospheric pressure as working fluids. Their findings concluded that the mechanism of heat transfer in the evaporator zone of a water heat pipe is that of conduction across a thin vapor layer near the heated wall, accompanied by a flow of vapor through the wick structure to the wick exterior. However, when liquid metals are used, heat is transferred by conduction across a liquid-saturated wick to the outer surface where vaporization of the working fluid takes place [15]. Ferrell and Davis [14] concluded with the same heat transfer mechanism in the wick as Winston et al. [15]. It was also pointed out the difficulties of determining the liquid-vapor interface in the wick with water as working fluid, which in turn makes it very difficult to accurately predict the heat transfer coefficient and the critical heat flux (burn out). Alleavitch and Ferrell [16] conducted experiments with a horizontal, heated stainless steel surface covered with a wick structure. The fluid used was water, and the wick was flooded. The authors concluded that for values of the heat flux below the critical, the mechanism of vaporization heat transfer from wick covered surfaces is one of conduction across a thin, liquid saturated film in contact with the heated surface, which is maintained by the capillary forces existing at a liquid-vapor interface within the wick [16]. Moss and Kelly [17] performed a neutron radiographic study of the vaporization processes which occur interior to the wick structure of a planar heat pipe employing water as working fluid. Their findings included two models of the heat transfer process, which were postulated and analytically formulated. The first model assumed that evaporation occurred only from the upper surface of the wick, whereas the second assumed that vapor was generated at the wicks base and released solely from the sides of the wick [17]. The second model proved to be more realistic for correlating the test data. This is corresponds well with [14] and [15] who also presented that with water as a working fluid the vaporization process occurs inside the wick structure.

One of the main incentive for coating surfaces with a porous material is to enhance the heat transfer performance. Porous coatings, wicks and other surface enhancing materials are often used to improve heat transfer performance in various applications. Bergles and Chyu [18], Allingham and Mcentire [19] and Xu et al. [20] all reported improved heat transfer performance on surfaces with porous structures in their experiments. Allingham and Mcentire [19] concluded that the wick fibers increase the effective heat transfer surface area and provide active sites for bubble formation. Another aspect concerning the improved heat transfer of porous surfaces is the needed superheat to incipience boiling. Janusz T. Cieslinski [21] reported that with porous coatings on a heated surface boiling commenced at lower wall superheat compared with those for a smooth surface. The lower wall superheat necessary is also reported by [22][23][24].

## 2.5 Pressure distribution in the wick

At the bottom of the evaporator in the proposed system the pressure inside the wick will be approximately equal to the vapor pressure. As the liquid moves upwards inside the wick, the liquid pressure is reduced due to gravitational and frictional pressure losses. This reduction of capillary pressure could be enough to lower the liquid pressure sufficiently, leading to the incipience of nucleate boiling. It is therefore important to investigate how the liquid pressure varies.

As pointed out earlier, the liquid pressure inside the wick will be a decisive factor for nucleation to occur at the wall or inside the wick. A low liquid pressure inside the wick will give a larger pressure difference between the liquid pressure and the saturation pressure, leading to a larger superheat, which again leads to greater risk of boiling. The pressure inside the wick can be represented by the following equation,

$$P_{wick} = P_o - \left( \rho g z + \int_0^z \frac{\mu_l \dot{m}_l}{\rho_l A_c K} dz \right), \quad (2.10)$$

where  $P_o$  is a reference pressure,  $K$  the permeability, and  $A_c$  the wick cross section area. The third term on the right hand side of equation (2.10) is the pressure drop of liquid flow in a wick structure due to frictional drag [5], also referred to as Darcy's law, while the second term on the right hand side is the gravitational pressure loss. Assuming that the liquid mass flow inside the wick decreases linearly with increasing  $z$  (See figure 2.6), a relation of the form,

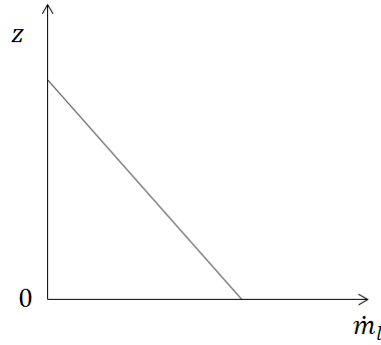


**Figure 2.6: Variation of the liquid mass flow as a function of the height  $z$ .**

$$\dot{m}_l = \frac{dm}{dt} = \dot{m}_{max} - \frac{\dot{m}_{max}}{h} z \quad (2.11)$$

can be used. Here  $h$  is the evaporator height and  $\dot{m}_{max} = \frac{Q}{h_{fg}}$ . Combining equation (2.10) and (2.11) the following expression is obtained,

$$P_{wick} = P_o - \left( \rho_l g z + \frac{\mu_l Q}{\rho_l A_c K h_{fg}} \int_0^z \left( 1 - \frac{z}{h} \right) dz \right). \quad (2.12)$$

Performing the necessary integration, the expression for the pressure inside the wick at height  $z$  yields,

$$P_{wick} = P_o - \left( \rho_l g z + \frac{\mu_l Q}{\rho_l A_c K h_{fg}} \left[ z - \frac{z^2}{2h} \right] \right). \quad (2.13)$$

There are several factors that may or may not play an important role when calculating the pressure loss. Temperature, which affect the physical properties of potassium, the applied heat flux, and the permeability of the wick all influence on the total pressure loss inside the wick. It is therefore necessary to evaluate all the different factors, and then evaluate the contribution of each factor.

## 2.6 Results and discussion

Since the wick pressure,  $P_{wick}$ , decreases with increasing  $z$ , the most likely place for boiling to occur is at the top of the evaporator. By making sure that no boiling occurs at the top of the evaporator, one can be confident that boiling is avoided in the entire wick. There is an ongoing study of identifying the best suitable wick for the proposed system, and at present there are two different nickel foam wicks being tested. In table 1 the permeability, effective pore radius, and porosity for the two foam wicks which will be used in the calculations are shown. The wick properties are determined by a "rate of rise" experiment with heptane done by Ph.D. candidate Geir Hansen. In the calculations no correction for the the contact angle against nickel is done for potassium. It is therefore expected that the actual performance of the wick

will be better due to the physical properties of potassium against nickel are more favorable compared with heptane.

**Table 1: Wick properties**

	Permeability (m <sup>2</sup> )	Effective pore radius (m)	Porosity (%)
Wick 1	31·10 <sup>-12</sup>	62·10 <sup>-6</sup>	79.7
Wick 2	205·10 <sup>-12</sup>	126·10 <sup>-6</sup>	88.6

An equation for the pressure distribution inside the wick was derived on the basis of Darcy's law and a gravitational pressure loss term in section 2.5. Using equation (2.13), one can calculate the pressure at the top of the evaporator, and then consider if there is any danger of boiling. In the sections to follow the effect of heat flux, wick thickness, and wick properties will be discussed. In the calculations in this section the reference pressure  $P_o$  has been set to 5000Pa, which corresponds to a saturation temperature of 773K (500°C).

### Pressure distribution inside the wick

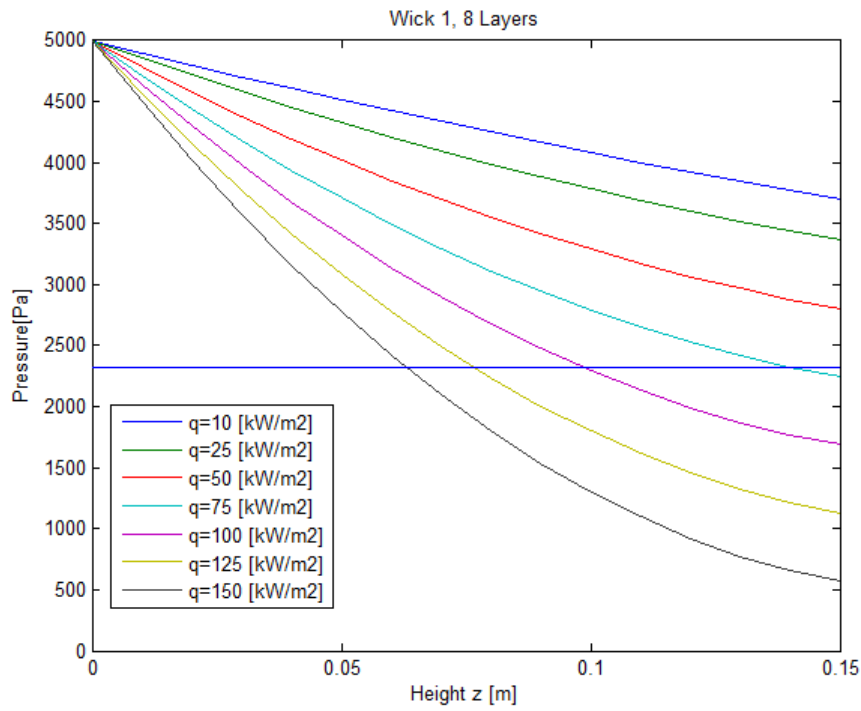
No decision has been made regarding the final number of wick layers in the proposed system, so a range from 8-15 layers were tested for different operating conditions. Figure 2.7 and 2.8 presents pressure curves for wick 1 (see table 1) with 8 and 12 layers with varying heat flux. It is seen that the performance of the wick is proportional to the thickness, where more layers gives less pressure drop. The wick with 8 layers has a pressure of 570Pa at the top of the evaporator with the highest heat flux (150kW/m<sup>2</sup>), while with 12 layers the pressure is 1688Pa at the top of the evaporator. However, it should be noted that it is not possible to achieve a pressure as low as 570Pa with 8 layers or 1688Pa with 12 layers. The reason for this is that the capillary limit is encountered before the pressure has decreased to the respective pressures. The horizontal lines in figures 2.7 and 2.8 represent the capillary limit, and if these lines are crossed by the declining pressure curves, dry out of the wick occurs. This is further discussed in section 3. Table 2 and 3 shows the values of the pressure inside the wick at the top of the evaporator for 8 and 12 layers of wick 1 for different heat fluxes. What can be seen both from table 2-3 and figure 2.7-2.8, is, that an increase in applied heat flux, yields an increase in the pressure drop within the wick.

**Table 2: Pressure within a 8 layer wick 1 at z=0.15m.**

Heat flux (kW/m <sup>2</sup> )	10	25	50	75	100	125	150
$P_{wick}$ (Pa)	3699	3364	2805	2246	1688	1129	570

**Table 3: Pressure within a 12 layer wick 1 at  $z=0.15\text{m}$ .**

Heat flux ( $\text{kW}/\text{m}^2$ )	10	25	50	75	100	125	150
$P_{wick}$ (Pa)	3773	3550	3177	2805	2433	2060	1688

**Figure 2.7: Pressure distribution inside a 8 layer thick wick 1 for different heat fluxes.**

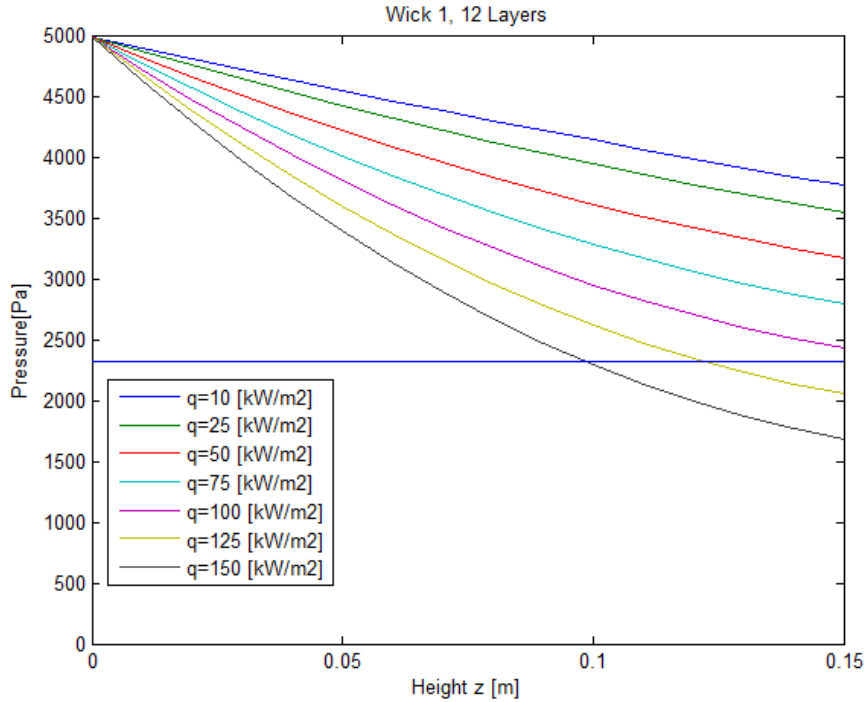


**Figure 2.8: Pressure distribution inside a 12 layer thick wick 1 for different heat fluxes.**

Figures 2.9 and 2.10 present pressure curves for wick 2 (see table 1) with 8 and 12 layers with varying heat flux. It is seen that wick 2 has a significantly less pressure drop throughout the evaporator both for 8 and 12 layers compared with wick 1. The big difference in the pressure loss is due to the permeability, which is evident by looking at equation (2.13), where the second term on the right hand side is proportional to permeability. In addition wick 2 is less compressed (i.e. thicker), leading to a bigger wick cross section, which also lowers the pressure drop. Although wick 2 yields a considerably less pressure drop, the maximum capillary pumping pressure sustainable by the wick is also much less (1317Pa for wick 2, 2667Pa for wick 1), which is seen from the horizontal lines in figures 2.9 and 2.10. It is seen that the capillary limit is encountered for heat fluxes above  $125\text{kW/m}^2$  with 8 layers, but for 12 layers the wick can tolerate heat fluxes well above  $150\text{kW/m}^2$ . Table 4 and 5 shows the values of the pressure inside the wick at the top of the evaporator for 8 and 12 layers of wick 2 for different heat fluxes. From a boiling point of view one could argue that wick 2 is the best choice since it has a much lower pressure drop inside the wick, leading to a favorable higher pressure at the top of the evaporator. However, in order to evaluate the possibility of boiling, the critical radius at which incipient boiling occurs has to be calculated.



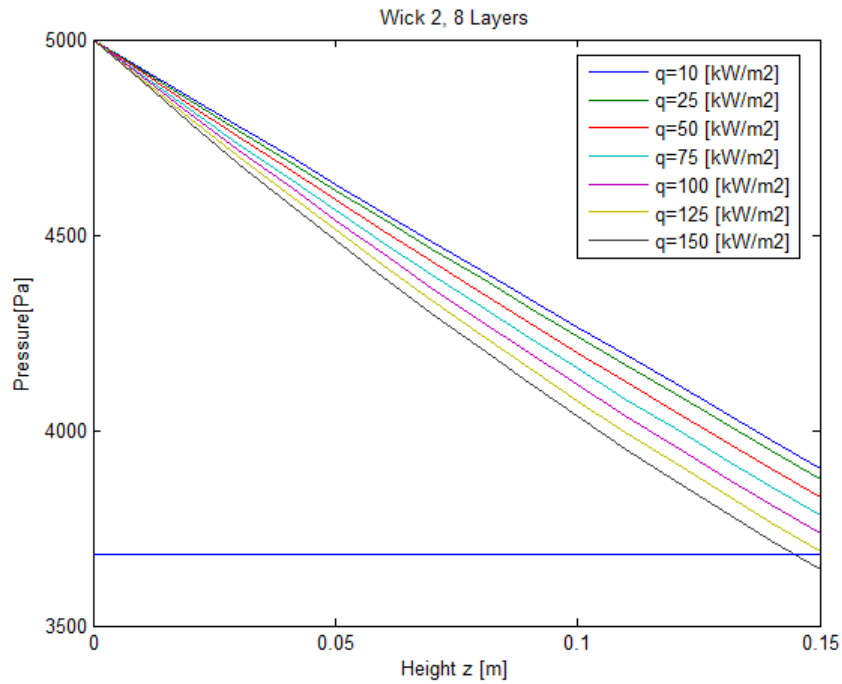
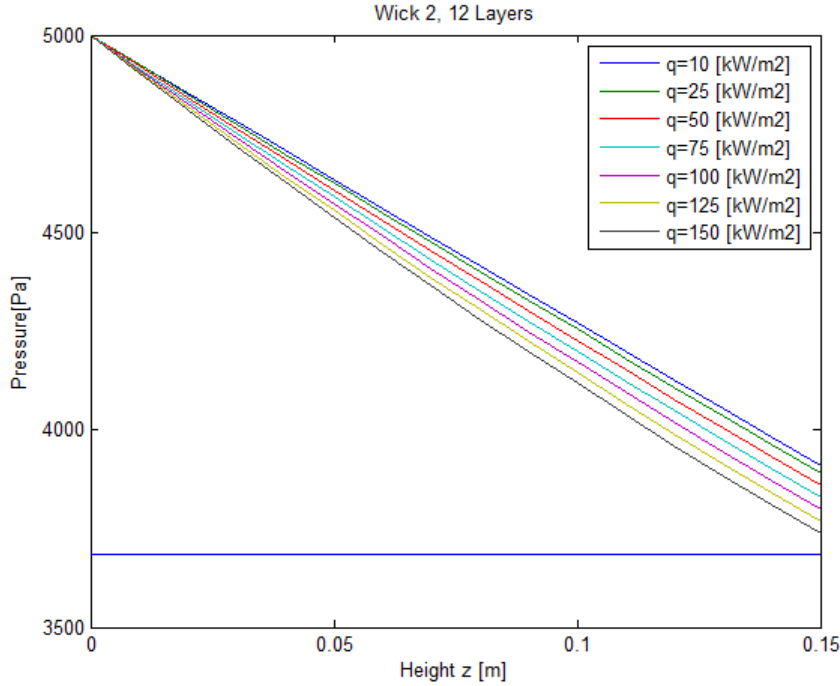


Figure 2.9: Pressure distribution inside a 8 layer thick wick 2 for different heat fluxes.

Table 4: Pressure within a 8 layer wick 2 at  $z=0.15\text{m}$ .

Heat flux ( $\text{kW}/\text{m}^2$ )	10	25	50	75	100	125	150
$P_{wick}$ (Pa)	3904	3876	3838	3783	3737	3691	3645



**Figure 2.10: Pressure distribution inside a 12 layer thick wick 2 for different heat fluxes.**

**Table 5: Pressure within a 12 layer wick 2 at  $z=0.15\text{m}$ .**

Heat Flux ( $\text{kW}/\text{m}^2$ )	10	25	50	75	100	125	150
$P_{wick}$ (Pa)	3910	3891	3860	3830	3799	3768	3737

### Homogeneous nucleation

In table 6 the saturation temperature and the corresponding necessary superheat for the onset of homogeneous nucleation (ohn) is calculated using equation 2.5. It is evident that there is no danger of homogeneous nucleation in the proposed system due to the very large superheat needed.

**Table 6: Necessary superheat for homogeneous nucleation.**

$T_{sat}$ (K)	573	673	773	873	973
$\Delta T_{ohn}$ (K)	1491.3	1391.3	1291.3	1191.4	1091.5

### Critical radius

Figures 2.12-2.19 were obtained by first calculating the wick pressure at the top of the evaporator using equation (2.13), then using this pressure and interpolate in a table containing the physical data of potassium to give a saturation temperature corresponding to the wick liquid pressure. This saturation temperature was then used to calculate the wall temperature based on an equation of the form,

$$q = \frac{T_w - T_{sat}}{R}, \quad (2.14)$$

where  $R$  is the resistance inside the wick defined as,

$$R = \frac{\delta}{k} + \frac{1}{h}, \quad (2.15)$$

where  $\frac{\delta}{k}$  represents conduction and  $\frac{1}{h}$  convection across the wick. A meeting with professor Erling Næss led to the conclusion that the contribution to  $R$  from convection inside the wick could be neglected because  $h$  is very large. Having the wall temperature, a saturation pressure based on this temperature was obtained by interpolating in table for potassium properties. Lastly equation (2.1) was used to calculate the necessary critical radius in order for a bubble to be stable and grow, the incipience of boiling. The reason for using (2.1) and not a Clausius-Clapeyron type of an equation, is because of the low pressure inside the heat pipe. When the pressure is very low there is a much larger error in using the Clausius-Clapeyron approximation (see figure 2.11).

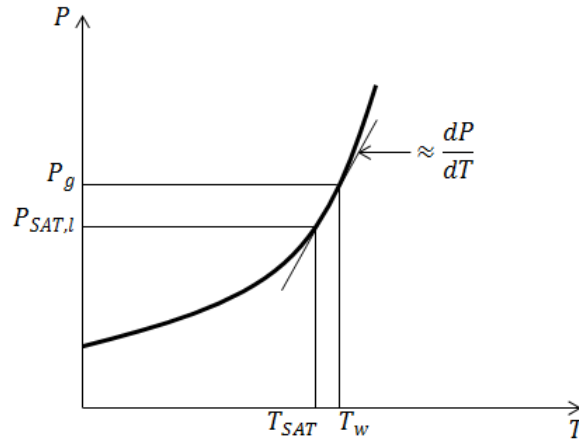


**Figure 2.11: Clausius-Clapeyrons equation / saturation curve.**

Professor Erling Næss suggested that two cases, or two different operating conditions were tested in the calculations of the critical radius. The two operating conditions tested are 450°C and 600°C. Figures 2.12 and 2.13 show the necessary critical radius for a bubble to be stable and grow with potassium as working fluid and an operating temperature of 450°C for wick 1 and 2, respectively. As can be seen from figure 2.12, with 15 layers the curve takes a sudden change of direction at 20000W. This curvature is not expected, but the approach used to calculate the critical radius, and the tabulated physical properties of potassium give the unexpected curvature with 15 layers. With wick 1 and an operating temperature of 450°C, the critical radius ranges from 2500 $\mu$ m-45000 $\mu$ m (ref. figure 2.12), and with wick 2 from 350 $\mu$ m-4500 $\mu$ m (ref. figure 2.13) depending on the applied heat flux and number of layers. There is not any data regarding the roughness of the

nickel casing, or any literature on how big the cavity size has to be in order to incipience boiling with potassium as working fluid. However, professor Erling Næss suggested that one could expect the critical radius to be around  $50\mu\text{m}$ . Since the calculated critical radius's are much greater than what could be expected, the possibility of boiling is very small.

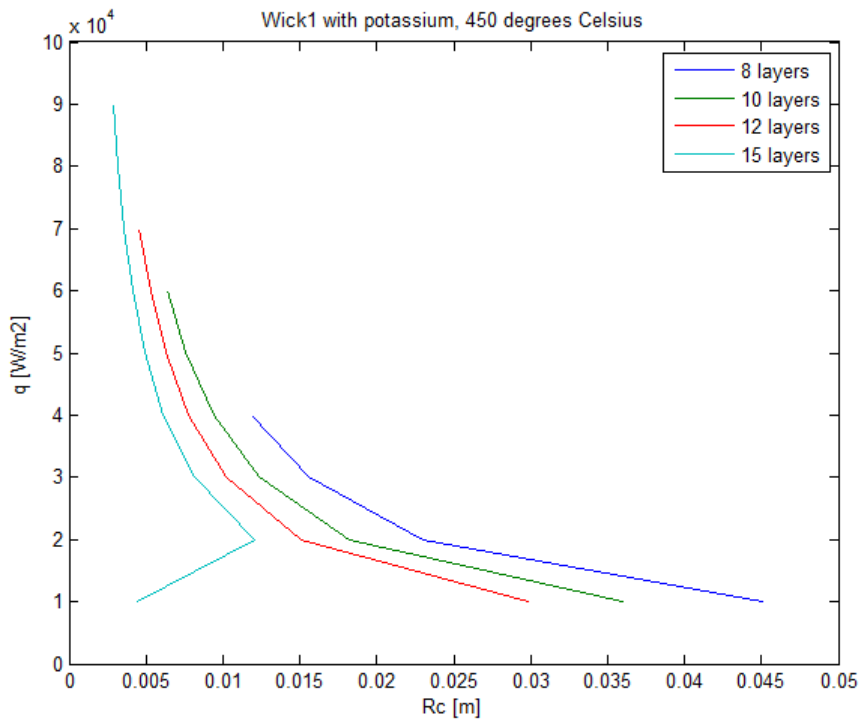
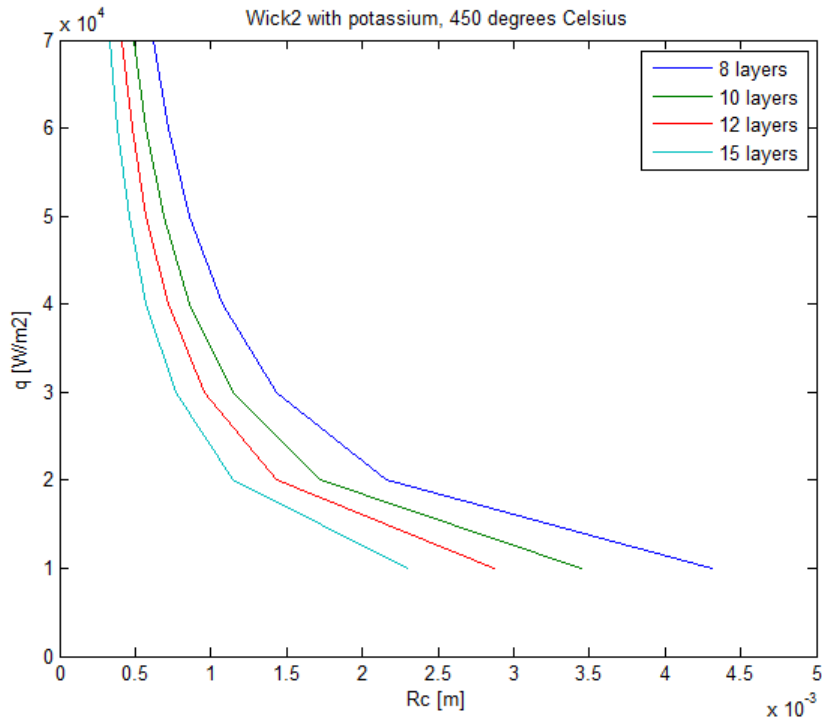


Figure 2.12: Critical radius as a function of heat flux with wick 1 at an operating temperature of  $450^\circ\text{C}$ .



**Figure 2.13: Critical radius as a function of heat flux with wick 2 at an operating temperature of 450°C.**

As a comparison the critical radius has also been calculated using water as working fluid at 100°C, where figure 2.14 and 2.15 presents the critical radius as a function of heat flux and number of layers. With water as working fluid the the critical radius lies in the range of 2 $\mu$ m-20 $\mu$ m with wick 1, and from 0.2 $\mu$ m-6 $\mu$ m with wick 2. If water had been intended for the proposed system the possibility of boiling would be of concern. The second case where the operating temperature is 600°C and potassium as working fluid are shown in figures 2.16 and 2.17. With wick 1 the critical radius ranges from 100 $\mu$ m-1800 $\mu$ m, and boiling should not be of concern. However, when wick 2 is used the critical radius ranges from about 25 $\mu$ m-900 $\mu$ m depending on applied heat flux and number of layers of the wick material. Remembering that the expected cavity size is around 50 $\mu$ m, caution should be taken when operating with a high heat flux combined with a 15 layer wick. Again as a comparison a case with water as working fluid operating at a temperature of 250°C, corresponding to a vapor operating pressure of 39.73bar are shown in figures 2.18 and 2.19. The critical radius for water at an operating temperature of 250°C lies in the range of 0.025 $\mu$ m-0.4 $\mu$ m with 1, and from 0.02 $\mu$ m-0.12 $\mu$ m with wick 2.

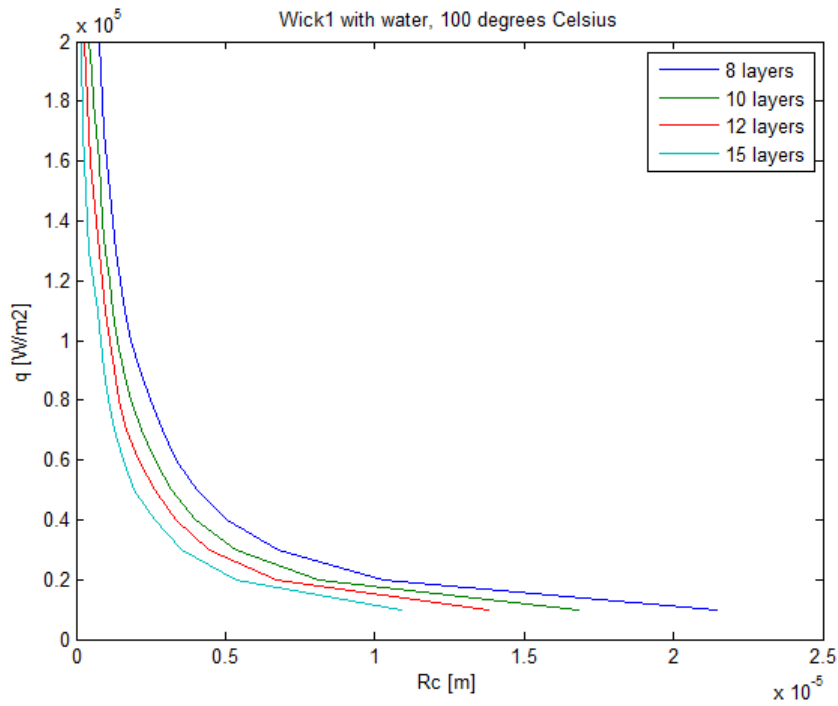


Figure 2.14: Critical radius as a function of heat flux with wick 1 at an operating temperature of 100°C.

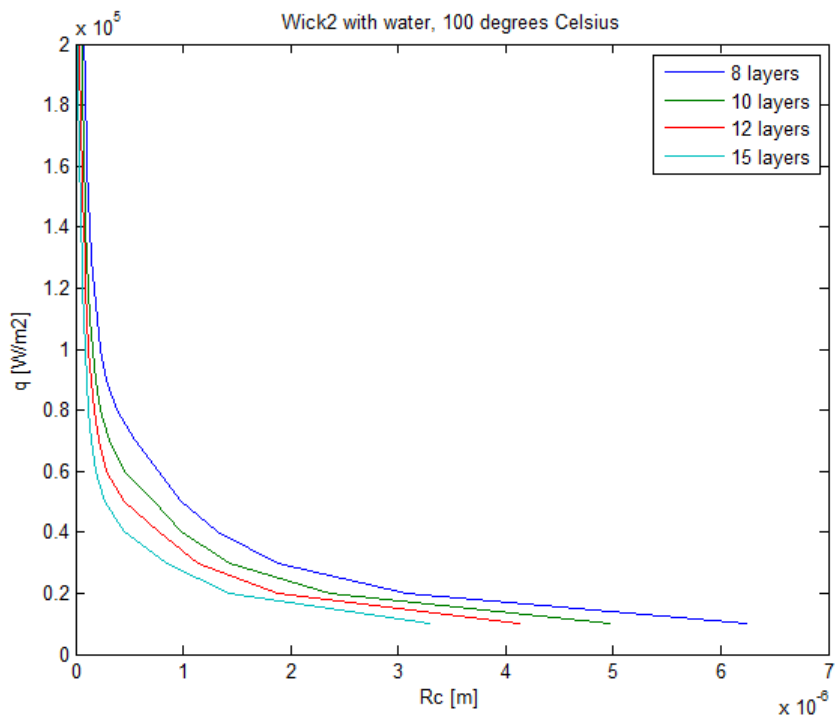


Figure 2.15: Critical radius as a function of heat flux with wick 2 at an operating temperature of 100°C.

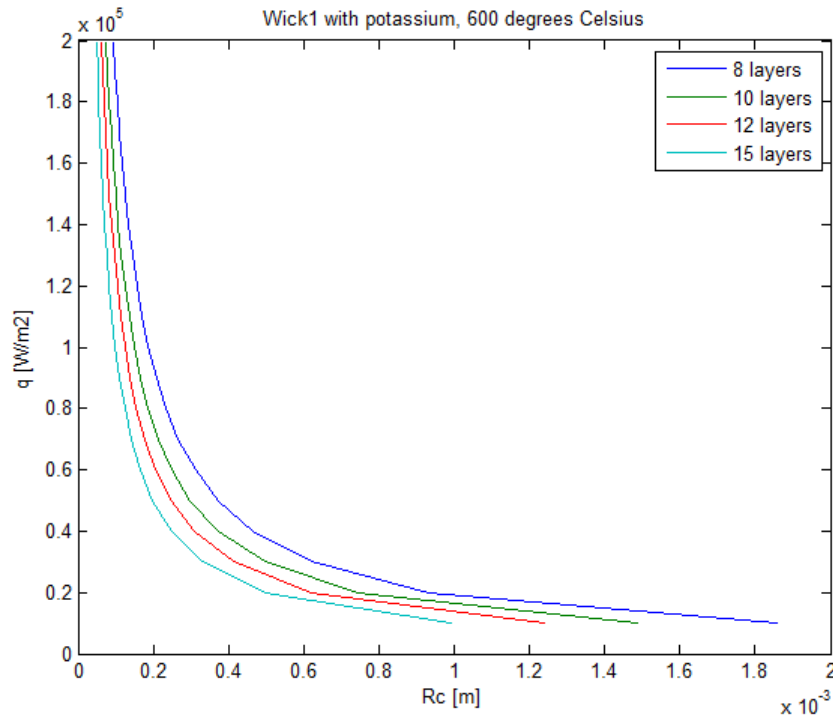


Figure 2.16: Critical radius as a function of heat flux with wick 1 at an operating temperature of 600°C.

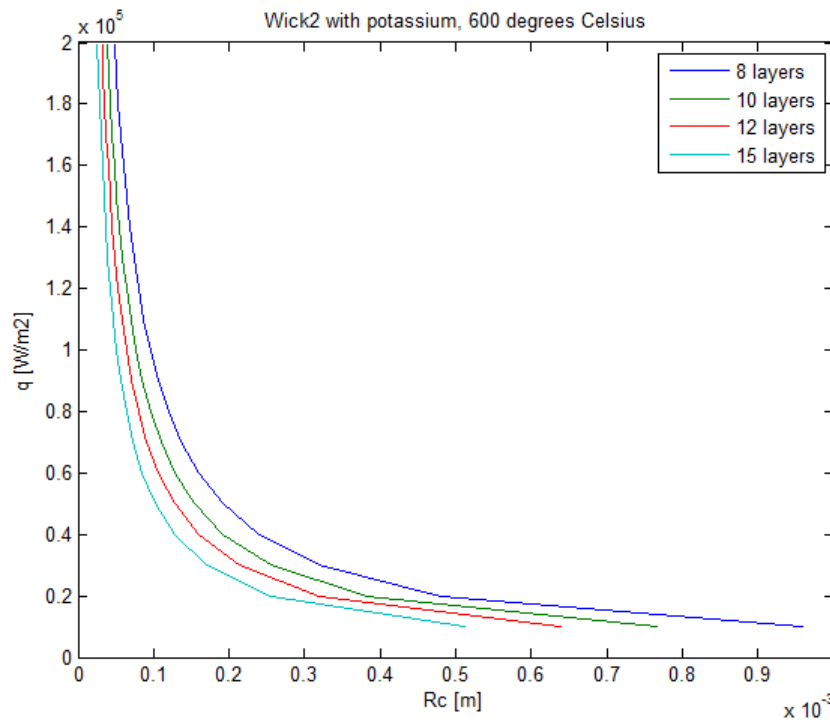


Figure 2.17: Critical radius as a function of heat flux with wick 2 at an operating temperature of 600°C.

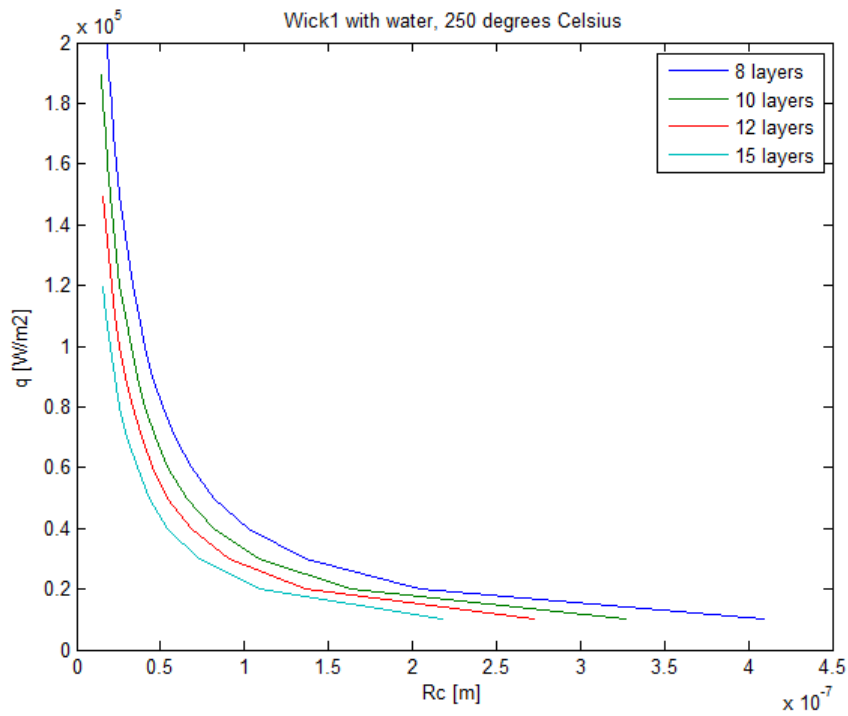


Figure 2.18: Critical radius as a function of heat flux with wick 1 at an operating temperature of 250°C.

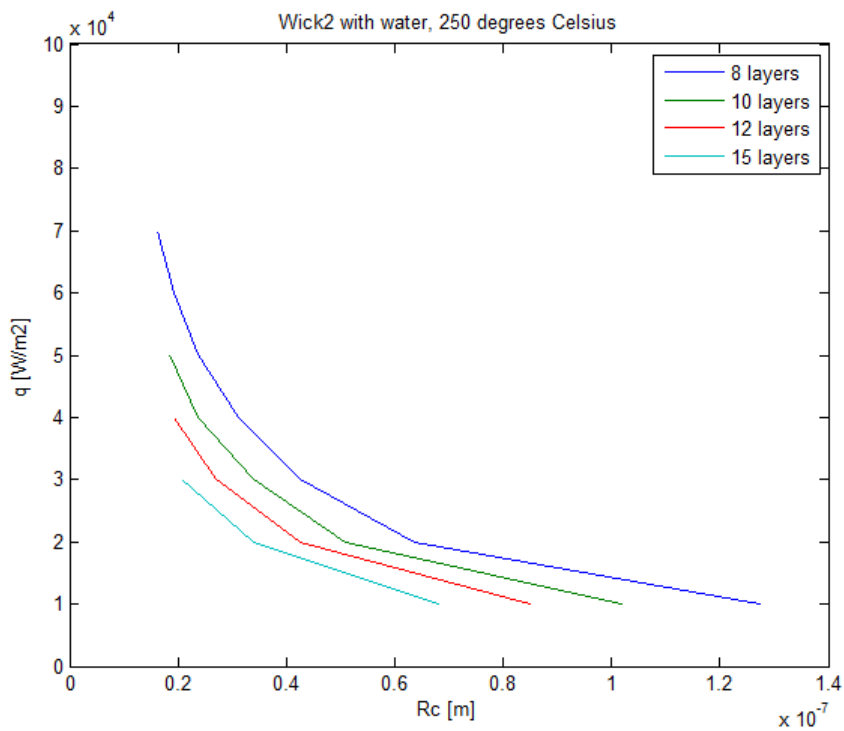


Figure 2.19: Critical radius as a function of heat flux with wick 2 at an operating temperature of 250°C.



## 2.7 Chapters conclusions

A literature survey regarding heat transfer and the incipience of boiling from porous surfaces was presented. From the literature survey it can be concluded that with porous coatings heat transfer is improved and less superheat is required for boiling to commence. The mechanism of heat transfer for liquid metals is most likely conduction across a liquid-saturated wick to the outer surface where vaporization of the working fluid takes place. However, an experimental setup with the proposed system should be done in order to verify the theory suggested in the literature survey. Also, it should be noted that depending on the applied heat flux the heat transfer model for the wick could change (ref. Figure 2.5).

The possibility of homogeneous nucleation in the proposed system is not of concern due to the large required superheat in order to incipience homogeneous nucleation. The chance of wick boiling is regarded as small for both wick 1 and wick 2. The calculated critical radius's lies significantly (order of 10 and more) above the expected value ( $50\mu\text{m}$ ) in most cases. However, caution should be taken if wick 2 and 15 layers is used with high heat fluxes at an operating temperature of  $600^\circ\text{C}$ . This is because the calculated radius's lie in the range  $25\mu\text{m}$ - $900\mu\text{m}$ , which is where the expected critical value should lie. This combined with the fact that porous coatings (wicks) generally lowers the required superheat for boiling to commence, makes it important to be careful at certain operating conditions for the proposed system. From a boiling perspective, wick 1 is the best choice because the critical radius's for all operating conditions tested are well above the expected critical radius.

### 3 Capillary limit

For the proposed system it is crucial that the capillary pressure sustainable by the wick is greater than, or equal to the sum of pressure losses along the heat pipe. If this criterion is not fulfilled, the heat pipe will not be able to wet the entire wick, leading to dry out of the wick, which in turn could destroy the heat pipe due to lack of cooling. For the heat pipe to operate properly the following pressure balance must be satisfied,

$$\Delta p_{cap,max} \geq \Delta p_l + \Delta p_v + \Delta p_{e,\delta} + \Delta p_{c,\delta} + \Delta p_g. \quad (3.1)$$

The maximum capillary head can be calculated by,

$$\Delta p_{cap,max} = \frac{2\sigma}{r_{eff}}, \quad (3.2)$$

where  $r_{eff}$  is the effective pore radius of the wick. The first and last pressure drop terms on the right hand side of equation (3.1),  $\Delta p_l$  and  $\Delta p_g$ , were introduced in section 2 and are the same here.  $\Delta p_v$  represents the vapor pressure drop, and to calculate this a numerical model is needed, which is not available at the time being. Although there is no model to calculate the vapor pressure drop, a worst case scenario when the vapor velocity equals the flooding velocity could be used as a first approximation. Using the recommended correlation from [25] for the prediction of the flooding velocity, a vapor velocity of 50m/s is found. By approximating the vapor pressure loss due to acceleration as  $\Delta p_v \approx \frac{1}{2}\rho v^2$ , a pressure loss of about 50Pa is obtained when a saturation temperature of 750K is assumed. A pressure drop of 50Pa is not very much compared with the gravitational and liquid pressure drop, but it should be kept in mind that the actual pressure drop will be slightly higher than what is calculated.  $\Delta p_{e,\delta}$  and  $\Delta p_{c,\delta}$  are the pressure drops due to the evaporation and condensation at the liquid-vapor interface, respectively, and usually can be neglected [5].

The proposed system has a 15cm wick, and there are at the time being two types of Nickel foam wicks (table 1) available for usage. The best wick is the one that gives the best performance, i.e. highest heat flux. In addition to simulating the performance of the wick for the proposed system, it is desired to find out how a larger system (30cm wick for example) performs, and how to achieve the best possible performance. The pressure loss inside the wick as function of  $z$  is given below,

$$P_{loss} = \rho g z + \frac{\mu_l Q}{\rho_l A_c K h_{fg}} \left[ z - \frac{z^2}{2h} \right] \leq P_{cap,max}. \quad (3.3)$$

The above equation will be used for calculating the pressure loss with varying heat flux, and then compared against the maximum capillary pressure of the wick.

### 3.1 Results and discussion

Equation (3.3) has been used to calculate the pressure loss distribution inside the wick as a function of the height  $z$  and a saturation temperature of 750K. The maximum capillary pressure for wick 1 and wick 2 is 2677Pa and 1317Pa, respectively. This will represent an upper limit for the pressure drop inside the wick, and cannot be surpassed. Or in other words, the heat flux that gives a higher pressure drop than the maximum capillary pressure sustainable by the wick will represent the capillary limit. Figures 3.1 and 3.2 shows the pressure loss for a 15cm wick 2 with 8- and 15 layers respectively. Figures 3.3 and 3.4 shows the pressure loss for a 15cm wick 1 with 8- and 15 layers respectively. The horizontal lines in the figures are the capillary limit for wick 1 and wick 2. From figures 3.1 and 3.2 it is seen that with 8 layers, one can achieve a maximum heat flux of about 125kW/m<sup>2</sup> for wick 2, while with 15 layers, a maximum heat flux 240kW/m<sup>2</sup> is possible. On the other hand, wick 1 only achieves a maximum heat flux of 70kW/m<sup>2</sup> and 130kW/m<sup>2</sup> with 8 and 15 layers respectively. It is evident that wick 2 is the best choice for a 15cm wick for the proposed system due to the significantly higher maximum heat flux (a factor of almost 2).

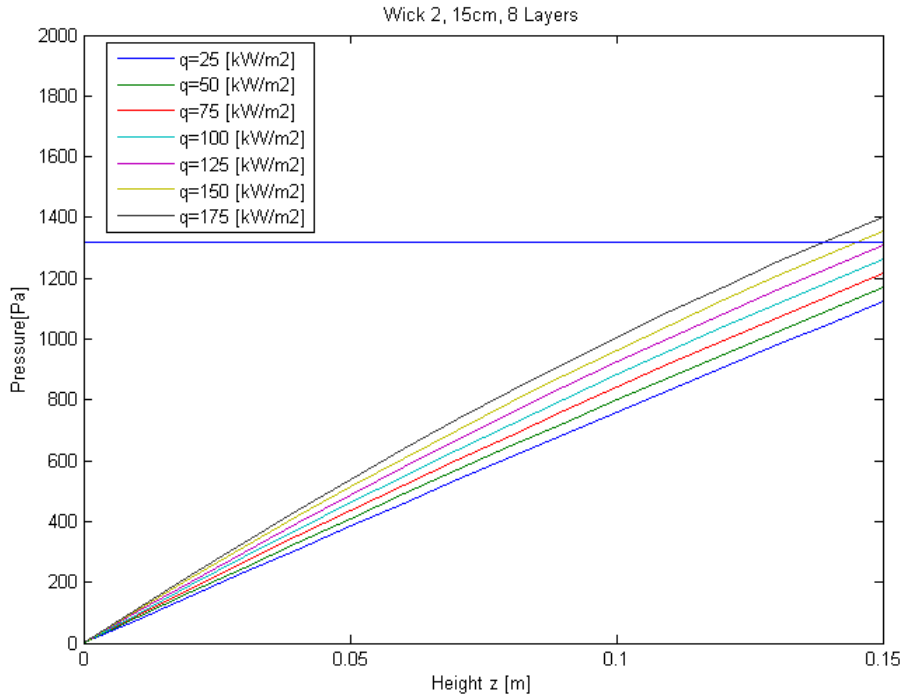


Figure 3.1: Pressure loss inside a 8 layer wick 2 as a function of  $z$ .

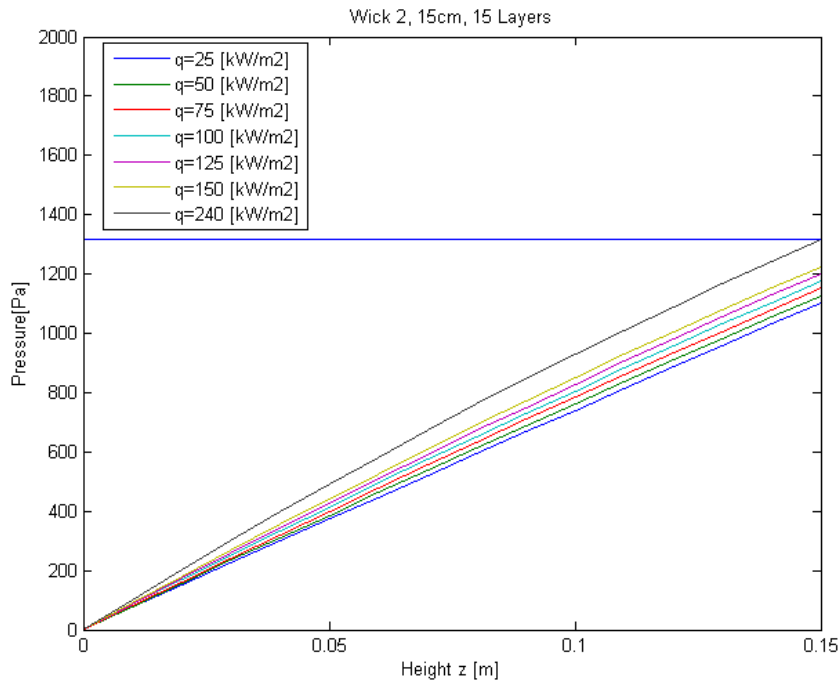


Figure 3.2: Pressure loss inside a 15 layer wick 2 as a function of  $z$ .

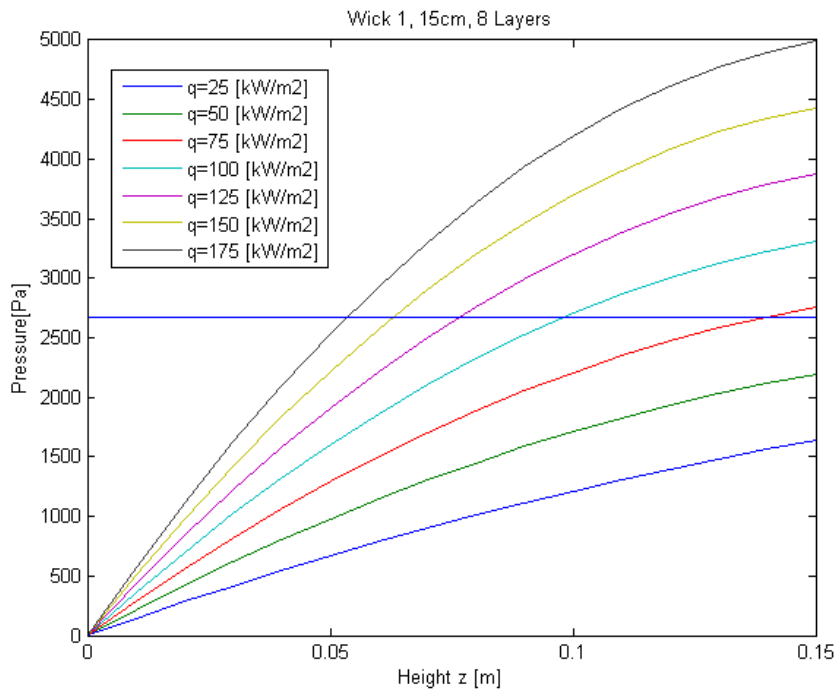
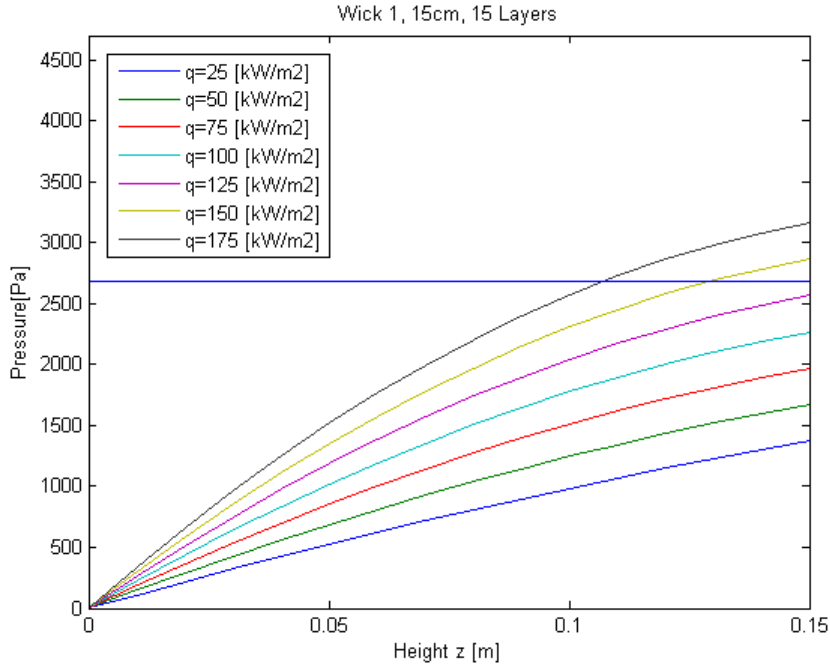


Figure 3.3: Pressure loss inside a 8 layer wick 1 as a function of  $z$ .



**Figure 3.4:** Pressure loss inside a 15 layer wick 1 as a function of  $z$ .

Further, it is desired to investigate how the two wick types performs when the length of the wick is increased. Wick lengths of 20cm, 25cm, and 30cm for wick 1 and wick 2 were tested to investigate the performance. Figures 3.5 and 3.6 show the pressure loss for a 20cm wick 2 with 8 and 15 layers. Again the horizontal line represents the capillary limit. As can be seen from figures 3.5 and 3.6, the capillary limit is reached for the entire range of heat fluxes for both 8 and 15 layers of a 20cm wick 2. The heat flux could be reduced to avoid the capillary limit, however, a heat flux of less than  $10\text{kW/m}^2$  would not be a realistic operating condition for the proposed system. Figures 3.7 and 3.8 shows the pressure loss for a 20cm wick1 with 8 and 15 layers. Opposed to wick 2, wick 1 does not encounter the capillary limit for all heat fluxes for a 20cm wick with 8 or 15 layers. With 8 layers wick 1 can sustain a heat flux of slightly above  $30\text{kW/m}^2$ , and almost  $60\text{kW/m}^2$  with 15 layers. Summarizing the above; when the length is increased to 20cm wick 1 performs considerably better than wick 2. This is in contrast to the case with a 15cm wick where wick 2 was the best choice. When the length is increased, Wick 2 can not be used because the capillary limit is encountered even for the lowest heat flux ( $10\text{kW/m}^2$ ).

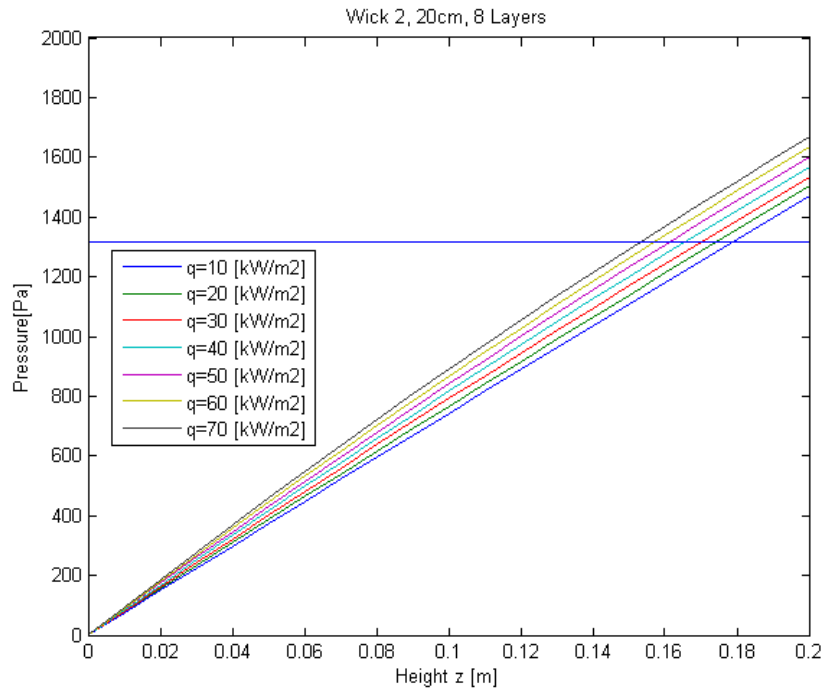


Figure 3.5: Pressure loss inside a 8 layer wick 2 as a function of  $z$ .

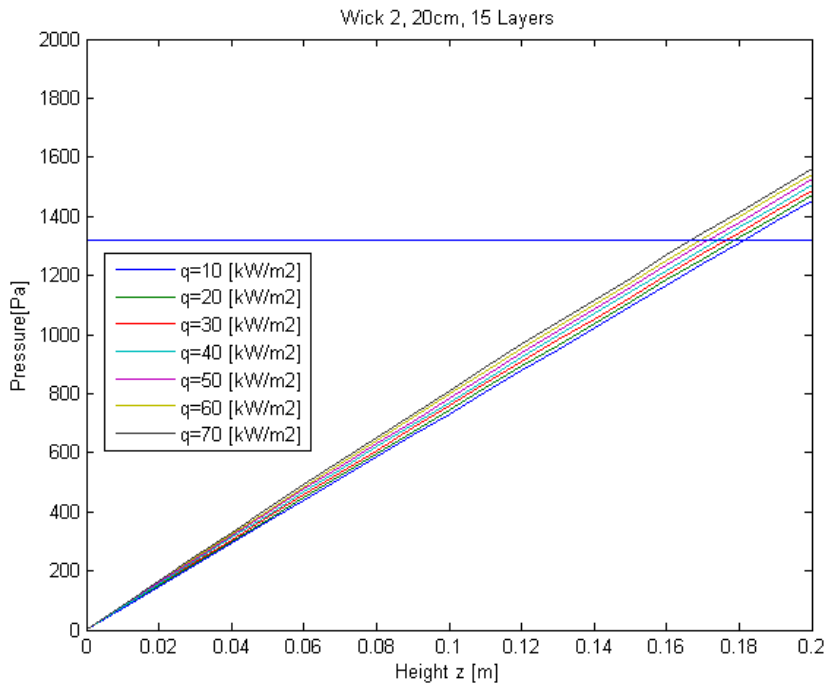


Figure 3.6: Pressure loss inside a 15 layer wick 2 as a function of  $z$ .

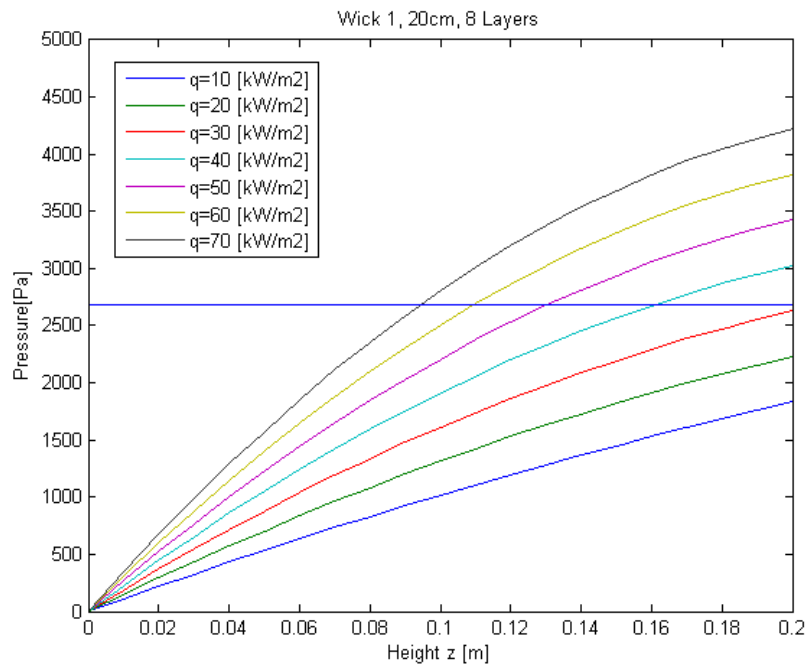


Figure 3.7: Pressure loss inside a 8 layer wick 1 as a function of  $z$ .

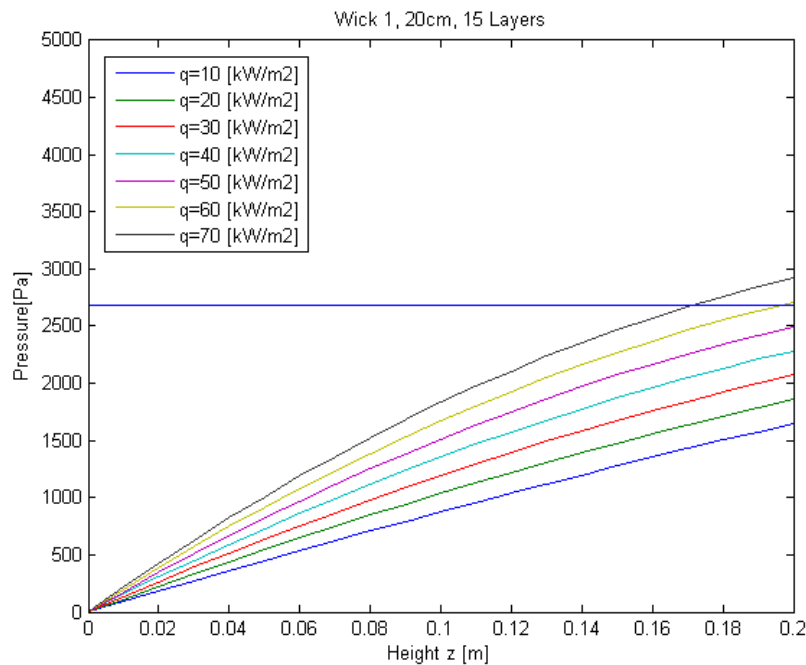
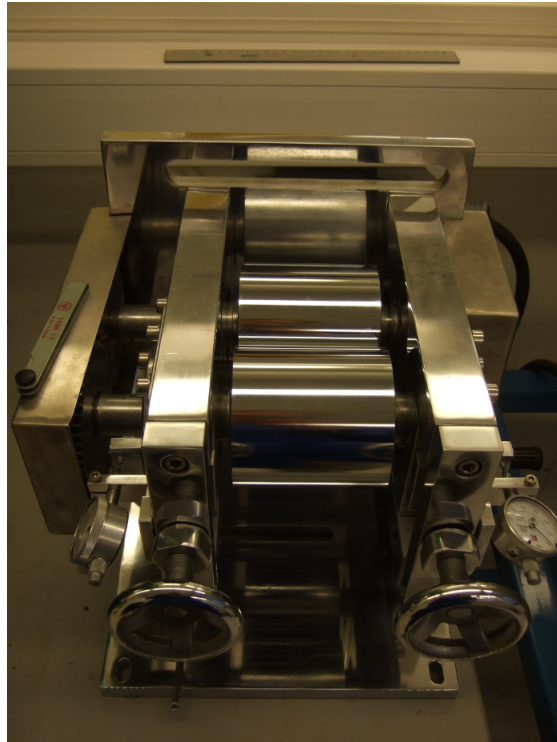


Figure 3.8: Pressure loss inside a 8 layer wick 1 as a function of  $z$ .

Figures 3.10-3.12 presents the pressure loss for a 25cm wick 1 with 8 and 15 layers, as well as a 30cm wick 1 with 15 layers. As expected the performance is reduced considerably when the length is further increased. With 8 layers and a length of 25cm the wick can operate at a maximum heat flux of about

14kW/m<sup>2</sup>, while with 15 layers the wick can tolerate a heat flux of nearly 30kW/m<sup>2</sup> before the capillary limit is encountered and the wick dries out. The maximum performance of a 30cm 15 layer wick 1 is only just above 10kW/m<sup>2</sup>, which is not enough for practical purposes. Since the performance of the longer wicks is very limited, there is a need for a solution to improve the performance in order to cool a larger surface. One way of doing this is to combine the two different wick types, having for instance a 15cm wick 2 at the bottom, and a 5cm wick 1 on top. The good thing about this kind of solution is that the production method is easy, and the extension between wick 2 and wick 1 will be smooth. In figure 3.9 a picture of the compression process is shown. The wanted parameters are set and then the wick is squeezed between the cylinders showed in figure 3.9. After the compression is complete, the layers are sintered together, and the wick is ready to be installed in the heat pipe.



**Figure 3.9:** Compression method for the wick.



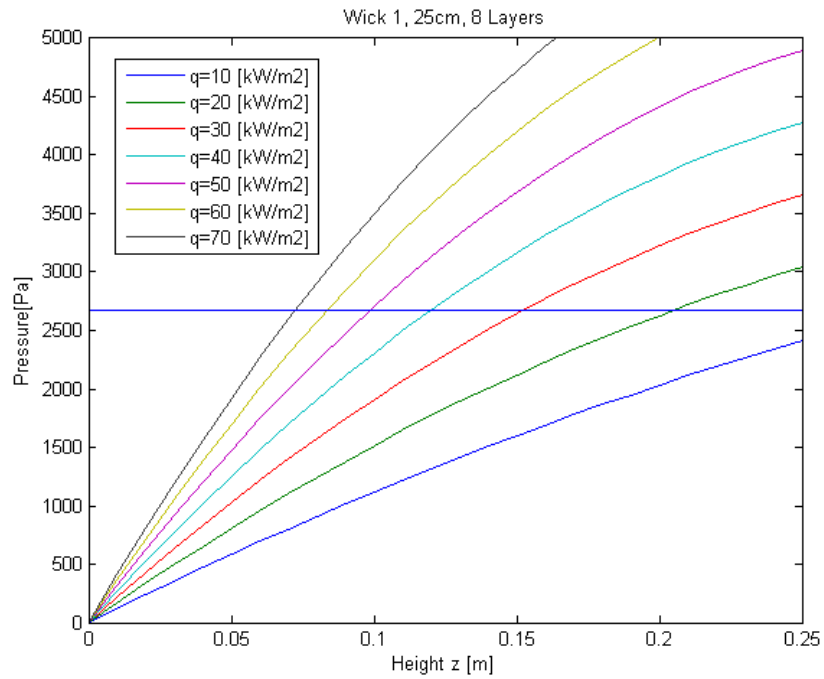


Figure 3.10: Pressure loss inside a 8 layer wick 1 as a function of  $z$ .

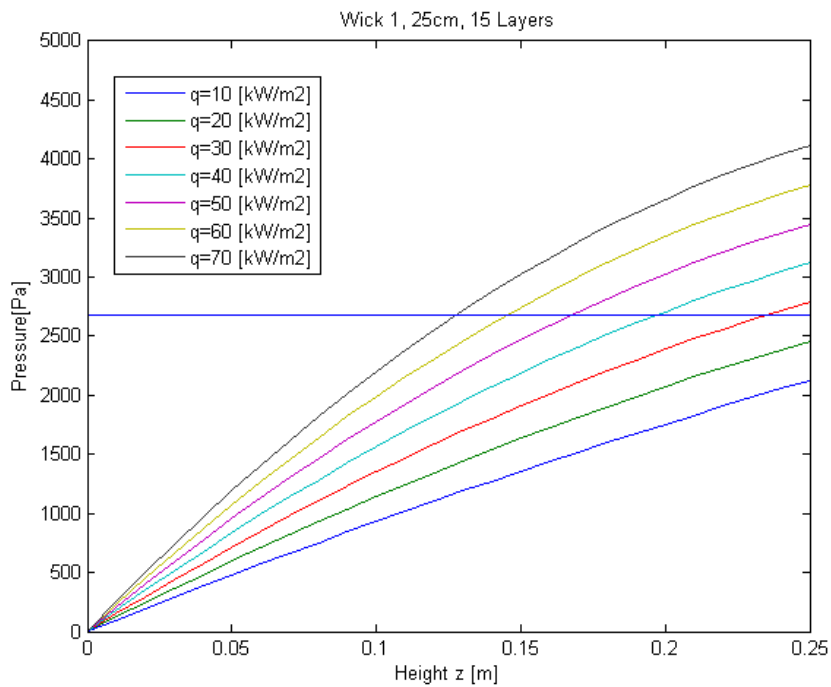


Figure 3.11: Pressure loss inside a 8 layer wick 1 as a function of  $z$ .

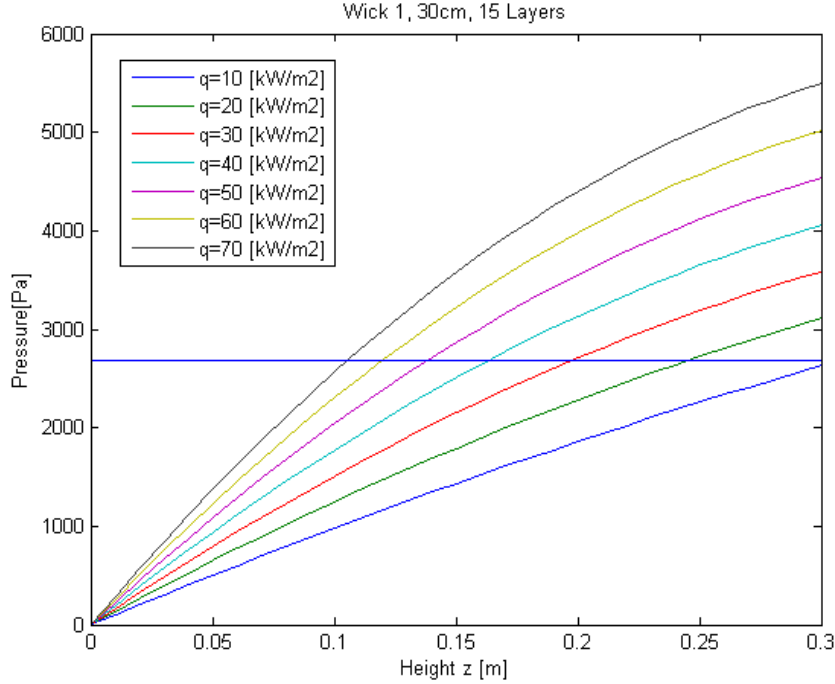


Figure 3.12: Pressure loss inside a 8 layer wick 1 as a function of  $z$ .

### 3.1.1 Combination of wicks

The incentive to combine two different types of wicks is to improve the performance (i.e. getting highest possible heat flux), or cool down a larger surface. An illustration of how a combined wick will look like is shown in the figure to the right. Since the two wick types (ref. table 1) have very different capillary limits, 1317Pa and 2677Pa for wick 2 and wick 1, respectively, there are two requirements that needs to be fulfilled. The first requirement is that for a given heat flux, the length of wick 2 can not be longer than a length which gives a maximum total pressure drop at the top of wick 2 of 1317Pa. Secondly, the total pressure drop in the combined wick can not exceed the maximum capillary pressure of wick 1 (2677Pa) which is the upper material. Because wick 2 has the lowest maximum allowable capillary pressure (1317Pa) and highest permeability (see table 1), it has to be placed in the lower region of the combined wick.

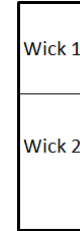


Figure 3.13: Combined wick.

As in the case with only one type of wick, equation (2.13), but without the reference pressure  $P_o$ , in addition to a gravitational pressure drop term is used. The resulting equation yields,

$$\Delta p_{drop} = \rho_l g z + \frac{\mu_l q A}{\rho_l A_c K h_{fg}} \left[ z - \frac{z^2}{2h} \right]. \quad (3.4)$$

First the extension point has to be figured out, and the most logical thing to do would be to utilize wick 2 as much as possible, i.e. set the capillary limit for wick 2 (1317Pa) as the upper boundary for calculating the height of wick 2. The reason for utilizing the maximum length of wick 2, is because wick 2 has a less steep pressure loss curve in the region of interest (see figure 3.1 and 3.3 as a comparison). For calculating the extension point, a total wick length and heat flux were set, and then equation (3.5) together with the goal seek (iteration) function in Microsoft Excel 2010 was used to find the height  $z$  where the pressure drop was 1317Pa, and this would then be the extension point.

$$0 = \rho_l g z + \frac{\mu_l q A}{\rho_l A_c K h_{fg}} \left[ z - \frac{z^2}{2h} \right] - 1317 \quad (3.5)$$

After the extension point has been determined, the total pressure drop is calculated and checked up against the maximum allowable capillary pressure for wick 1 which is seated at the upper part of the combined wick.

In table 7-10 the results of calculations with a combined wick for different lengths and number of layers are presented. More calculations for different lengths and layers can be found in appendix B. From table 7 it is evident that the combined wick performs much better than wick 1 and wick 2 separately. Where wick 2 could sustain a heat flux of 130kW/m<sup>2</sup>, and wick 1 70kW/m<sup>2</sup>, the combined wick can actually sustain heat fluxes up to around 370kW/m<sup>2</sup>. This is a significant improvement, and because of the easy production process of the combined wick, it would be a very good solution if high heat fluxes are desired. The numbers in bold in tables 7-10 are highlighted to show that at these heat fluxes the capillary limit is encountered.

**Table 7: Performance of a 15cm 8 layer combined wick**

Heat Flux (kW/m <sup>2</sup> )	Wick2 length (cm)	Total pressure drop (Pa)
150	14.5	1359
200	13.2	1507
250	12.1	1732
300	11.1	2049
350	10.2	2459
400	9.4	<b>2960</b>

When the wick length was increased to 20cm, 25cm, and 30cm for wick 1 and wick 2, it was shown that the performance dropped a lot, and with a 30cm 15 layer wick 1 the maximum heat flux had dropped to slightly above 10kW/m<sup>2</sup>. Studying the tables below, it is clear that with a combined wick the performance will increase considerably even when the length is increased. Table 26 shows that the performance has improved by almost a factor of four compared with the 30cm 15layer wick 1. Where wick 1 only achieved a maximum heat flux of slightly above 10kW/m<sup>2</sup>, the combined wick can sustain a heat flux of 40kW/m<sup>2</sup>.

**Table 8: Performance of a 20cm 8 layer combined wick**

Heat Flux (kW/m <sup>2</sup> )	Wick2 length (cm)	Total pressure drop (Pa)
10	17.9	1474
50	16.1	1671
100	14.1	2094
120	13.4	2307
140	12.8	2559
150	12.4	<b>2720</b>

**Table 9: Performance of a 25cm 8 layer combined wick**

Heat Flux (kW/m <sup>2</sup> )	Wick2 length (cm)	Total pressure drop (Pa)
20	17	2016
40	15.9	2304
60	14.8	2671
70	14.3	<b>2877</b>

**Table 10: Performance of a 30cm 8 layer combined wick**

Heat Flux (kW/m <sup>2</sup> )	Wick2 length (cm)	Total pressure drop (Pa)
10	17.5	2372
20	16.7	2626
30	15.9	<b>2923</b>

It is evident that by utilizing the properties of both wick 1 and 2, one can achieve a significantly better performance by using a combined wick compared with using separate wicks.

### 3.1.2 Different operating conditions

The proposed experimental system allows for an uneven heat flux distribution when operating the heat pipe. The evaporator has three regions, each 5cm, and one can choose to have a higher heat flux at the bottom section, and then a lower heat flux at the two upper regions for instance. In figures 3.14-3.16 HLL, LHL and LLH represents the heat distribution in the three 5cm regions in the evaporator, where H=high and L=low. HLL will then represent high low low, where there is a higher heat flux in the bottom region and a lower heat flux in the two upper regions. Figure 3.14 illustrates how the liquid mass flow varies in the wick for the two cases of HLL and LLH heat flux distribution, and in the calculations it has been taken into account that the liquid mass flow changes with the operating conditions.

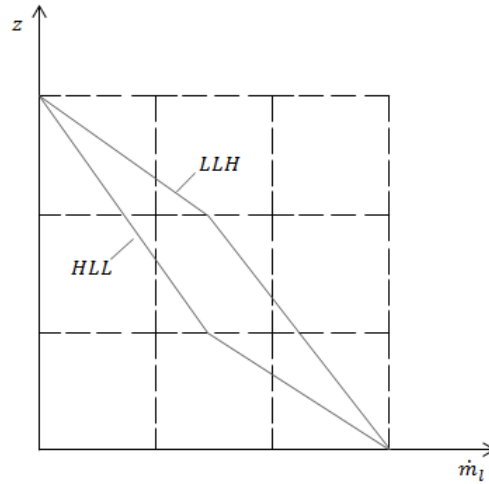


**Figure 3.14: Liquid mass flow with different operating conditions.**

Three different flux distribution cases are simulated in the figures 3.15 and 3.16. One with a high flux at the bottom 5cm and low flux at the top, one with high flux in the middle 5cm and low flux at the bottom and top, and lastly one case with low flux at the bottom 10cm and high flux at the top 5cm. In figure 3.15 an even heat flux distribution of  $70\text{kW/m}^2$ , a high heat flux of  $150\text{kW/m}^2$  and a low heat flux of  $30\text{kW/m}^2$  are used. The vertical axis in figures 3.15 and 3.16 shows the pressure drop divided by a reference pressure drop. The reference pressure drop has been set to the pressure drop corresponding to the even heat flux distribution. From figure 3.15 it is clear that it is more favorable to have a high heat flux at the bottom of the evaporator, and then a low heat flux at the top. The HLL distribution gives 22.6% less pressure drop compared with the even heat flux distribution. In contrast the LLH distribution gives 22.6% higher pressure drop compared with the even heat flux distribution. The LHL arrangement will give the same total pressure drop as the even heat flux distribution. For wick 2 the same results are seen, only that the percentage gain/loss is less than for wick 1. Where wick 1 yielded a 22.6% loss/gain for the LLH and HLL distribution, wick 2 yields a 4.9% loss/gain for the LLH and HLL distribution. The results are consistent with the physical aspect of the system. When the HLL distribution is used, more mass is evaporated in the lower region, thus resulting in less mass being transported to the upper region. This will lead to less pressure drop since less mass has to be transported over the entire length of the evaporator. For the LLH distribution the opposite is the case, less mass is evaporated at the lower region, resulting in more mass being transported over the entire length of the evaporator, and thus leading to a higher total pressure drop compared with the even heat flux distribution.

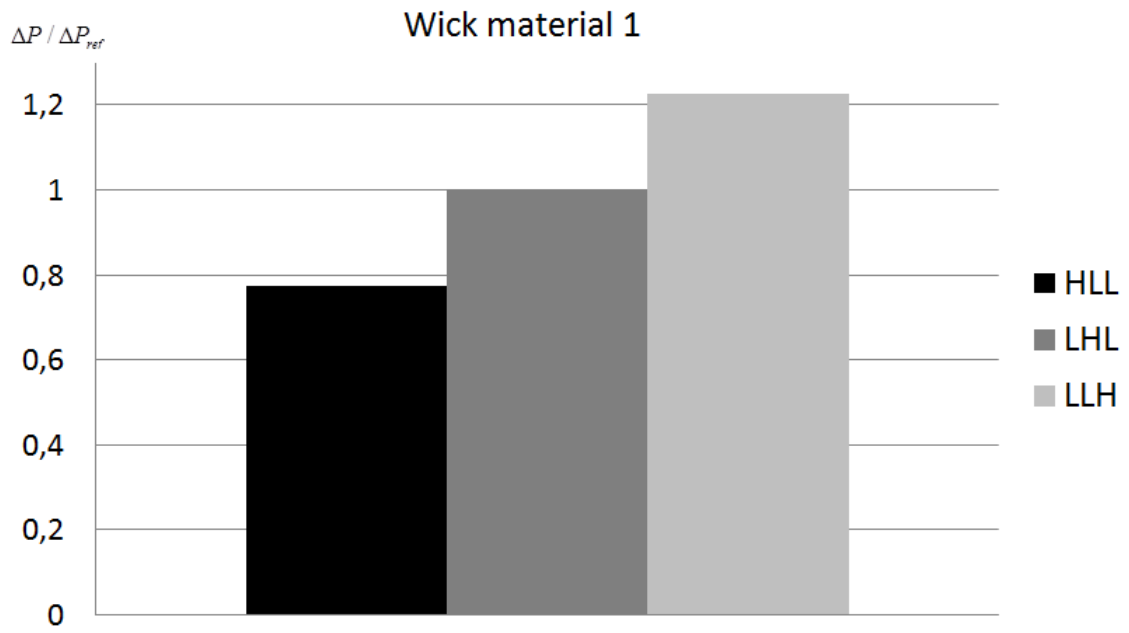


Figure 3.15: Uneven heat flux distribution with wick 1

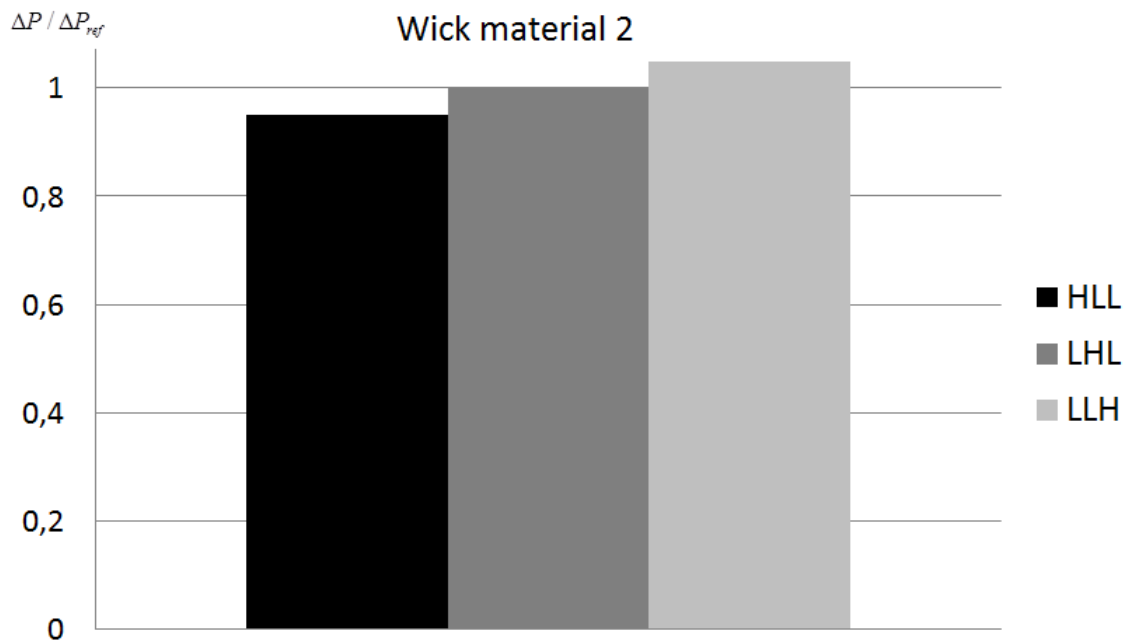


Figure 3.16: Uneven heat flux distribution with wick 2

### 3.2 Chapters conclusions

The performance limitations of two wick types for different lengths, combination of wick types and uneven heat flux distribution have been presented. Wick 2 is found to be the best choice for the proposed system. Wick 2 can sustain heat fluxes up to  $125\text{kW/m}^2$  for the proposed system, while wick 1's performance stops at  $70\text{kW/m}^2$ . The performance is proportional to the number of layers, and more layers can be sintered together in order to increase the performance. However, when the length of the wick is extended, the picture is very different. Wick 2 encounters the capillary limit before the top of the evaporator is reached with a 20cm 15 layer wick for all heat fluxes, but wick 1 is able to withstand heat fluxes up to almost  $60\text{kW/m}^2$  with 15 layers. If the length is further increased to 30cm neither wick 1 or wick 2 is suitable for usage.

However, by combining the two wick types a larger surface (e.g. wick length of 30cm) can be cooled. There is a significant (factor of almost 4) improvement of the performance when the wicks are combined, and the production method is also very easy. Combination of wick types is highly recommended due to the good performance and easiness of production.

If the operating conditions are changing, leading to uneven heat flux distribution, it is important to know how the performance of the wick changes. A higher heat flux at the bottom section, leading to more liquid mass being evaporated at the lower region leads to less pressure drop. In contrast, a low heat flux at the bottom region, and a higher heat flux at the top, leads to a higher total pressure drop, thus lowering the performance of the wick.

## 4 Energy balance of test rig

The proposed heat pipe is cooled using a nitrogen cooling circuit. Figure 4.1 shows the process and instrumentation diagram (P&ID) for the cooling circuit. Inside the safety chamber is where the heat pipe will be located during tests, but for the experiments and simulations that will be presented in this master thesis there will be a bypass tube instead of actual the heat pipe. This is because the construction and testing of wick material for the heat pipe has not yet been completed. The circulation of nitrogen in the cooling circuit is produced by a side channel blower, and the tracing will provide the necessary heating in order to control the temperature at the inlet of the bypass tube. After the bypass tube the hot nitrogen flow is cooled with tap water in a counterflow plate heat exchanger, before it again enters the side channel blower. The purpose of the experiments is to study the dynamics and response time of the cooling circuit, in addition to making a total energy balance for the test rig where heat loss from the components is accounted for.

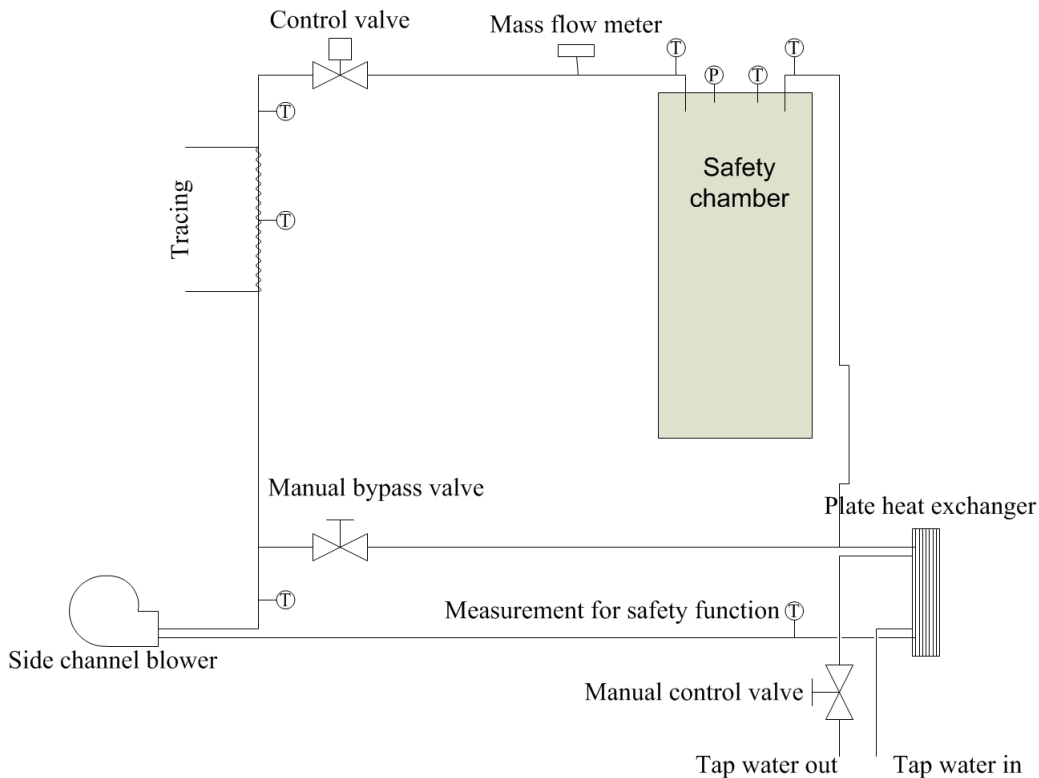


**Figure 4.1: Process and instrumentation diagram for the test rig**

### 4.1 Heat transfer theory

Since a total energy balance is to be performed of the cooling circuit there are several different heat transfer phenomena that are encountered in the process. Conduction, forced convection and free convection will all be investigated in order to account for heat losses in the different components and tubing. The



contribution from radiation heat transfer has been neglected due to the low temperatures ( $<100^\circ\text{C}$ ) associated with the experiments. All heat transfer theory in the following subsections are based on the book by Incropera et al. [4] unless other sources are cited.

#### 4.1.1 Conduction

The heat equation shown in Cartesian and cylindrical coordinates below is the basic tool for conduction heat transfer analysis.

$$\frac{\partial}{\partial x} \left( k \frac{\partial T}{\partial x} \right) + \frac{\partial}{\partial y} \left( k \frac{\partial T}{\partial y} \right) + \frac{\partial}{\partial z} \left( k \frac{\partial T}{\partial z} \right) + \dot{q} = \rho c_p \frac{\partial T}{\partial t}, \quad (4.1)$$

$$\frac{1}{r} \frac{\partial}{\partial r} \left( kr \frac{\partial T}{\partial r} \right) + \frac{1}{r^2} \frac{\partial}{\partial \phi} \left( k \frac{\partial T}{\partial \phi} \right) + \frac{\partial}{\partial z} \left( k \frac{\partial T}{\partial z} \right) + \dot{q} = \rho c_p \frac{\partial T}{\partial t}. \quad (4.2)$$

For the conduction heat transfer in the tubing, steady-state conduction with no heat generation will be assumed. Equation (4.2) then reduces to,

$$\frac{1}{r} \frac{\partial}{\partial r} \left( kr \frac{\partial T}{\partial r} \right) = 0. \quad (4.3)$$

Integrating equation (4.3) twice, and applying the appropriate boundary conditions (i.e. inner or outer) the resulting temperature distribution yields,

$$T(r) = \frac{T_i - T_o}{\ln(r_i/r_o)} \ln \left( \frac{r}{r_o} \right) + T_o, \quad (4.4)$$

where the subscripts i and o refers to the inner and outer radius of the tube. Combining the above equation together with Fourier's law the resulting equation for the heat transfer rate yields,

$$q_r = \frac{2\pi Lk(T_i - T_o)}{\ln(r_o/r_i)}. \quad (4.5)$$

#### 4.1.2 Convection

For internal tube flow the mean fluid temperature, or bulk temperature is a convenient reference temperature to use when calculating the convective heat transfer. Newton's law of cooling using the mean temperature yields,

$$q_s'' = h(T_s - T_m), \quad (4.6)$$

where h is the local convection heat transfer coefficient, and the subscripts s and m refers to the surface and mean temperature respectively. For a tube of finite length the convective heat transfer rate can be written as,

$$q_{conv} = \dot{m}c_p(T_{m,o} - T_{m,i}). \quad (4.7)$$

It should be noted that the equation above is derived based on a few assumptions; viscous dissipation is negligible, the fluid is incompressible or an

ideal gas with negligible pressure variation, and axial conduction is neglected. This equation applies irrespectively of the nature of the surface or tube flow conditions because it is a general expression. Equation (4.7) applied to the control volume in figure 4.2 yields,

$$dq_{conv} = \dot{m}c_p[(T_m + dT_m) - T_m] \Rightarrow dq_{conv} = \dot{m}c_p dT_m. \quad (4.8)$$

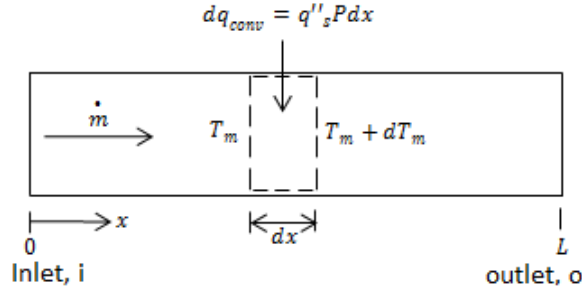


**Figure 4.2: Control volume for internal flow in a tube based on figure from [4].**

Using the perimeter  $P$ , which for a circular tube is  $\pi D$ , the rate of convection heat transfer can be expressed as  $dq_{conv} = q''_s P dx$ . Combined with equation (4.6) it follows that

$$\frac{dT_m}{dx} = \frac{q''_s P}{\dot{m}c_p} = \frac{P}{\dot{m}c_p} h(T_s - T_m). \quad (4.9)$$

Solving equation (4.9) for the temperature  $T(x)$  requires knowledge about the boundary conditions. The two cases which are of interest are the cases with constant heat flux and constant surface temperature.

### Constant heat flux

The heat flux  $q''_s$  is independent of  $x$ , so that the total heat transfer rate yields,

$$q_{conv} = q''_s (P \cdot L), \quad (4.10)$$

and the above equation can be used together with equation (4.7) to determine the temperature change,  $(T_{m,o} - T_{m,i})$ . Moreover, by integrating equation (4.9) from 0 to  $x$ , and remembering that  $q''_s$  is independent of  $x$ , it follows that,

$$T_m(x) = T_{m,i} + \frac{q''_s P}{\dot{m}c_p} x. \quad (4.11)$$

It can be seen from the above equation that the mean temperature varies linearly with  $x$  along the tube.

### Constant surface temperature

Opposed to the case with constant heat flux, a constant surface temperature

leads to a very different result when equation (4.9) is solved for temperature. Defining  $\Delta T = T_s - T_m$ , equation (4.9) can be expressed as

$$\frac{dT_m}{dx} = -\frac{d(\Delta T)}{dx} = \frac{P}{\dot{m}c_p}h\Delta T \quad (4.12)$$

Separating variables and integrating from the tube inlet to some distance  $x$  it follows that,

$$\ln \frac{\Delta T_x}{\Delta T_i} = -\frac{Px}{\dot{m}c_p} \left( \frac{1}{x} \int_0^x h dx \right). \quad (4.13)$$

Rearranging the above expression, and using the definition of the average heat transfer coefficient  $\bar{h} = \frac{1}{x} \int_0^x h dx$ , the resulting equation yields,

$$\frac{T_s - T_m(x)}{T_s - T_{m,i}} = \exp \left( -\frac{Px}{\dot{m}c_p} \bar{h} \right). \quad (4.14)$$

As can be seen from the above equation is that the temperature difference ( $T_s - T_m$ ) decays exponentially with  $x$  along the tube. This is in contrast to the case with constant heat flux where the temperature varied linearly. The expression for the total heat transfer rate  $q_{conv}$  requires a little manipulation, but the resulting equation yields

$$q_{conv} = \bar{h}A_s\Delta T_{lm}, \quad \Delta T_{lm} \equiv \frac{\Delta T_o - \Delta T_i}{\ln(\Delta T_o/\Delta T_i)} \quad (4.15)$$

Equation (4.15) is a form of Newton's law of cooling for the entire tube, and  $\Delta T_{lm}$  is the log mean temperature difference over the tube. Figure 4.3 shows the temperature variation for the two cases.

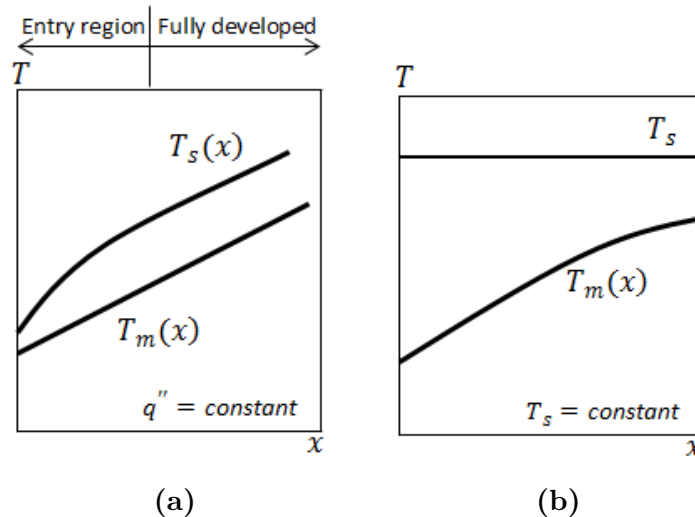


**Figure 4.3: Temperature variation for internal pipe flow. (a) Constant heat flux. (b) Constant surface temperature. Based on figure from [4].**

### Flow conditions

The internal flow conditions in circular tubes are important for calculating

the heat transfer coefficient. Depending on the mass flow, laminar, transition or turbulent flow conditions can arise, which in turn decide the Nusselt correlation. Below the range of Reynolds numbers and appropriate flow classification are given,

$$\begin{cases} \text{Laminar} & \text{for } Re_D \leq 2300; \\ \text{Transition} & \text{for } 2300 \leq Re_D \leq 10000; \\ \text{Fully Turbulent} & \text{for } Re_D \geq 10000. \end{cases}$$

For fully developed laminar flow, the Nusselt number is a constant, but differs depending on the boundary conditions,

$$Nu_D \equiv \frac{hD}{k} = 4.36 \quad q_s'' = \text{constant} \quad (4.16)$$

$$Nu_D \equiv \frac{hD}{k} = 3.66 \quad T_s = \text{constant} \quad (4.17)$$

For turbulent flow the following correlation has been confirmed experimentally for  $0.6 \leq Pr \leq 160$ ,  $L/D \geq 10$ ,  $Re_D \geq 10000$  [4],

$$Nu_D = 0.023 Re_D^{4/5} Pr^n, \quad n=0.4 \text{ for } T_s > T_m, \quad n=0.3 \text{ for } T_s < T_m \quad (4.18)$$

For the transition region a correlation by Gnielinski [4] is valid,

$$Nu_D = \frac{(f/8)(Re_D - 1000)Pr}{1 + 12.7(f/8)^{1/2}(Pr^{2/3} - 1)}, \quad (4.19)$$

where  $f$  is the friction factor. A correlation by Petukhov [4] for smooth pipes can be used to find the friction factor,

$$f = (0.79 \ln Re_D - 1.64)^{-2}, \quad 300 \leq Re_D \leq 5 \cdot 10^6. \quad (4.20)$$

### Entry length

Like determination of the flow conditions (e.g. laminar or turbulent flow), the effect of the hydrodynamic and thermal entry length is important. In the hydrodynamic entrance region, the boundary layer is developing and the velocity profile is a function of  $r$  and  $x$ . After a finite length, the boundary layer merges at the centerline, and the flow can be said to be fully developed, meaning that the velocity profile is only a function of  $r$ . The thermal boundary layer develops in the same manner as the hydrodynamic boundary layer, and when the thermal boundary layer merges at the centerline a thermally fully developed condition is reached. The Prandtl number,  $Pr = \frac{\nu}{\alpha}$ , is the ratio of momentum diffusivity to thermal diffusivity. Moreover, a Prandtl number larger than 1 means that the hydrodynamic boundary layer develops faster than the thermal boundary layer, and vice versa if the Prandtl number is less than 1. The laminar hydrodynamic entry length can be obtained from the following expression,

$$\left(\frac{x_{fd,h}}{D}\right)_{lam} \approx 0.05Re_D, \quad (4.21)$$

while the turbulent hydrodynamic entry length may be found from,

$$10 \leq \left(\frac{x_{fd,h}}{D}\right)_{turb} \leq 60. \quad (4.22)$$

The thermal entry length may be obtained from similar expressions. The laminar thermal entry length expression yields,

$$\left(\frac{x_{fd,t}}{D}\right)_{lam} \approx 0.05Re_DPr, \quad (4.23)$$

and the turbulent thermal entry length can be approximated by  $x_{fd,t} = 10D$ . For the laminar entry region a correlation due to Sieder and Tate[4] is suitable,

$$\overline{Nu}_D = 1.86 \left(\frac{Re_DPr}{L/D}\right)^{1/3} \left(\frac{\mu}{\mu_s}\right)^{0.14}. \quad (4.24)$$

### 4.1.3 Free Convection

The fluid motion in free convection is due to buoyancy forces within the fluid, unlike forced convection where the the motion is externally subjected. "*Buoyancy is due to the combined presence of a fluid density gradient and a body force that is proportional to density*" [4]. The geometry, or system of interest is quiescent air (the surroundings) and the circular tubing of the cooling circuit. There are different empirical correlations depending on the geometry and/or angle of the tube. For the long horizontal cylinder, Churchill and Chu [28] recommended the following correlation for a wide range of Rayleigh numbers,

$$\overline{Nu}_D = \left[0.6 + \frac{0.387Ra_D^{1/6}}{[1 + (0.559/Pr)^{9/16}]^{8/27}}\right]^2, \quad Ra_D \leq 10^{12} \quad (4.25)$$

The Rayleigh number ( $Ra_D$ ) is defined as

$$Ra_D = \frac{g\beta(T_s - T_\infty)D^3}{\nu\alpha}, \quad (4.26)$$

where  $\beta$  is the volumetric expansion coefficient,  $\beta = -\frac{1}{\rho} \left(\frac{\partial \rho}{\partial T}\right)_p$ . For an ideal gas,  $\beta = \frac{1}{T}$ . This correlation is also valid for vertical cylinders if the criterion below is satisfied [27]

$$D \geq \frac{35L}{Gr_L^{1/4}}, \quad Gr_L \frac{g\beta(T_s - T_\infty)L^3}{\nu^2}, \quad (4.27)$$

where  $Gr_L$  is the Grashof number.

#### 4.1.4 Heat exchanger

The steady flow energy equation with negligible heat transfer between the heat exchanger and the surroundings, in addition to negligible kinetic and potential energy changes yields,

$$q = \dot{m}_h(h_{h,i} - h_{h,o}), \quad q = \dot{m}_c(h_{c,o} - h_{c,i}), \quad (4.28)$$

where  $h$  is the enthalpy, and the subscripts  $h$  and  $c$  refers to the hot and cold fluid, respectively. With no phase change and constant specific heats, equation (4.28) may be written as

$$q = \dot{m}_h c_p (T_{h,i} - T_{h,o}), \quad q = \dot{m}_c c_p (T_{c,o} - T_{c,i}). \quad (4.29)$$

In the figure below the temperature distribution for a counterflow heat exchanger is shown. The temperature difference notation in figure 4.4 is

$$\Delta T_1 \equiv T_{h,1} - T_{c,1} = T_{h,i} - T_{c,o}, \quad \Delta T_2 \equiv T_{h,2} - T_{c,2} = T_{h,o} - T_{c,i}. \quad (4.30)$$

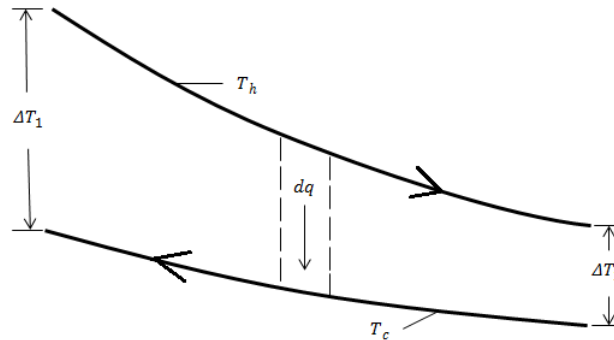


**Figure 4.4: Temperature distribution in a counterflow heat exchanger based on figure from [4].**

#### 4.1.5 Side channel blower

Assuming that the specific heats  $c_v$  and  $c_p$  are constant, the entropy change of an ideal gas can be written as [31],

$$s(T_2, p_2) - s(T_1, p_1) = c_p \ln \frac{T_2}{T_1} - R \ln \frac{p_2}{p_1}. \quad (4.31)$$

For an ideal gas the following relations can be useful,

$$c_p = \frac{\gamma R}{\gamma - 1}, \quad c_v = \frac{R}{\gamma - 1}, \quad \gamma = \frac{c_p}{c_v} \quad (4.32)$$

Combining equation (4.31) with the ideal gas relations above, the resulting equation yields,

$$\frac{T_2}{T_1} = \left( \frac{p_2}{p_1} \right)^{(\gamma-1)/\gamma} \quad (4.33)$$

Equation (4.33) can be used together with the data sheet (see appendix C) to estimate the temperature rise over the side channel blower.

## 4.2 Geometry and dimensions

In the figures below the dimensions and geometry of the insulated tubes with and without tracing are shown, as well as the dimensions of the bypass tube. The yellow color in figure 4.5 illustrates that this part of the bypass tube is made of brass, while the rest of the bypass tube is made of stainless steel. The inner tubes of figure 4.6-4.7 are also made of stainless steel. It should be noted that the diameters shown in figure 4.5 are the inner diameters, and that the wall thickness is 2mm. The geometry and dimensions shown in figure 4.6 are the same for the vertical tube shown in figure 4.7, except for the tracing which is 4mm thick. The gray shaded areas in figures 4.6 and 4.7 illustrates the Rockwool which is used for insulation around the tubes.

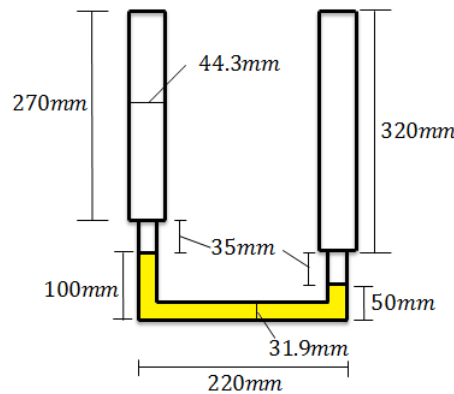


Figure 4.5: Bypass tube dimensions.

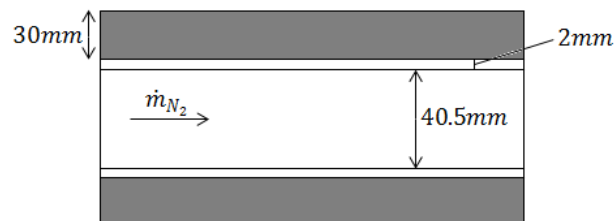
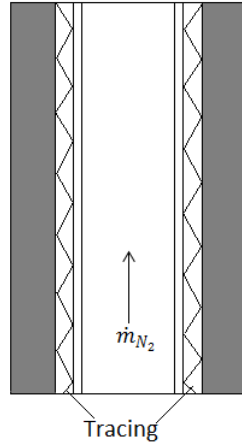


Figure 4.6: Horizontal insulated tube main dimensions.



**Figure 4.7: Vertical insulated tube.**

Figure 4.8 shows the resistance network from the inside of the horizontal tube to the surrounding room temperature.  $T_{m,i}$  is the mean gas temperature of nitrogen at the inlet of the tube section,  $h_i$  and  $h_y$  are the convection coefficients for forced and free convection heat transfer, respectively, while  $k_{steel}$  and  $k_{RW}$  are the thermal conductivity of stainless steel and Rockwool, respectively.



**Figure 4.8: Resistance network for the heat transfer from the inside of the tube to the surroundings.**

The total resistance per unit length of tube based on the resistance network of figure 4.8 yields,

$$R'_{tot} = \frac{1}{2\pi r_i h_i} + \frac{\ln(r_2/r_i)}{2\pi k_{steel}} + \frac{\ln(r_y/r_2)}{2\pi k_{RW}} + \frac{1}{2\pi r_y h_y}, \quad (4.34)$$

where  $r_i$  is the inner stainless steel radius,  $r_2$  is the outer stainless steel radius and  $r_y$  is the outer Rockwool radius. For the vertical pipe the wall temperature of the tracing is known, so the heat loss for the vertical pipe will only consist of the last two resistances,  $k_{RW}$  and  $h_y$ . Since the outer Rockwool surface temperature is unknown, an initial guess has to be made, the total resistance calculated, and then iterate using an energy balance at the insulated surface yielding,

$$\frac{k_{RW}(T_w - T_s)}{\ln(R_y/R_i)} = h_y(T_s - T_{air}). \quad (4.35)$$



### 4.3 Controller - Tracing

The tracing, or temperature controller can be tuned to give an accurate fixed temperature. It can be used either as a P controller, PI controller or PID controller depending on the users desire. All control theory in the following sections is based on the book by Finn Haugen [29], expect for the tuning section which is based by another book by Finn Haugen [30].

#### **P controller**

The P controller is the simplest, and it calculates the control output  $u$  by multiplying the deviation  $e$  by a proportional gain constant  $K_p$ . The deviation is the set point (desired temperature) minus the actual temperature. The P controller is not able to remove the deviation completely, so there will always be a stationary deviation if a P controller is used.

#### **PI controller**

By introducing the integral term I, the stationary error present with the P controller can be eliminated or reduced significantly. The effect of the integral term is to increase the control output based on the accumulated error over time, and correct for this.

#### **PID controller**

The derivative term D is very different from the integral term. It gives an extra addition/reduction in the control output when the deviation changes. The derivative term gives an addition when the error is increased, which can give less transient control deviation, and it gives a reduction in the control output when the error is decreased, which can give a more damped settling of the output signal.

#### **Stability**

The stability of the system depends on all three parameters mentioned above, proportional gain, integral time and the derivative time. To achieve good stability these parameters have to be tuned differently depending on the kind of system the controller is regulating. In figure 4.9 three stability properties are shown.

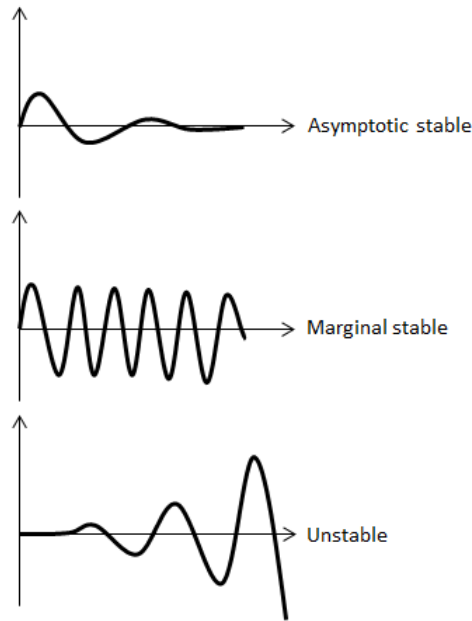


**Figure 4.9: Stability properties for a system.**

The horizontal line in the graphs could represent a set point or reference value for the system. The asymptotic stable system is the kind of system which is desired for the temperature controlled system in the cooling circuit. If a temperature of 50°C is set at the inlet of the heat pipe, it is important to get this temperature to control the cooling of the heat pipe, and not a sinusoidal oscillating system (marginally stable system). An unstable system illustrated by the bottom graph in figure 4.9 is not accepted when the experiments are running. It is therefore necessary to tune the PID controller in order to get a satisfactory stable system.

### Manual tuning - Good Gain method

The aim of controller tuning is to achieve good stability and fast response. In a PID controller these two wishes cannot be achieved simultaneously in most cases. So for practical purposes it is enough to have acceptable stability, meaning good stability, but not extremely good because this would give very slow response. One way to define acceptable stability is, "*Acceptable stability is when the undershoot that follows the first overshoot of the response is small, or barely observable*" [30]. A simple method for achieving acceptable stability is the Good Gain method. It has proven to give good results on laboratory processes, and the procedure is as follows,

- \* Bring the process to the normal specified operating point with the controller in manual mode.
- \* Make sure that the controller is a P controller with  $K_p = 0$  (set the integral time  $T_i = \infty$  and derivative time  $T_d = 0$ ). Increase  $K_p$  until the control loop gets satisfactory stability as seen in the response in the measurement signal after e.g. a step in the setpoint. One could

also try to start with  $K_p = 1$  instead of zero. The value of  $K_p$  is then increased/decreased until some overshoot and barely an undershoot is seen. This kind of response is assumed to represent good stability of the control system.

- \* Set the integral time  $T_i$  equal to  $T_i = 1.5T_{ou}$ , where  $T_{ou}$  is the time between the overshoot and the undershoot of the step response with the P controller (see figure 4.10). The offset from the set point in figure 4.10 is because the controller at this point only is a P controller.
- \* The introduction of the integral term could compromise the stability of the system compared with the P controller, and to compensate for this  $K_p$  could be reduced to  $0.8K_p$ .
- \* The derivative term D could be included by setting  $T_d = \frac{T_i}{4}$ .
- \* One should check the stability of the system after the parameters have been tuned by applying a step change of the setpoint. If the stability is poor, the controller gain could be reduced, possibly in combination with increasing the integral time.

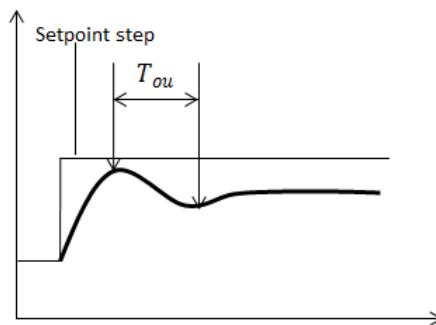


Figure 4.10: Good gain method.

## 4.4 Instrumentation

The flow of nitrogen is induced by a side channel blower type SAH 55. It can deliver 750W at maximum rpm (revolutions per minute). The nitrogen gas is heated using a temperature regulated heating tape series MIL-HT-CN. It consists of a copper-nickel wire that can withstand temperatures up to 250°C. In addition to being able to control the mass flow of nitrogen using the side channel blower, a pneumatic control valve type 3241 together with an electric actuator type 3374, both from Samson, lets the operator control the percentage of opening in the valve. The mass flow is measured using a Sierra series 620S fast-flow insertion mass flow meter. The hot nitrogen gas is cooled in an Alfa Laval fusion-brazed plate heat exchanger type AlfaNova 14-10H, and it is made of 100% stainless steel. Temperature measurements throughout the circuit are done using thermocouples type N with length 1m and

diameter of 1mm. The measurements are calculated from the voltage signal from the thermocouples to temperatures using a table that is programmed in LabView (logging program). The tables come from a standard called ITS-90, and it is the same standard that the calibration certificates uses. The temperatures are measured where there is a "T" symbol in the P&ID (figure 4.1). In addition a loose compensation cable has been hooked up so that measurements at other places can be done by only mounting a thermocouple to the wanted spot, and then connect the compensation cable. This has been done to the copper tubing of the water flowing in and out of the heat exchanger. One thermocouple has been mounted to the inlet, and one to the outlet of the heat exchanger. By connecting the compensation cable to one of these thermocouples the temperature is logged, and then one could switch to the other thermocouple in order to get the temperature difference of the water inside the heat exchanger. The thermocouples on the water inlet and outlet are insulated using Rockwool. Rockwool is also used for insulation on the rest of the test rig. A simple control valve with several positions for controlling the mass flow of water has been installed. This is manually controlled by using a turning wheel.

## 4.5 Uncertainty analysis

The equipment which is used have uncertainties which need to be taken taken into account when the results are investigated. The N-type thermocouples have an uncertainty of  $\pm 0.5^\circ\text{C}$  calculated by Ph.D. candidate [2]. The uncertainty includes the uncertainty related to the measured voltage of the thermocouples to the IEC (International Electrothechnical Commission) table for N-type thermocouples, the calibration uncertainty and the NI 9214 thermocouple input module uncertainty. In addition the mass flow meter has a uncertainty of 1% of full scale and 0.5% of the reading. Full scale correspond to  $23.45\text{Nm}^3/\text{h} = 0.00767\text{kg/s}$ .

## 4.6 Experimental procedure

Before each experiment the pressure is checked to make sure that there is an overpressure in the circuit to prevent air from leaking in. Also, the mass flow meter is calibrated for an overpressure of 0.2barg, and the operating pressure should be maintained at this level to ensure correct measurements. If the pressure is too low, nitrogen is refilled. The tracing controlled temperature (temperature at bypass tube inlet) is set to  $50^\circ\text{C}$ , which is the temperature to be used when the actual heat pipe is ready for usage. The temperature is gradually increased by controlling the maximum allowed power of the tracing. By gradually increasing the control temperature one ensures that the safety function that turns off the tracing if the measured tracing wall temperature reaches  $100^\circ\text{C}$  is not encountered. This safety temperature has been set because the pneumatic control valve cannot withstand too high temperatures ( $\approx 70^\circ\text{C}$ ) and it is located near the tracing (see P&ID). At startup the mass flow of water has to be decided. Then the position of the water valve turning

wheel is positioned correctly and the electric power supply is switched on. After Labview is started the experiment is ready to begin. During the experiments there are a multiple number of parameters that can be changed. The rotational speed of the side channel pump, the regulating tracing temperature, the opening of the pneumatic control valve and the water valve position can all be regulated.

## 4.7 Results and discussion

### Controller tuning

The graph of figure 4.11 presents the temperature variation regulated by the PID controller (tracing). The x and y axis in figures 4.11-4.16 are temperature ( $^{\circ}\text{C}$ ) and minutes, respectively. From figure 4.11 it is seen that the temperature increases to the set point temperature of  $50^{\circ}\text{C}$ , before it starts to oscillate around this temperature, which indicate that the system is marginally stable. Figure 4.12 shows an enlarged picture of figure 4.11 where the marginally stable temperature variation is more clear. This is explained by the fact that no tuning of the controller had been done at this point. The proportional gain, integral time and derivative time were all at preset values (see table 11). Since the system was marginally stable, manual tuning of the controller parameters were tested (test 1 in table 11). The results of test 1 can also be seen in figure 4.11 after approximately 100 minutes where a sharp increase of temperature is seen. At first eyesight it could look like the system is asymptotic stable, however, in figure 4.13 the same graph has been enlarged to show how the temperature variation in more detail. It is clear that the system is not asymptotic stable, but rather unstable because after the temperature seem to set on the set point temperature, a larger overshoot follows which indicate that the system is unstable.

Figure 4.14 and 4.15 shows the temperature variation after the Good Gain procedure (section 4.3) has been followed in order to tune the controller. It is evident that the Good Gain method gives a stable temperature output after the controller temperature reaches the set point. Opposed to both the preset case and test 1, the Good Gain method gives a stable system with a temperature variation of only  $\pm 0.05^{\circ}\text{C}$ . The parameters given in table 11 for the Good Gain method is recommended for usage when running experiments due to the good results obtained. The system is stable for these parameters.

**Table 11: PID controller parameters**

Case	$K_p$	$T_i(\text{min})$	$T_d(\text{min})$
Preset	1	0.01	0
Test 1	0.4	7	1.75
Good Gain method	25	5	1.25

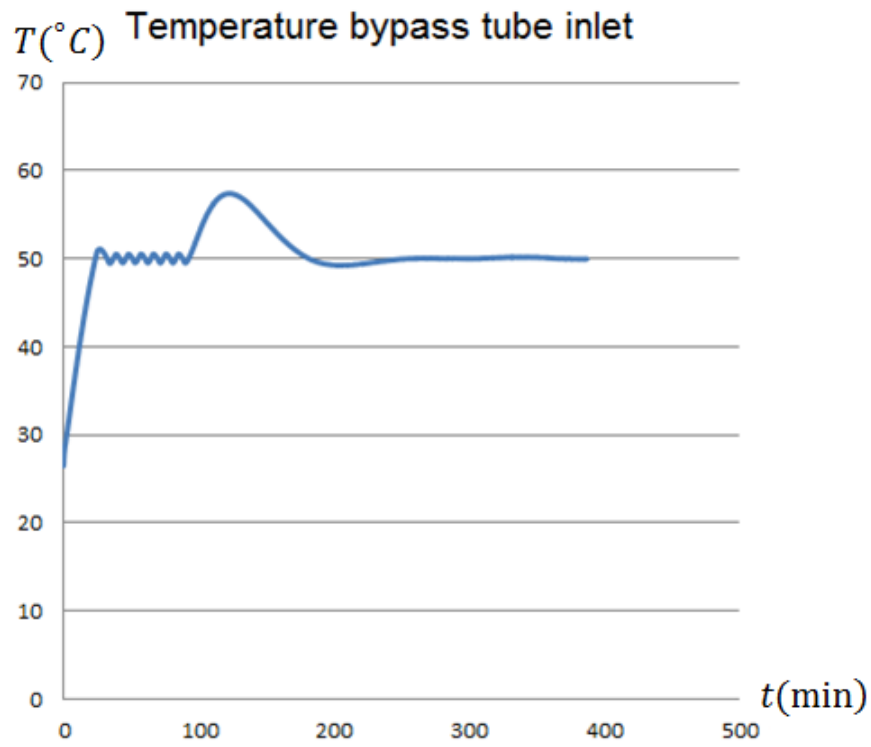


Figure 4.11: Temperature at heat pipe inlet for different controller parameters.

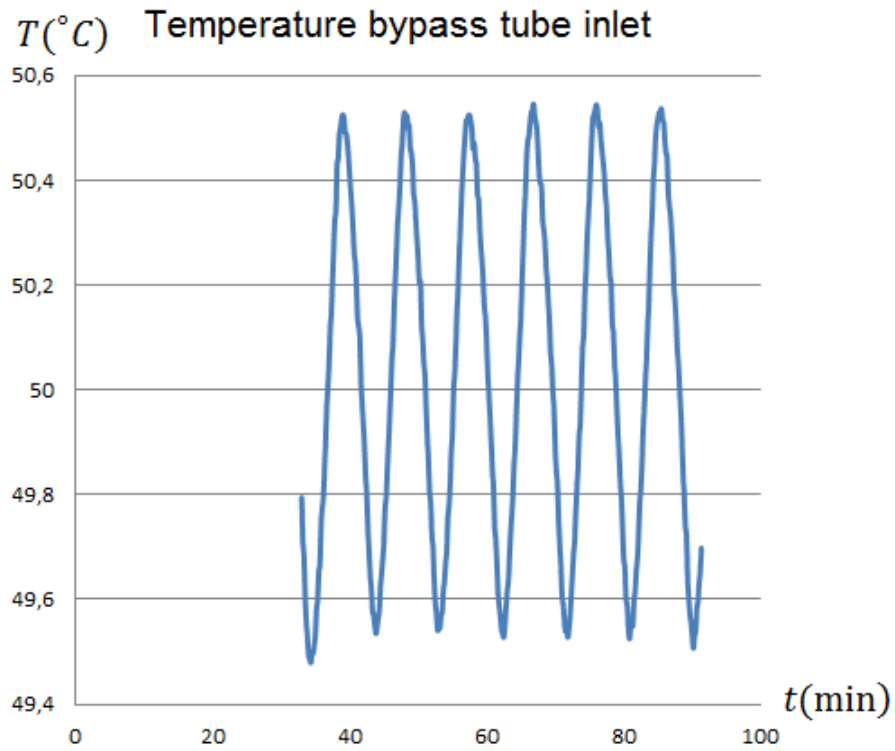


Figure 4.12: Marginal stable PID controller.

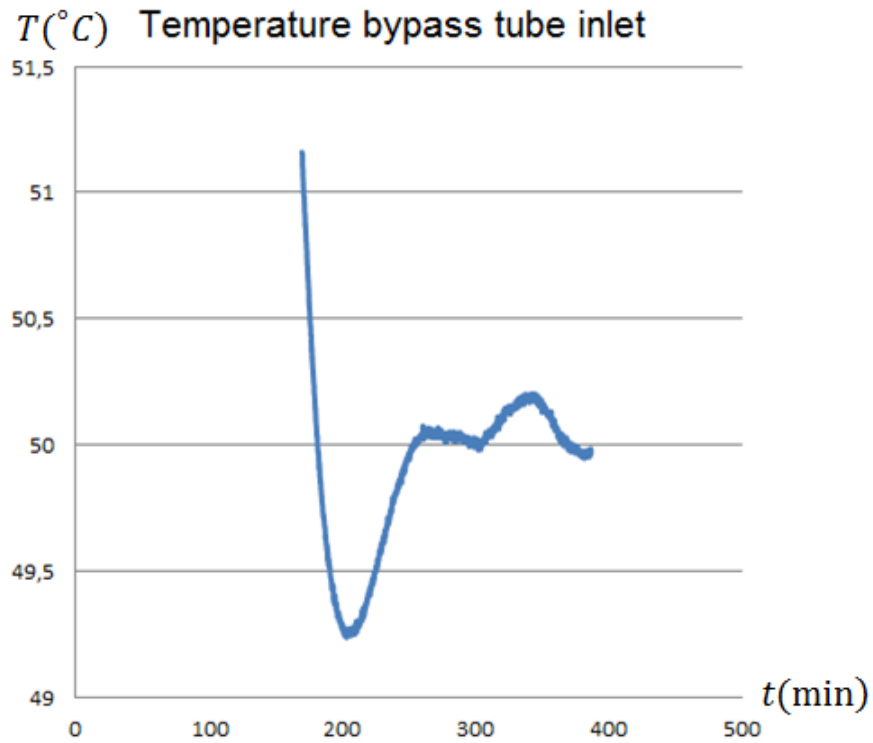


Figure 4.13: Unstable PID controller.

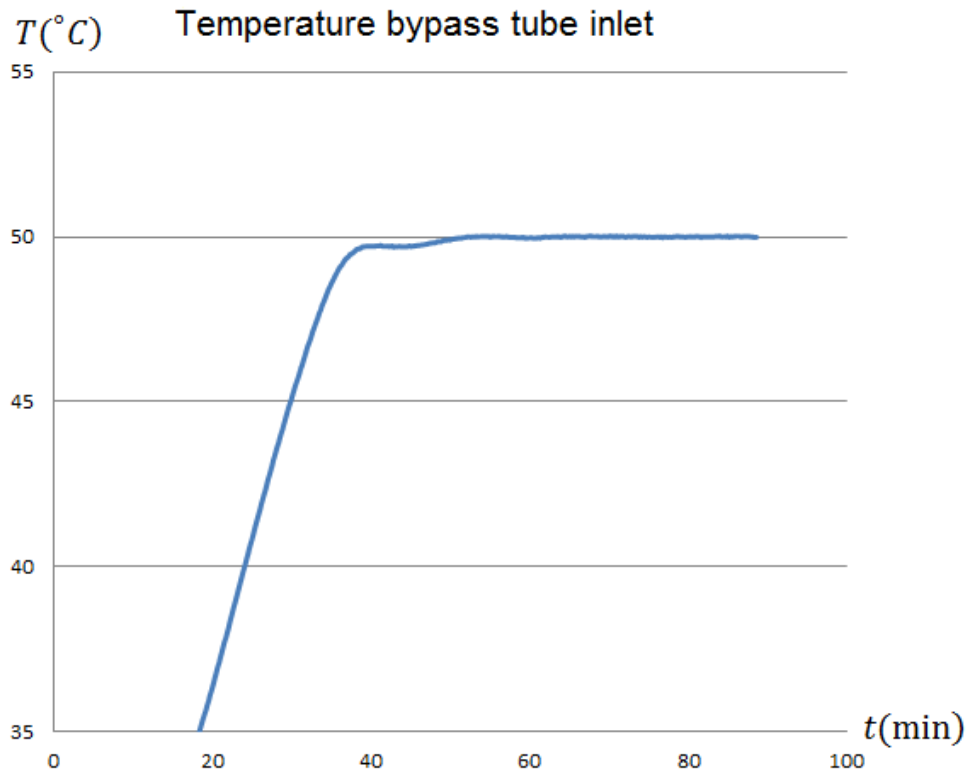


Figure 4.14: Stable PID controller.

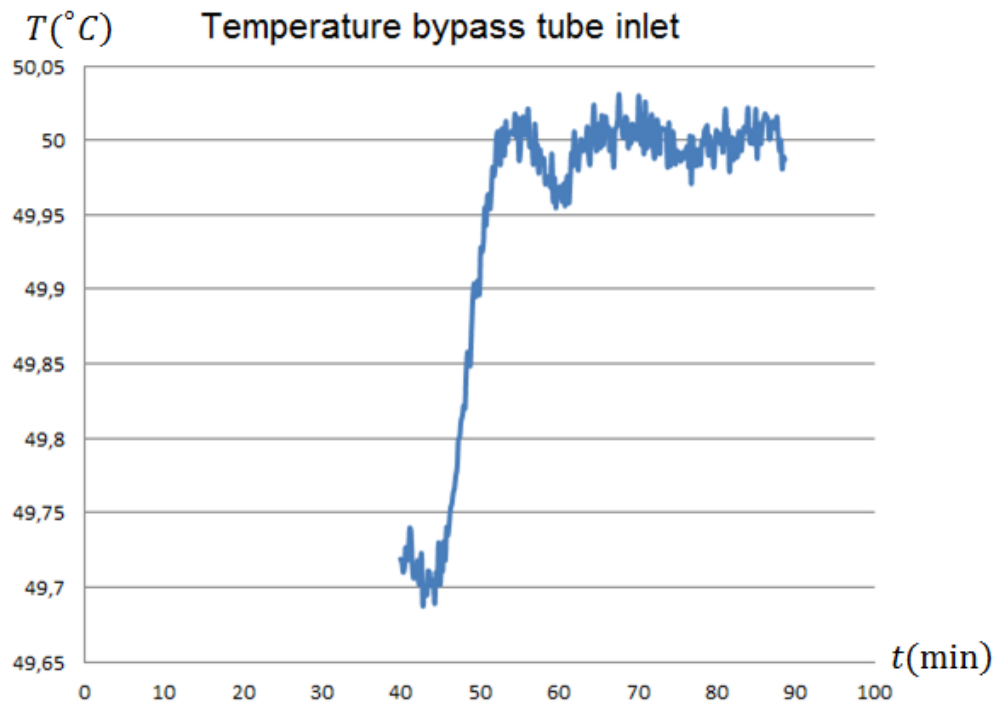
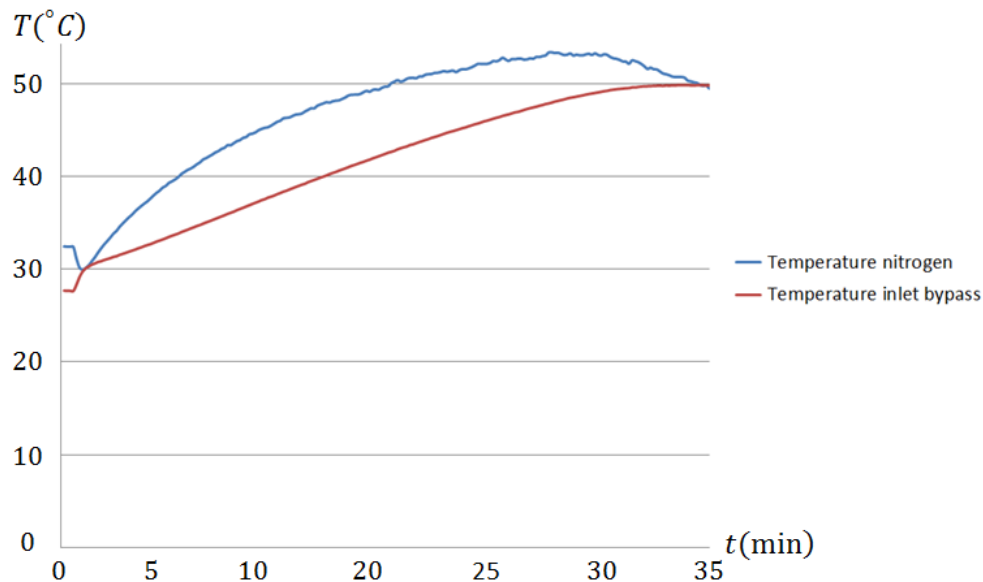


Figure 4.15: Stable PID controller.



### Heating of control valve and mass flow meter

In figure 4.16 the temperature of nitrogen at the outlet of the vertical pipe section and nitrogen temperature at the inlet of the bypass tube are shown as a function of time. It can be seen that it takes about 32 minutes for the controller temperature (bypass inlet temperature) to reach the set point value of 50°C. However, it only takes approximately 19 minutes for the gas temperature to reach a temperature of 50°C. This is because of all the steel (i.e. pipes, control valve and flow meter) in between the tracing and controller temperature which needs to be heated. This makes the system response much slower than what it could have been had the tracing been placed closer to the control temperature. If changes are to be made to the test rig, effort should be put in rearranging the tracing in order to obtain faster system response.



**Figure 4.16: Time difference due to heating of steel in cooling circuit.**

### Pipe Heat loss

For all calculations where parameters (e.g. mass flow, wall temperature etc.) are taken from the LabView logging files, the values are taken after stable operating conditions are reached, i.e. after the controller temperature has settled at the set point. In table 12 selected parameters from tests in the laboratory are presented for a range of revolutions per minute (rpm).  $\Delta T_{bp}$  is the temperature difference from inlet to outlet of the bypass tube,  $T_w$  is the tracing wall temperature,  $\Delta T_H$  is the temperature drop from inlet to outlet of the horizontal insulated pipe section,  $\Delta T_V$  is the temperature drop from inlet to outlet of the vertical insulated pipe section,  $\dot{m}_{N_2}$  is the mass flow of nitrogen circulating in the circuit and  $T_{m,i}$  is the mean temperature of nitrogen at the inlet of the horizontal pipe section, or the outlet of the vertical pipe section where the tracing is located. It should be noted that Ph.D. candidate Geir Hansen pointed out that the thermocouple measuring  $T_{m,i}$  is actually located somewhat down in the heated tracing section, which

means that the gas temperature will increase more before it reaches the outlet of the tracing section (see figure 4.3a).

**Table 12: LabView logging parameters**

rpm	653	983	1310	1638	1971	2469	2956
% of max rpm	20	30	40	50	60	75	90
$\dot{m}_{N_2}$ (kg/s)	0.00124	0.00209	0.00311	0.00406	0.00468	0.00579	0.0068
$T_{m,i}$ (°C)	47.5	47.4	46.1	46.3	48.2	50.6	52.5
$\Delta T_H$ (°C)	-2.5	-2.6	-3.9	-3.7	-1.8	0.6	2.5
$T_w$ (°C)	86.3	82.4	77.1	74.3	71.3	64.6	56.7
$\Delta T_{bp}$ (°C)	8.86	7	5	4.16	4	3.3	3.1
$\Delta T_V$ (°C)	20.3	18	15.1	14	12.3	7	1.6

As can be seen from table 12, it seems to be a temperature increase from the inlet to the outlet of the horizontal pipe section for some of the mass flows. This can not be the case because there is no heat source located along the pipe section. The only explanation is as was mentioned earlier, that the thermocouple which is measuring the inlet temperature is located at an uncertain position inside the heated region. With a mass flow of 0.00124kg/s, there seems to be a temperature increase of 2.5 degrees from table 12. However, looking at the wall temperature of 86.3°C, and taking into account that the thermocouple is located inside the heated region, it is expected that the actual inlet temperature is several degrees higher. Comparing with the calculated horizontal tube results from table 13, where a temperature decrease of 4.97 degrees is obtained for a rpm of 653, one could expect the actual temperature to be around 55°C at the horizontal tube inlet. When a mass flow of 0.0068kg/s is used, a temperature increase is no longer seen, and a temperature decrease of 2.5°C is obtained in the experiments (see table 12). The temperature drop calculated with the same mass flow yields 1.74°C. The difference between the calculated temperature drop and the drop obtained in the experiments can be explained by the fact that the correlations which are used have uncertainties, and that there is a lot of steel (control valve and mass flow meter) which needs to be heated between the measured inlet temperature and outlet temperature. In addition the thermocouples have an uncertainty of  $\pm 0.5^\circ\text{C}$ .

**Table 13: Horizontal insulated tube calculations**

rpm	653	983	1310	1638	1971	2469	2956
% of max rpm	20	30	40	50	60	75	90
Reynolds number	2083	3512	5242	6840	7849	9657	11292
Flow region	Laminar	Transition	Transition	Transition	Transition	Transition	Turbulent
Entrance length (m)	4.2(3) <sup>1</sup>	0.405	0.405	0.405	0.405	0.405	0.405
$R'_{tot}$ (mK/W)	7.88	5.68	5.37	5.23	5.17	5.09	5.02
$q'$ (W/m)	2.85	3.95	3.93	4.07	4.49	5.03	5.48
$Q_H$ (W)	6.41	8.89	8.84	9.16	10.10	11.32	12.33
$\Delta T_H$ (°C)	4.97	4.08	2.73	2.17	2.07	1.88	1.74

In table 14, the total heat loss and temperature difference from inlet to outlet of the bypass tube are presented as a function of rpm. The total heat loss includes heat loss for the 3 regions in the bypass tube which is illustrated in figure 4.5. As opposed to the horizontal tube, the thermocouples at the inlet and outlet of the bypass tube should be positioned more correctly, which leads to less error in the measured experimental results. Comparing the calculated bypass tube results in table 14 with the experimental results in table 12 it is seen that the calculated temperature drop from inlet to outlet of the bypass tube is less than what is obtained from the experiments. Although there are differences between the calculated and experimental values, the trend is the same. What could explain the deviation is the uncertainty in the thermocouples of  $\pm 0.5^\circ\text{C}$ , the uncertainty regarding the position of the thermocouples and the uncertainty of the correlations which are used.

**Table 14: Bypass tube calculations**

rpm	653	983	1310	1638	1971	2469	2956
$Q_{bp}$ (W)	10.15	11.06	12.71	13.63	14.08	14.76	15.35
$\Delta T_{bp}$ (K)	7.86	5.08	3.93	3.23	2.89	2.45	2.18

Table 15 presents the calculated results for the vertical pipe section. The heated section is 1m long, and the tracing band gives a constant heat flux temperature variation (ref. figure 4.3a).  $T_s$  is the outer surface temperature of the insulation in table 15, and the wall temperature  $T_w$  of the tracing can be found in table 12. It should be noted that the position of the measured  $T_w$  is located approximately in the middle of the vertical tube section [2], but for the calculations it will be assumed that this measurement yields the average over the entire tube section. The total heat generation by the tracing is not known because no logging or instrumentation is measuring this. However, an estimate of the total heat  $Q$ , as well as the heat flux could be done by summing the heat loss ( $Q_V$ ) presented in table 15 and the heat added to the nitrogen gas by using  $\dot{m}c_p\Delta T_V$ . As can be seen from table 16 is that the heat added by the tracing to the gas ( $\dot{m}c_p\Delta T$ ) increases as a function of rpm at first, but then decreases again as a function of rpm. This is explained by the fact that the temperature of the outlet of the side channel blower increases with rpm. As the outlet temperature of the side channel blower increases (which is the temperature used as the inlet temperature for the vertical pipe section), the tracing doesn't need to apply that much heat in order to reach the set point temperature at the bypass tube inlet. Figure 4.17 shows the side channel blower outlet temperature as a function of rpm. It should be noted that the thermocouple measuring the "outlet" temperature of the side channel blower is in fact located after the gas has passed through a non-insulated tube, which means that the actual side channel outlet temperature is higher.

<sup>1</sup>The number in parenthesis is the thermal entry length. For transition and turbulent flow conditions the thermal and hydrodynamic entry lengths are assumed to be equal.

It is seen from figure 4.17 that in the lower rpm-region the temperature gradient is quite different from the upper rpm-region. This is because of the non-insulated tube connecting the side channel blower to the vertical pipe section, and for non-insulated tubes in the lower rpm-region (low mass flow) the heat losses are much greater (ref. table 14). The non-insulated tube connecting the side channel blower and the vertical pipe section will most likely have a similar temperature drop as the bypass tube has from inlet to outlet.

The heat flux from the tracing is shown as a function of rpm in table 16. It is clear that the largest part of the heat generated by the heating tape is given to the gas flow, and less is lost to the environment.

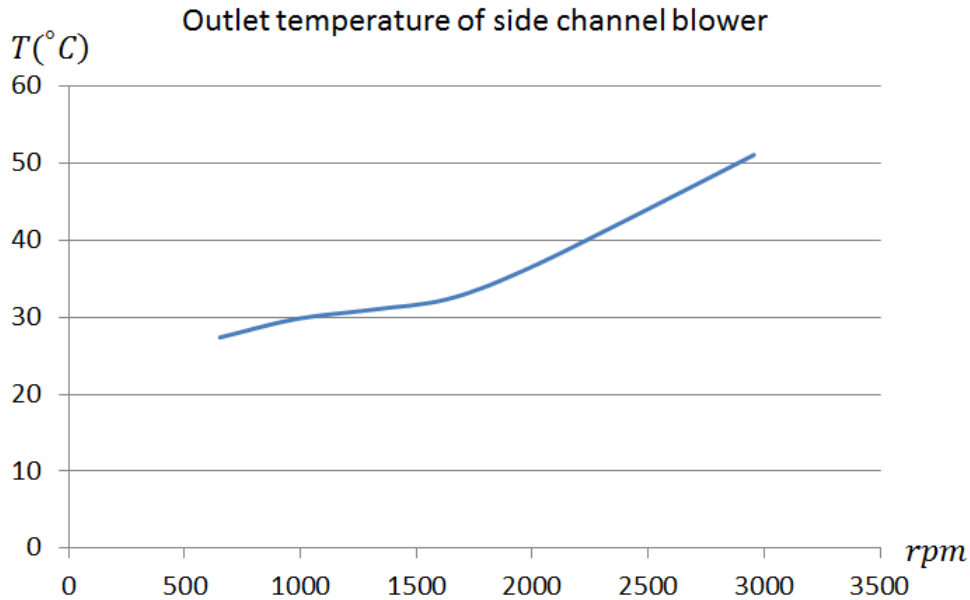


Figure 4.17: Outlet temperature of side channel blower as a function of rpm.

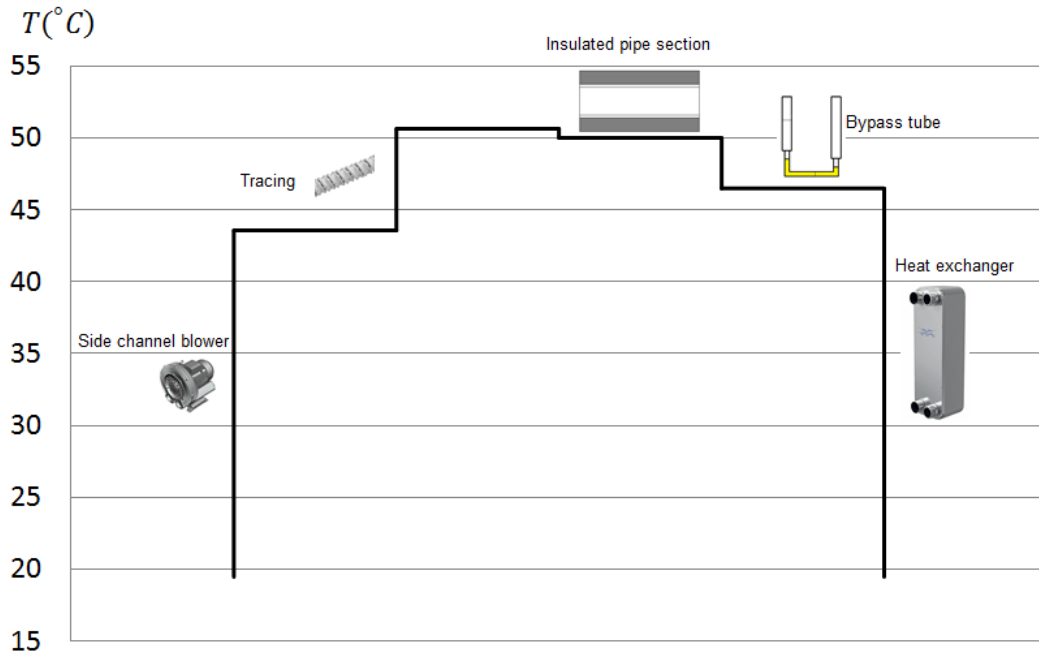
Table 15: Vertical insulated tube calculations

rpm	653	983	1310	1638	1971	2469	2956
% of max rpm	20	30	40	50	60	75	90
$T_s$ (K)	310.8	310	309.2	308.7	308.2	306.9	305.4
$R'_{tot}$ (mK/W)	3.55	3.56	3.57	3.58	3.6	3.62	3.67
$q'$ (W/m)	17.28	16.12	14.58	13.76	12.88	10.93	8.65
$Q_V$ (W)	17.28	16.12	14.58	13.76	12.88	10.93	8.65

**Table 16: Heat added by tracing**

rpm	653	983	1310	1638	1971	2469	2956
$Q_V$ (W)	17.28	16.12	14.58	13.76	12.88	10.93	8.65
$\dot{m}c_p\Delta T$ (W)	26.2	39.16	48.89	59.17	59.92	42.19	11.33
$Q_{trac}$ (W)	43.48	55.28	63.47	72.93	72.8	53.12	19.98
$q''_{trac}$ (W/m <sup>2</sup> )	311	395.4	454	521.7	520.7	380	142.9

As an illustration the mean gas temperature sequence throughout the cooling circuit for 2469rpm has been plotted in figure 4.18. The small pictures (e.g picture of side channel blower) in figure 4.18 illustrates what component that causes the temperature increase/decrease in the circuit. The largest temperature difference of the nitrogen gas is across the plate heat exchanger, while the side channel blower provides the largest temperature lift. It should be noted that the temperature plot in figure 4.18 does not show the temperature profiles at the different components, but rather just an illustration of the how the mean temperature varies in the circuit.

**Figure 4.18: Temperature sequence throughout cooling circuit.**

### Heat exchanger and side channel blower

A heat balance for the plate heat exchanger at 2469rpm is done using the known values of the cold stream (water). The mass flow of water was calibrated manually by setting a position on the water valve, filling a bucket while taking the time, weighing the filled bucket and then calculate the mass flow in kg/s. In figure 4.19 the calibration of the water mass flow is shown. As can be seen is that there are only two positions which have been measured twice, so it is expected to be some deviation in the calibrated mass flow and the actual mass flow. In addition the water valve turning wheel could from experience not be said to be precise to the millimeter. The total heat transferred between the hot and cold stream yields,

$$Q = \dot{m}_w c_{p,w} (T_{w,o} - T_{w,i}) = 0.065 \text{kg/s} \cdot 4187 \text{J/kgK} \cdot 0.8 \text{K} = 217 \text{W} \quad (4.36)$$

For the hot stream(nitrogen) the following yields,

$$Q = 217.7 \text{W} = \dot{m}_{N_2} \cdot 1041 \text{J/kgK} (44 - 12.5) \text{K} \quad (4.37)$$

$$\Rightarrow \dot{m}_{N_2} = 0.00664 \text{kg/s} \quad (4.38)$$

Comparing the calculated value above with the value in table 12, a difference of 0.00085kg/s is seen. An explanation of the difference is most likely due to the measurement of  $\Delta T_W$  which was measured to 0.8K. However, the insulation around these thermocouples is not very good from the authors point of view, and should explain the difference. The total heat transferred Q is very sensitive to the temperature difference of the cooling water. A decrease of  $\Delta T_w$  from 0.8 to 0.7K would give a decrease of Q from 217.7W to 190.5W, which would decrease the mass flow from 0.00664kg/s to 0.00581kg/s. Given that the insulation is not sufficient, the calculated mass flow will always differ compared with the measured.

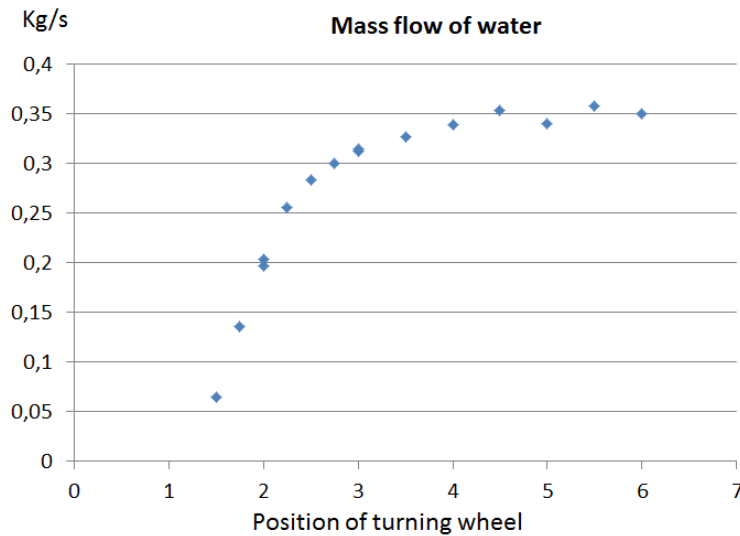


Figure 4.19: Calibration of the water mass flow

In table 17 the calculated outlet temperatures using equation (4.33), and the measured outlet temperatures from the laboratory experiments are shown.  $\dot{V}$  is the volumetric flow rate,  $\Delta P$  is the pressure loss over the side channel blower obtained from data sheet,  $T_1$  is the inlet temperature (taken from labview logging file),  $T_{2,calc}$  is the calculated outlet temperature, and  $T_{2,exp}$  is the measured value from the laboratory experiments. It is seen that difference between the calculated and measured values varies from 0.2°C to 2.7°C. This can be explained by the fact that even though the same inlet temperature is used, the measured outlet temperature is located after an uninsulated tube section, which would make the actual outlet temperature higher. However for 2469rpm the measured outlet temperature is higher than the calculated, but the reason for this is not known. It could be related to measurement error, and that the isentropic relation used to calculate only gives an estimate.

**Table 17: Side channel blower calculations**

rpm	1638	1971	2469
$\dot{V}$ ( $m^3/h$ )	12.4	14.2	17.7
$\Delta P$ (mbar)	389	365	337
$T_1$ (K)	284.2	286.2	292.5
$T_{2,calc}$ (K)	307.9	309.4	313.9
$T_{2,exp}$ (K)	305.4	309.2	316.6

## 4.8 Chapter conclusions

Results of a series of experiments on a cooling circuit for a heat pipe were reported. PID controller tuning for temperature regulation was successful. The tuned PID controller parameters are recommended for further use when the actual heat pipe is ready. The response time of the temperature regulated thermocouple was found to be slow due to the positioning of the heating tape. It is advised to change the layout and move the heating tape closer to the temperature regulated thermocouple to achieve faster response time. The heating tape series provided more heat to the gas than what was lost to the environment.

As expected, the largest heat loss in the cooling circuit was at low rotational speeds (little mass flow), and the bypass tube section is where the biggest temperature drop in the piping was seen. The large uncertainty regarding the positioning of the thermocouples should be addressed by opening the circuit and clarify the actual position if possible.

The obtained results are satisfactory considering that the system had never been tested before, by working properly with no major unforeseen problems.





## 5 Conclusions

Results from two important performance limitations, the boiling- and capillary limitation and a series of experiments on a cooling circuit for a heat pipe have been presented.

From the literature survey in section 2 it can be concluded that with porous coated surfaces heat transfer is improved and less superheat is required for boiling to commence. The mechanism of heat transfer for liquid metals is most likely conduction across a liquid-saturated wick to the outer surface where vaporization of the working fluid takes place. The possibility of homogeneous nucleation is considered not to be of concern. Boiling inside the wick is only of concern for wick 2 with 15 layers combined with high heat fluxes in the higher (600°C) temperature region.

For the proposed system wick 2 is the best choice if high heat fluxes is of the essence. However, when the wick length is increased to 20cm, wick 2 becomes inferior to wick 1 and wick 1 would be the best choice. The performance of the wick is proportional to the wick thickness, and several layers can be sintered together in order to improve the performance. Combination of wick types is found to give a significant (factor of almost 4) improvement of the performance and using a combined wick makes it possible to cool down a larger surface. Uneven heat flux distribution in the wick could lower the maximum sustainable heat flux. A higher heat flux at the bottom section of the evaporator increases the performance compared with the even heat flux distribution, while a lower heat flux at the bottom section of the evaporator lowers the performance.

The results obtained from tuning the PID controller were satisfactory, and stable operating conditions with the tuned parameters were seen. The response time of the temperature regulation was found to be slow due to the positioning of the heating tape. It is recommended to change the layout and move the heating tape closer to the temperature regulated thermocouple in order to achieve faster response time. Heat loss localization and energy balances for the components and tubing in the cooling circuit were done. The uncertainty regarding the positioning of the thermocouple proved to be the largest source of error in the heat balance calculations.



## 6 Further work

No literature is found regarding boiling in nickel foam wicks with potassium as working fluid. There is also a large uncertainty regarding the maximum critical radius of potassium with respect to wetting of a cavity. Therefore, if possible, laboratory experiments using a nickel foam wick and potassium should be done in order to get a better understanding of the boiling mechanism in the proposed heat pipe.

When the actual heat pipe is ready and experiments is to be performed, it is important that the maximum heat flux is measured and compared with the calculated values. Due to the easiness of the production method for the combined wick type, a combined wick should be made, tested and evaluated against the theory presented in this thesis. Ph.D. candidate Geir Hansen has already established a procedure for a "rate of rise" experiment, and experimental results for single wick types for a "rate of rise" experiment are available, so a comparison should be made.

Time and effort should be put in changing the layout of the cooling circuit in order to achieve faster response. The thermocouples should be positioned at different **known** locations to obtain accurate measurements, and then make an improved energy analysis of the cooling circuit. Also, a study of where to add additional thermocouples throughout the circuit should be done, and then add these.



## References

- [1] Annette Hultin, *Evaporation and condensation in heat pipes with potassium as working fluid*. Master thesis,
- [2] Ph.D. candidate Geir Hansen *Ref. meetings*. 2012.
- [3] N.B. Vargaftik, Y.K. Vinogradov, V.S. Yargin *Handbook of physical properties of liquids and gases*. Begell house, 1996.
- [4] Frank P. Incropera, David P. Dewitt, Theodore L. Bergman, Adrienne S. Lavine, *Fundamentals of Heat and Mass Transfer*. 6th edition, John Wiley & Sons, 2007.
- [5] Amir Faghri, *Heat Pipe Science and Technology*. Taylor Francis, Massachusetts, 2nd Edition, 1994.
- [6] <http://i-am-fast.com/cpucooling.aspx>.
- [7] David Reay, Peter Kew, *Heat Pipes*. Linacre House, Jordan Hill, Oxford, 5th Edition, 2006.
- [8] P.D. Dunn, D.A. Reay, *Heat Pipes*. Pergamon, Elsevier Science Ltd 1994.
- [9] M.N. Ivanovskii, V.P. Sorokin, I.V. Yagodkin, *The physical principles of heat pipes*. Oxford University Press, New York, 1982.
- [10] Erling Næss, Martin Løvland, *Compendium in TEP07 - Industrial Heat Engineering*. NTNU, Department of Energy and Process Engineering, 2011.
- [11] John G. Collier, John R. Thome *Convective boiling and condensation*. 3rd edition, Oxford University Press, 1994.
- [12] Lienhard, J. H. *Correlation of the limiting liquid superheat*. Chemical Engineering Science, Vol.31, pp. 847-849, 1976.
- [13] O. E. Dwyer, *On incipient-boiling wall superheats in liquid metals*. International Journal of Heat and Mass Transfer, Vol. 12, pp. 1403-1419 Pergamon Press, 1969.
- [14] W.R. Davis, J.K. Ferrell, *Evaporative heat transfer of liquid potassium in porous media*. AIAA/ASME Thermophysics and Heat Transfer Conference, Boston, 1974.
- [15] H.M. Winston, J.K. Ferrell, R. Davis, *The mechanism of heat transfer in the evaporator zone of the heat pipe*. 2nd International Heat Pipe Conference, 1976.
- [16] J.K. Ferrell, Jack Alleavitch, *Vaporization Heat Transfer in Capillary Wick Structures*. Chemical Engineering Progress Symposium Series, No. 102, Vol. 66, pp 82-91, 1970.

- [17] Richard A. Moss, Arnold J. Kelly, *Neutron Radiographic Study of Limiting Planar Heat Pipe Performance*. International Journal of Heat and Mass Transfer, Vol. 13, pp. 491-502, Pergamon Press 1970.
- [18] A.E. Bergles, M.C. Chyu *Characteristics of Nucleate Pool Boiling From Porous Metallic Coatings*. Transactions of the ASME, Journal of Heat Transfer, Vol. 104, May, pp. 279-285 1982.
- [19] William D. Allingham, Jack A. Mcintire, *Determination of Boiling Film Coefficient for a Heated Horizontal Tube in Water-Saturated Wick Material*. Transactions of the ASME, presented at the ASME-AIChE Heat Transfer Conference, Buffalo, N.Y., 1960.
- [20] Z.G. Xu, Z.G. Qu, C.Y. Zhao, W.Q. Tao *Pool boiling heat transfer on open-celled metallic foam sintered surface under saturation condition*. International Journal of Heat and Mass Transfer, May, 2011.
- [21] Janusz T. Cieslinski *Augmentation of heat transfer in boiling of water on surfaces with capillary-porous layers*. Advances in Engineering Heat Transfer, pp 395-402, 1995.
- [22] Naim H. Afgan, Larisa A. Jovic, Sergey A. Kovalev, Victor A: Lenykov *Boiling heat transfer from surfaces with porous layers*. International Journal of Heat and Mass Transfer, Vol. 28, pp. 415-422, Pergamon Press 1985.
- [23] P.J. Marto, Lt. V.J. Lepere *Pool Boiling Heat Transfer From Enhanced Surfaces to Dielectric Fluids*. Transactions of the ASME, Journal of Heat Transfer, Vol. 104, May, pp. 292-299 1982.
- [24] Janusz T. Cieslinski *Nucleate pool boiling on porous metallic coatings*. Experimental Thermal and Fluid Science, Vol. 25, pp. 557-564 2002
- [25] Dan Adrian Odden *Investigation of heat transfer and flow conditions in heat pipes using potassium as working fluid*. Project thesis, 2011,
- [26] Chen Li, G.P. Peterson, Yaxiong Wang *Evaporation/Boiling in Thin Capillary Wicks - Wick Thickness Effects*. Transactions of the ASME, Journal of Heat Transfer, Vol. 128, pp. 1312-1319, 2006. 2011.
- [27] Yunus a. Cengel, *Heat and mass transfer - A practical approach*. 3rd edition, McGrawHill, 2006.
- [28] Stuart W. Churchill, Humbert H. S. Chu *Correlating Equations for Laminar and Turbulent Free Convection from a Horizontal Cylinder*. International Journal of Heat and Mass Transfer, Vol. 18, pp. 1049-1053,
- [29] Finn Haugen *Anvendt reguleringssteknikk*. Tapir forlag, 1990.
- [30] Finn Haugen *Basic dynamics and control*. TechTeach, 2010.

- [31] Michael J. Moran, Howard N. Shapiro *Fundamentals of Engineering Thermodynamics*. 5th edition, John Wiley & Sons, 2006.





---

# Appendices

## Appendix A

This appendix includes the tables for the physical properties of potassium, nitrogen and air. Most of the potassium values are taken from Vargaftik et al.[3], but for the lowest temperature(600K) values from Faghri[5] are taken. The air and nitrogen properties are both taken from Incropera et al.[4]. The thermal conductivity for steel,  $k_{steel} = 14$  W/mK, and brass,  $k_{brass} = 109$  W/mK are also taken from Incropera et al. [4]. For Rockwool the thermal conductivity used is taken from the data sheet.

Table A.33: Thermophysical Properties of Saturated Potassium

Potassium, K, Molecular Weight: 39.1, ( $T_b = 1032.2$ K; $T_m = 336.4$ ) [1]											
Temp. K	$p_v$ Saturation Pressure ( $10^5$ Pa)	$h_{fg}$ Latent Heat (kJ/kg)	$\rho_\ell$ Liquid Density ( $\text{kg/m}^3$ )	$\rho_v$ Vapor Density ( $10^{-3}$ $\text{kg/m}^3$ )	$\mu_\ell$ Liquid Viscosity ( $10^{-4}$ $\text{N}\cdot\text{s/m}^2$ )	$\mu_v$ Vapor Viscosity ( $10^{-7}$ $\text{N}\cdot\text{s/m}^2$ )	$k_\ell$ Liquid Thermal Conductivity ( $\text{W/m}\cdot\text{K}$ )	$k_v$ Vapor Thermal Conductivity ( $\text{W/m}\cdot\text{K}$ )	$\sigma$ Liquid Surface Tension ( $10^{-3}$ $\text{N/m}$ )	$c_{p,\ell}$ Liquid Specific Heat (kJ/kg·K)	$c_{p,v}$ Vapor Specific Heat ( $10^{-1}$ kJ/kg·K)
600	0.0009258	2143	766.9	0.69	2.380		33.85		98.2	0.771	0.8194
700	0.01022	2108	743.3	6.68	1.981		40.72		92.2	0.762	0.9646
800	0.06116	2068	719.6	36.44	1.707	134	37.58	0.0142	86.2	0.761	1.066
900	0.2441	2023	695.7	134.80	1.507	148	34.45	0.0175	80.2	0.769	1.116
1000	0.7322	1970	671.6	380.20	1.354	163	31.32	0.0228	74.2	0.792	1.121
1100	1.864	1924	647.3	871.50	1.233	178	28.19	0.0248	68.2	0.816	1.100
1200	3.913	1872	622.9	1703.00	1.135	196	25.05	0.0266	62.2	0.846	1.064
1300	7.304	1820	598.4	2969.10	1.053	212	22.00	0.0280	56.2	0.873	1.022
1400	12.44	1765	573.6	4768.70	0.984	228	19.00	0.0303	50.0	0.899	
1500	20.0	1711	548.8	7062.10	0.925	242	16.00	0.0303	47.0	0.924	0.9796

Thermophysical properties of saturated potassium taken from Faghri [5]

continued

$T, \text{K}$	$\rho', 10^3 \text{ kg/m}^3$	$\alpha'_p, 10^{-5} \text{ K}^{-1}$	$\beta'_T, 10^{-5} \text{ MPa}^{-1}$
700	0.7441	31.1	56.2
800	0.7209	32.3	64.0
900	0.6974	33.9	73.4
1000	0.6736	35.8	84.5
1100	0.6491	38.1	97.4
1200	0.6241	40.6	112
1300	0.5985	43.2	129
1400	0.5724	46.2	149
1500	0.5456	49.7	173
1600	0.5180	54.2	205
1700	0.4892	60.7	248
1800	0.4583	70.8	309
1900	0.4238	87.2	393
2000	0.3834	115	510
2100	0.3341	165	
2200	0.2712	263	
2280	0.194	$\infty$	

Correlation equation for density of saturated liquid potassium:

$$\rho' \cdot 10^{-3} = 0.90287 - 0.17015\tau - 0.26817\tau^2 + 0.50513\tau^3 - 0.46506\tau^4 + 0.20365\tau^5 - 3.475 \cdot 10^{-2}\tau^6,$$

where  $\rho$  is in  $(\text{kg/m}^3)$ ,  $\tau = 10^{-3} T$ ,  $T_{\text{melt}} \leq T \leq T_{\text{cr}}$ 

Accuracy of the tabulated values:

for  $\rho$  - 0.25% ( $T \leq 1300 \text{ K}$ ), 0.5% ( $1300 < T \leq 1800 \text{ K}$ ), 1% ( $T > 1800 \text{ K}$ );for  $\alpha'_p$  - 2% ( $T \leq 1300 \text{ K}$ ), 3% ( $1300 < T \leq 1800 \text{ K}$ ), 5% ( $T > 1800 \text{ K}$ );for  $\beta'_T$  - 5%, 10%, and 15%, respectively.

Thermodynamic properties of saturated potassium vapor :

 $\rho''$  ( $\text{kg/m}^3$ ),  $i''$  ( $\text{MJ/kg}$ ),  $r$  ( $\text{MJ/kg}$ ),  $s''$  ( $\text{kJ}/(\text{kg}\cdot\text{K})$ ),  $c_p''$  ( $\text{kJ}/(\text{kg}\cdot\text{K})$ ),  $(\frac{c_p}{c_v})''$  and  $z''$  [413]

$T_s, \text{K}$	$\rho''$	$i''$	$r$	$s''$	$c_p''$	$(\frac{c_p}{c_v})''$	$z'' = \frac{p\mu}{\rho RT}$
800	0.3947-1*	2.657	2.024	5.136	1.155	1.452	0.9543
900	0.1417+0	2.682	1.973	4.888	1.193	1.480	0.9352
1000	0.3893+0	2.707	1.920	4.698	1.181	1.515	0.9162
1100	0.8822+0	2.732	1.865	4.550	1.146	1.552	0.8976
1200	0.1733+1	2.759	1.810	4.434	1.102	1.590	0.8798
1300	0.3057+1	2.785	1.750	4.340	1.060	1.631	0.8605
1400	0.4963+1	2.811	1.685	4.264	1.021	1.674	0.8390
1500	0.7570+1	2.835	1.614	4.203	0.985	1.717	0.8143
1600	0.1098+2	2.858	1.535	4.152	0.951	1.749	0.7845
1700	0.1532+2	2.880	1.449	4.110	0.914	1.764	0.7504
1800	0.2065+2	2.902	1.356	4.077	0.874	1.756	0.7146
1900	0.2701+2	2.927	1.256	4.052	0.834	1.727	0.6788
2000	0.3437+2	2.954	1.150	4.035	0.796	1.683	0.6440

Notation : 0.3387-2 denote  $0.3387 \cdot 10^{-2}$ 

The accuracy of the data are the same as for saturated sodium vapor.

Thermophysical properties of saturated potassium taken from Vargaftik [3]

T, K	$\lambda_1$	P, kPa													At saturation curve	
		1	5	10	30	50	80	100	200	400	600	800	1000	1200		1500
1325	204.6	204.7	205.0	205.4	207.0	208.6	210.7	212.0	217.7	225.1	229.4					234.4
1350	208.4	208.5	208.8	209.1	210.5	211.8	213.7	214.9	219.9	226.7	230.8	233.0	233.5			236.7
1375	212.2	212.3	212.5	212.9	214.0	215.2	216.8	217.8	222.3	228.5	232.3	234.5	236.2			238.9
1400	216.0	216.1	216.3	216.6	217.6	218.6	220.0	220.9	224.8	230.5	234.0	236.2	237.4			241.0
1425	219.9	219.9	220.1	220.3	221.2	222.1	223.3	224.1	227.6	232.7	236.0	238.0	239.2	239.8		243.1
1450	223.7	223.7	223.9	224.1	224.9	225.6	226.7	227.4	230.4	235.0	238.1	240.0	241.2	241.8		245.2
1475	227.5	227.5	227.7	227.9	228.5	229.2	230.1	230.7	233.4	237.5	240.3	242.1	243.3	243.9	244.1	247.3
1500	231.3	231.4	231.5	231.6	232.2	232.8	233.6	234.1	236.5	240.1	242.7	244.4	245.5	246.1	246.3	249.4

Accuracy of the tabulated values is  $\pm 4\%$  at  $T \leq 1200$  K, and  $\pm 4.5\%$  at  $T > 1200$  K.

Thermal conductivity  $\lambda$  of liquid potassium [413]

T, K	336.76	400	500	600	700	800	900	1000	1100	1200	1300	1400	1500	1600	1800	2000	2200
$\lambda$ , W/(m·K)	51.8	50.2	47.6	45.0	42.4	39.9	37.3	34.7	32.1	29.5	27.0	24.4	21.8	19.2	14.1	8.9	3.7

Correlation equation for temperatures  $T_{\text{melt}} \leq T \leq 2200$  K is [467, 413]:  $\lambda = 60.5 - 25.8 \cdot 10^{-3} T$ . Accuracy of the tabulated values ranges from 5% at  $T_{\text{melt}}$  to 15% at  $T > 1600$  K.

Surface tension of  $\sigma$  potassium [413]

T, K	336.76	400	500	600	700	800	900	1000	1100	1200	1300	1400	1500	1600	1700
$\sigma$ , mN·m <sup>-1</sup>	112	108	101	94	87	79	72	64	57	49.5	42.5	35.7	29.3	23.4	17.9

Tabulated values are accurate within 5% and can be correlated by the equation:

$$\sigma = 130.48 - 45.72 \cdot 10^{-3} T - 32.65 \cdot 10^{-6} T^2 + 12.12 \cdot 10^{-9} T^3$$

Thermophysical properties of saturated potassium taken from Vargaftik [3]

*continued*

T, K	$\eta$	p, kPa												At saturation curve	
		1	5	10	30	50	80	100	200	400	600	800	1000		1200
1325	256.1	256.0	255.3	254.6	251.8	249.0	245.1	242.6	231.3	213.5	200.0				187.0
1350	260.9	260.7	260.2	259.5	256.9	254.3	250.6	248.3	237.7	220.6	207.3				189.0
1375	265.7	265.5	265.1	264.4	262.0	259.6	256.2	253.9	243.9	227.5	214.5				191.1
1400	270.4	270.3	269.8	269.3	267.0	264.8	261.5	259.5	250.0	234.3	221.7			202.6	193.1
1425	275.2	275.1	274.7	274.1	272.0	269.9	266.9	265.0	256.0	240.9	228.7			209.9	195.2
1450	280.8	279.9	279.5	279.0	277.0	275.1	272.3	270.5	261.9	247.5	235.6			217.1	197.3
1475	284.8	284.7	284.3	283.9	282.0	280.2	277.5	275.8	267.8	253.9	242.4			224.2	199.4
1500	289.6	289.5	289.1	288.7	287.0	285.3	282.7	281.1	273.5	260.2	249.1			231.2	201.5

Accuracy of the data is  $\pm 2.5\%$  at  $T \leq 1200$  K,  $\pm 3.0\%$  at  $T > 1200$  K.

Viscosity  $\eta$  of liquid potassium [466, 467, 413]

T, K	336.76	400	500	600	700	800	900	1000	1100	1200
$\eta \cdot 10^4$ , Pa·s	5.313	3.930	2.802	2.204	1.838	1.591	1.414	1.281	1.176	1.092
T, K	1300	1400	1500	1600	1700	1800	1900	2000	2280	
$\eta \cdot 10^4$ , Pa·s	1.023	0.965	0.916	0.873	0.835	0.802	0.773	0.746	0.49	

Correlation equation for temperatures  $T_{\text{melt}} \leq T \leq 2000$  K is [467, 413]:

$$\ln \eta = -6.4846 - 0.42903 \ln T + 485.32 T^{-1}$$

Marginal uncertainty of the data calculated from this equation is  $\pm(3-5)\%$  at temperatures below 1300 K and  $\pm(5-10)\%$  at temperatures between 1300 and 2000 K.

**TABLE A.4** Thermophysical Properties  
of Gases at Atmospheric Pressure<sup>a</sup>

$T$ (K)	$\rho$ (kg/m <sup>3</sup> )	$c_p$ (kJ/kg · K)	$\mu \cdot 10^7$ (N · s/m <sup>2</sup> )	$\nu \cdot 10^6$ (m <sup>2</sup> /s)	$k \cdot 10^3$ (W/m · K)	$\alpha \cdot 10^6$ (m <sup>2</sup> /s)	$Pr$
Air							
100	3.5562	1.032	71.1	2.00	9.34	2.54	0.786
150	2.3364	1.012	103.4	4.426	13.8	5.84	0.758
200	1.7458	1.007	132.5	7.590	18.1	10.3	0.737
250	1.3947	1.006	159.6	11.44	22.3	15.9	0.720
300	1.1614	1.007	184.6	15.89	26.3	22.5	0.707
350	0.9950	1.009	208.2	20.92	30.0	29.9	0.700
400	0.8711	1.014	230.1	26.41	33.8	38.3	0.690
450	0.7740	1.021	250.7	32.39	37.3	47.2	0.686
500	0.6964	1.030	270.1	38.79	40.7	56.7	0.684
550	0.6329	1.040	288.4	45.57	43.9	66.7	0.683
600	0.5804	1.051	305.8	52.69	46.9	76.9	0.685
650	0.5356	1.063	322.5	60.21	49.7	87.3	0.690
700	0.4975	1.075	338.8	68.10	52.4	98.0	0.695
750	0.4643	1.087	354.6	76.37	54.9	109	0.702
800	0.4354	1.099	369.8	84.93	57.3	120	0.709
850	0.4097	1.110	384.3	93.80	59.6	131	0.716
900	0.3868	1.121	398.1	102.9	62.0	143	0.720
950	0.3666	1.131	411.3	112.2	64.3	155	0.723
1000	0.3482	1.141	424.4	121.9	66.7	168	0.726
1100	0.3166	1.159	449.0	141.8	71.5	195	0.728
1200	0.2902	1.175	473.0	162.9	76.3	224	0.728
1300	0.2679	1.189	496.0	185.1	82	238	0.719
1400	0.2488	1.207	530	213	91	303	0.703
1500	0.2322	1.230	557	240	100	350	0.685
1600	0.2177	1.248	584	268	106	390	0.688
1700	0.2049	1.267	611	298	113	435	0.685
1800	0.1935	1.286	637	329	120	482	0.683
1900	0.1833	1.307	663	362	128	534	0.677
2000	0.1741	1.337	689	396	137	589	0.672
2100	0.1658	1.372	715	431	147	646	0.667
2200	0.1582	1.417	740	468	160	714	0.655
2300	0.1513	1.478	766	506	175	783	0.647
2400	0.1448	1.558	792	547	196	869	0.630
2500	0.1389	1.665	818	589	222	960	0.613
3000	0.1135	2.726	955	841	486	1570	0.536

Air properties at atmospheric pressure

**TABLE A.4** *Continued*

$T$ (K)	$\rho$ (kg/m <sup>3</sup> )	$c_p$ (kJ/kg · K)	$\mu \cdot 10^7$ (N · s/m <sup>2</sup> )	$\nu \cdot 10^6$ (m <sup>2</sup> /s)	$k \cdot 10^3$ (W/m · K)	$\alpha \cdot 10^6$ (m <sup>2</sup> /s)	$Pr$
<b>Hydrogen (H<sub>2</sub>) (continued)</b>							
600	0.04040	14.55	142.4	352	305	519	0.678
700	0.03463	14.61	157.8	456	342	676	0.675
800	0.03030	14.70	172.4	569	378	849	0.670
900	0.02694	14.83	186.5	692	412	1030	0.671
1000	0.02424	14.99	201.3	830	448	1230	0.673
1100	0.02204	15.17	213.0	966	488	1460	0.662
1200	0.02020	15.37	226.2	1120	528	1700	0.659
1300	0.01865	15.59	238.5	1279	568	1955	0.655
1400	0.01732	15.81	250.7	1447	610	2230	0.650
1500	0.01616	16.02	262.7	1626	655	2530	0.643
1600	0.0152	16.28	273.7	1801	697	2815	0.639
1700	0.0143	16.58	284.9	1992	742	3130	0.637
1800	0.0135	16.96	296.1	2193	786	3435	0.639
1900	0.0128	17.49	307.2	2400	835	3730	0.643
2000	0.0121	18.25	318.2	2630	878	3975	0.661
<b>Nitrogen (N<sub>2</sub>)</b>							
100	3.4388	1.070	68.8	2.00	9.58	2.60	0.768
150	2.2594	1.050	100.6	4.45	13.9	5.86	0.759
200	1.6883	1.043	129.2	7.65	18.3	10.4	0.736
250	1.3488	1.042	154.9	11.48	22.2	15.8	0.727
300	1.1233	1.041	178.2	15.86	25.9	22.1	0.716
350	0.9625	1.042	200.0	20.78	29.3	29.2	0.711
400	0.8425	1.045	220.4	26.16	32.7	37.1	0.704
450	0.7485	1.050	239.6	32.01	35.8	45.6	0.703
500	0.6739	1.056	257.7	38.24	38.9	54.7	0.700
550	0.6124	1.065	274.7	44.86	41.7	63.9	0.702
600	0.5615	1.075	290.8	51.79	44.6	73.9	0.701
700	0.4812	1.098	321.0	66.71	49.9	94.4	0.706
800	0.4211	1.22	349.1	82.90	54.8	116	0.715
900	0.3743	1.146	375.3	100.3	59.7	139	0.721
1000	0.3368	1.167	399.9	118.7	64.7	165	0.721
1100	0.3062	1.187	423.2	138.2	70.0	193	0.718
1200	0.2807	1.204	445.3	158.6	75.8	224	0.707
1300	0.2591	1.219	466.2	179.9	81.0	256	0.701

Nitrogen properties at atmospheric pressure



---

## Appendix B

This appendix includes tables for calculations of the combined wick.

---

**Table 18: Performance of a 20cm 10 layer combined wick**

Heat Flux (kW/m <sup>2</sup> )	Wick2 length (cm)	Total pressure drop (Pa)
100	14.9	1890
150	13.4	2308
170	12.9	2508
180	12.6	2630
200	12.1	2873

**Table 19: Performance of a 25cm 10 layer combined wick**

Heat Flux (kW/m <sup>2</sup> )	Wick2 length (cm)	Total pressure drop (Pa)
20	17.3	1965
40	16.3	2182
60	15.4	2444
70	15	2591
80	14.5	2772

**Table 20: Performance of a 30cm 10 layer combined wick**

Heat Flux (kW/m <sup>2</sup> )	Wick2 length (cm)	Total pressure drop (Pa)
10	17.6	2327
20	17	2520
30	16.3	2744

**Table 21: Performance of a 20cm 12 layer combined wick**

Heat Flux (kW/m <sup>2</sup> )	Wick2 length (cm)	Total pressure drop (Pa)
50	16.8	1578
100	15.4	1785
150	14.1	2083
200	13	2471
220	12.5	2670
250	11.9	2981

**Table 22: Performance of a 25cm 12 layer combined wick**

Heat Flux (kW/m <sup>2</sup> )	Wick2 length (cm)	Total pressure drop (Pa)
20	17.5	1933
40	16.6	2105
60	15.9	2302
80	15.1	2550
90	14.7	2687

---

**Table 23: Performance of a 30cm 12 layer combined wick**

Heat Flux (kW/m <sup>2</sup> )	Wick2 length (cm)	Total pressure drop (Pa)
10	17.8	2295
20	17.2	2453
30	16.7	2626
40	16.2	2815

**Table 24: Performance of a 20cm 15 layer combined wick**

Heat Flux (kW/m <sup>2</sup> )	Wick2 length (cm)	Total pressure drop (Pa)
100	16	1690
150	14.9	1890
200	13.9	2150
250	13	2471
270	12.6	2628
300	12.1	2873

**Table 25: Performance of a 25cm 15 layer combined wick**

Heat Flux (kW/m <sup>2</sup> )	Wick2 length (cm)	Total pressure drop (Pa)
20	17.6	1904
60	16.3	2180
90	15.4	2448
110	14.8	2657
120	14.5	2771

**Table 26: Performance of a 30cm 15 layer combined wick**

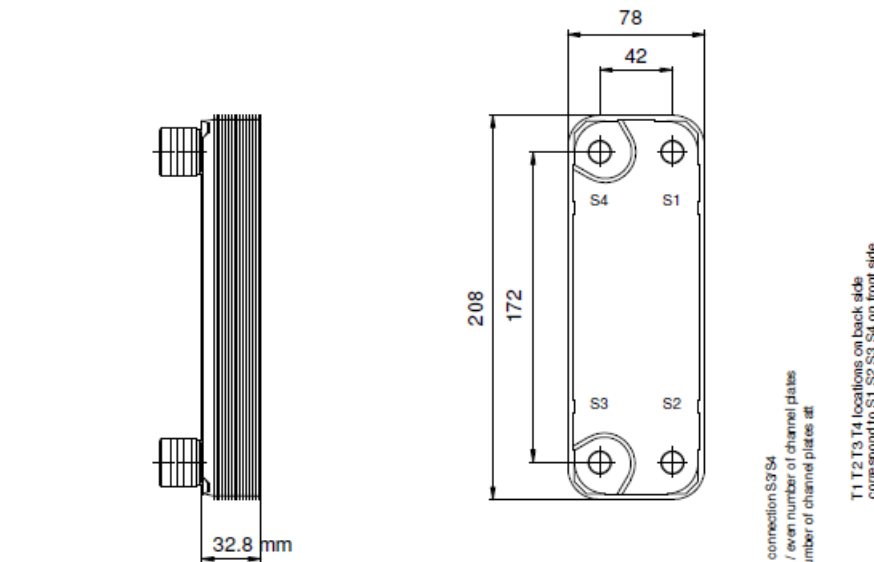
Heat Flux (kW/m <sup>2</sup> )	Wick2 length (cm)	Total pressure drop (Pa)
10	17.9	2266
20	17.4	2389
30	17	2521
40	16.6	2662
50	16.2	2814

---

## Appendix C

This appendix contains specifications of the plate heat exchanger, side channel blower, control valve, tracing, rockwool and calibration certificate for the insertion mass flow meter. All information are given from the producer of the components.

Plate package length upper tolerance +/-3.0 mm



Frameplate is depressed 2 mm at connection S3/S4  
 Pressedplate is depressed 2 mm / even number of channel plates  
 all connections T3/T4 / une en number of channel plates at  
 connections T1/T2.

T1, T2, T3, T4 locations on back side  
 correspond to S1, S2, S3, S4 on front side

ALL DIMENSIONS IN MILLIMETERS

HEATING SURFACE	0.1040 m <sup>2</sup>	PLATE MATERIAL	Alloy 316	TOTAL LENGTH	56.8
NETWEIGHT	1.200 kg	PLATE THICKNESS	0.3 mm	TOTAL WIDTH	77.0
OPERATING WEIGHT	1.200 kg	PLATE GROUPING	1*5H/1*4H	TOTAL HEIGHT	207.0

MEDIA	INLET	OUTLET	TEMP. °C	TEMP. °C	FLOW RATE kg/s	PRESSURE DROP kPa	LIQUID VOL. dm <sup>3</sup>
Nitrogen Water	S1	S2	200.0 °C	25.0 °C	0.004931 kg/s	4.277 kPa	0.08000 dm <sup>3</sup>
	S3	S4	15.0 °C	25.0 °C	0.02147 kg/s	0.3055 kPa	0.1000 dm <sup>3</sup>

SUPPLIER	REF.	MP NO.	PLATE HEAT EXCHANGER		
AGENT / REF.			AlfaNova 14-10H		
CUSTOMER NAME / REF. NO.					ITEM ID: 32870 5066 1
SIGN.			PED		DATE: 2010-07-15

# Daten



A Thomas Industries Company



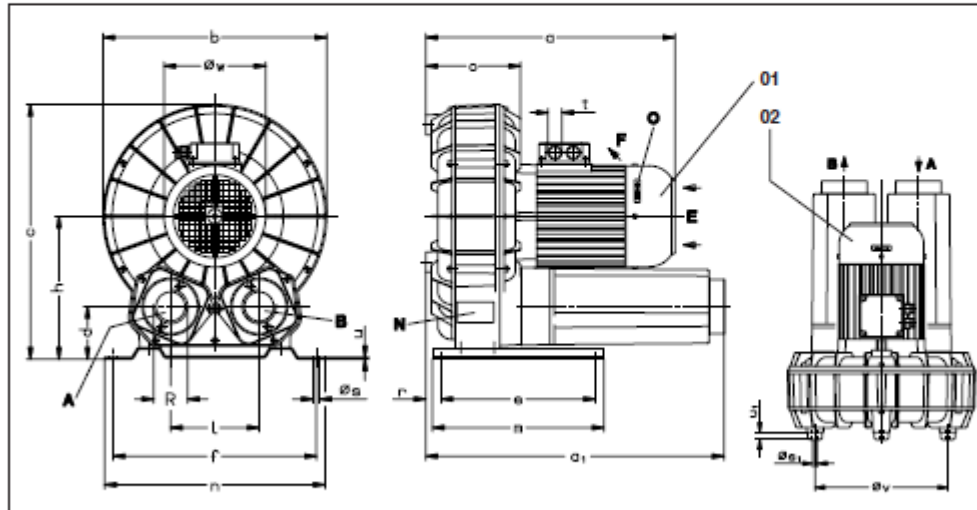
Seitenkanal-Verdichter

Side channel compressors

Turbine latérale pression

Compressori a canali laterali

SAH



- SAH 25
- SAH 45
- SAH 55
- SAH 75
- SAH 95

01	Normal-Ausführung Vertikal-Ausführung	Standard version Vertical version	Exécution standard Exécution verticale	Esecuzione standard Esecuzione verticale
A	Ansaug-Anschluß	Suction connection	Raccord d'aspiration	Attacco aspirazione
B	Druck-Anschluß	Pressure connection	Raccord surpression	Attacco pressione
E	Kühlluft-Eintritt	Cooling air entry	Entrée air refroidissement	Entrata aria di raffreddamento
F	Kühlluft-Austritt	Cooling air exit	Sortie air refroidissement	Uscita aria di raffreddamento
N	Datenschild	Data plate	Etiquette caractéristique	Targhetta dati
O	Drehrichtungsschild	Direction of rotation	Flèche sens rotation	Targhetta senso rotazione

SAH	25	45	55	75	95
a	3- 312 1- 350	335 350	343 378	344 # 379	377 381 377 416
a <sub>i</sub>	337	375	388	389	445
b	238	255	296	282	336
c	269	299	324	322	385
d / h	58 / 150	68 / 171	68 / 181	68 / 181	80 / 215
e / f	220 / 226	220 / 226	220 / 226	220 / 226	270 / 275
m / n	240 / 246	240 / 246	240 / 246	240 / 246	300 / 305
l	104	110	110	110	133
o / r	117 / 37	127 / 24	141 / 15	142 / 16	141 / 23
os / os <sub>i</sub>	11 / M8	11 / M8	11 / M8	11 / M8	11 / M8
t	M 20 x 1,5	M 20 x 1,5	M 20 x 1,5	M 20 x 1,5	M 20 x 1,5
u / u <sub>i</sub>	2 / 20	2 / 20	2 / 20	2 / 20	3 / 30
øv	190	204	230	230	290
øw	139	139	157	157	157 178
R	G 1	G 1 1/4	G 1 1/2	G 1 1/2	G 2

ZRK		25 (03)	32 (03)	40 (03)	40 (03)	50 (03)
ZED / ZUV / ZBD	50 Hz	-	ZUV 32	ZBD 40	ZBD 40	ZBD 40
	60 Hz	ZED 25	ZUV 32	ZBD 40	ZBD 40	ZBD 40
ZAF		25 (00)	32 (00)	40 (00)	40 (00)	50 (00)
ZGD		25 (06)	32 (06)	40 (06)	40 (06)	50 (06)
ZFP		145 (06)	216 (07)	216 (06)	216 (06)	216 (01)
ZMS (3-)	50 Hz	25/16	25/16 40/25	40/25	40/25 63/40	63/40 100/63
	60 Hz	25/16	25/16 40/25	40/25	40/25 63/40	63/40 100/63
ZMS (1-)	50 Hz	40	40 63	100	# 100	100 100
	60 Hz	40	40 63	100	# 100	100 #
ZWS		61 (10)	61 (11)	61 (12)	61 (12)	83 (10)

ZRK	Zubehör Rückschlagventil	Optional extras Non-return valve	Accessoires Clapet anti-retour	Accessori Valvola di non ritorno
ZED-ZBD	Druck-Begrenzungsventil	Pressure limitation valve	Limiteur surpression	Valvola limitatrice di pressione
ZAF	Ansaugfilter	Suction filter	Filtre d'aspiration	Filtro di aspirazione
ZGD	Zusätzlicher Schalldämpfer	Additional silencer	Silencieux complémentaire	Silenziatore supplementare
ZFP	Staubabscheider	Dust separator	Filtre séparateur	Separatore polveri
ZMS	Motorschutzschalter	Motor starter	Disjoncteur moteur	Interruttore magnetotermico
ZWS	Wechselschaltung	Change over valve	Inverseur de débit	Valvola di inversione

D 656/1

4.7.2000

Rietschle Thomas  
GmbH + Co. KG

Postfach 1260

79642 SCHOPFHEIM

GERMANY

☎ 07622 / 392-0

Fax 07622 / 392300

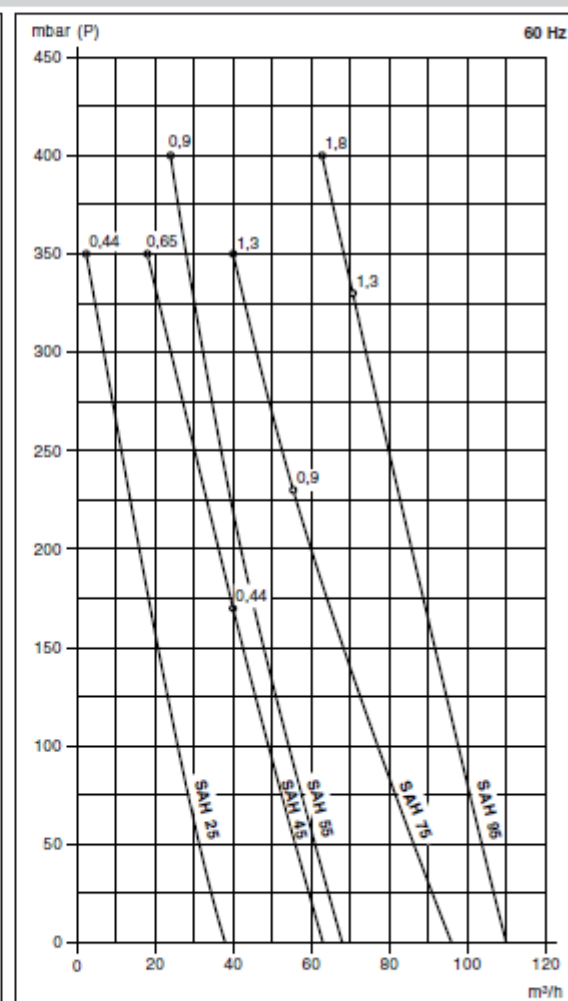
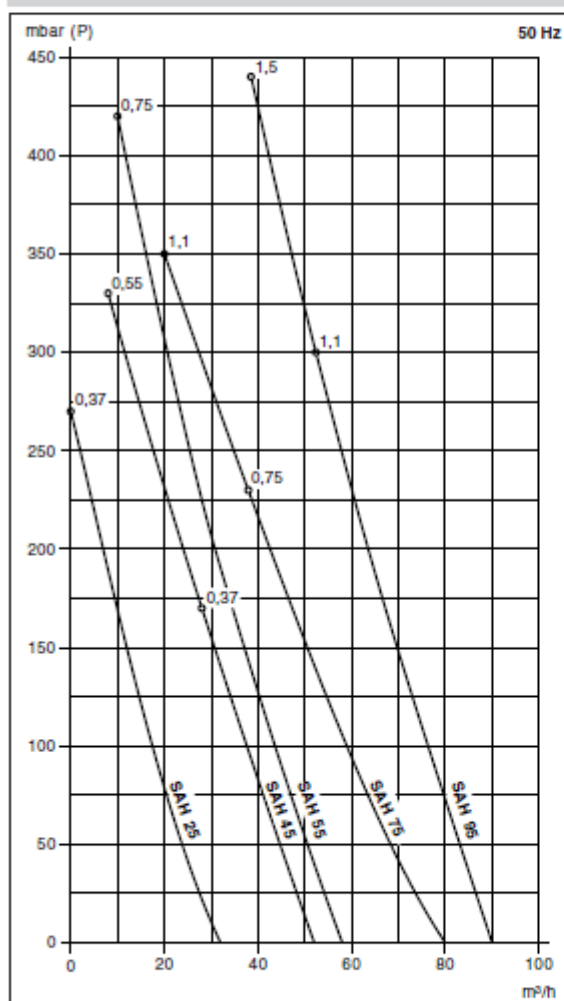
e-mail:

Info.sch@rtpumps.com

http://www.rietschle.com

SAH		25	45	55	75	95			
m³/h	50 Hz	32	52	58	80	90			
	60 Hz	38	63	68	98	110			
mbar (P)	50 Hz	270	170	330	420	230	350	300	440
	60 Hz	350	170	350	400	230	350	330	400
3-	50 Hz	200-255/346-440 V ± 5%							
	60 Hz	200-277/346-480 V ± 5%							
1-	50 Hz	230 V ± 10%							
	60 Hz	230 V ± 10%							
kW	50 Hz	0,37	0,37	0,55	0,75	1,1	1,1	1,5	
	60 Hz	0,44	0,44	0,65	0,90	0,90	1,3	1,8	
A (3-)	50 Hz	2,1/1,20	2,1/1,20	3,0/1,70	4,0/2,3	4,0/2,3	5,7/3,3	5,7/3,3	8,7/5,0
	60 Hz	2,1/1,20	2,1/1,20	3,46/2,0	4,0/2,3	4,0/2,3	6,1/3,5	5,7/3,3	7,7/4,5
A (1-)	50 Hz	3,0	3,7	4,3	6,9	#	9,2	9,2	9,5
	60 Hz	3,0	3,5	5,6	6,1	#	8,4	7,9	#
min⁻¹	50 Hz	2850							
	60 Hz	3450							
dB(A)	50 Hz	57	59	60	60	61	62	63	63,5
	60 Hz	61	62	63	63	63	64	67	67,5
kg	3-	16	18	19	23,5	25,5	26,5	31	34
	1-	16,5	20	20	24,5	25,5	26,5	31	34

m³/h	Volumenstrom	Capacity	Volume engendré	Portata volumetrica
mbar	Druckdifferenz	Pressure difference	Pression différentielle	Differenza di pressione
P	Druckbetrieb	Pressure operation	Fonction surpression	Pressione di esercizio
3-/1-	Motorausführung	Motor version	Exécution moteur	Esecuzione motore
kW	Motorleistung	Motor rating	Puissance moteur	Potenza motore
A	Stromaufnahme	Current drawn	Intensité absorbée	Corrente nominale
min⁻¹	Drehzahl	Speed	Vitesse rotation	Numero giri
dB(A) → DIN 45635	Mittlerer Schalldruckpegel (Ansaugung über Schlauchleitung)	Average noise level (Inlet connected to a pipeline)	Niveau sonore moyen (Aspiration au travers d'un tuyau)	Rumorosità media (Aspirazione tramite tubazione flessibile)
kg	Max. Gewicht	Maximum weight	Poids maxi.	Peso massimo



Die Kennlinien haben eine Toleranz von ± 10% und beziehen sich auf freie atmosphärische Luft von 1 bar (abs.) und 20°C./ The curves have a tolerance of ± 10% and refer to free atmospheric air at 1 bar (abs.) and 20°C./ Les courbes ont une tolérance de ± 10% et sont établies à l'atmosphère de 1 bar (abs.) à 20°C./ Le curve hanno una tolleranza del ± 10% e si riferiscono alla pressione atmosferica di 1 bar (ass.) a 20°C.

Technische Änderungen vorbehalten! / We reserve the right to alter technical information! / Sous réserve de modification technique! / Salvo modifiche tecniche! / # auf Anfrage / # on request / # sur demande / # a richiesta

## Electric Actuator Type 3374



### Application

Electric actuator designed for use in industrial plants and in heating, ventilation and air-conditioning systems.



The Type 3374 Electric Actuators are linear actuators available with or without fail-safe action. They can be combined with valves from various SAMSON series.

### Special features:

- 15 or 30 mm travel
- Voltage supply 230 V or 24 V with 50 Hz or 60 Hz or 110 V/60 Hz
- Synchronous motor with planetary gear
- Motor switched off by torque-dependent switches
- Mechanical override

### Standard version

**Type 3374** - Actuator optionally available with either integrated yoke or central attachment using a M30 x 1.5 ring nut including necessary coupling parts.

**Typetested version** - Actuator with fail-safe action "actuator stem extends" for various SAMSON valves. Register number available on request.

### Further versions with

- Two adjustable two-way limit switches
- Two potentiometers

### Digital positioner

- Automatic travel calibration
- Different operating modes can be selected using selector switch

Setting by means of TROVIS-VIEW:

- Additional functions can be set and transferred using a PC or a memory pen
- Characteristic either linear, equal percentage or freely determinable by entering the desired points
- Priority position
- Action selectable when input signal fails

No further potentiometers are available for version with digital positioner.



Fig. 1 - Type 3374 Electric Actuator with integrated yoke attached to V2001 Globe Valve



### Principle of operation

The electric actuators consist of a reversible synchronous motor and a maintenance-free planetary gear with ball screw. The motor is switched off by torque-dependent switches when the end positions are reached or in case of overload.

The Type 3374 Actuators with integrated yoke (Fig. 3a) are primarily combined with the following valves:

- V2001 Series
- Type 3260 in DN 65 to DN 150
- Type 3214 in DN 65 to DN 100.

The Type 3374 Actuators with central attachment are primarily combined with valves with yokes of their own:

- Series 240 (Fig. 3b)
- Type 3214 in DN 125 to 250 (Fig. 3c)

### Fail-safe action

The Type 3374 Actuators are optionally available with fail-safe action:

#### Actuator stem extends

Upon the power supply failure, the actuator stem extends

#### Actuator stem retracts

Upon the power supply failure, the actuator stem retracts

### Ordering text

Electric Actuator	Type 3374- ...
Rated travel	15 or 30 mm
Version with fail-safe action	Actuator stem extends or retracts only with 15 mm travel
Electrical connection	230 V/50 Hz or 60 Hz, 24 V/50 Hz or 60 Hz or 110 V/60 Hz

Additional electrical equipment (see Table 1)

Two limit switches	
Two potentiometers	0 to 1000 $\Omega$
Digital positioner	

Specifications subject to change without notice.

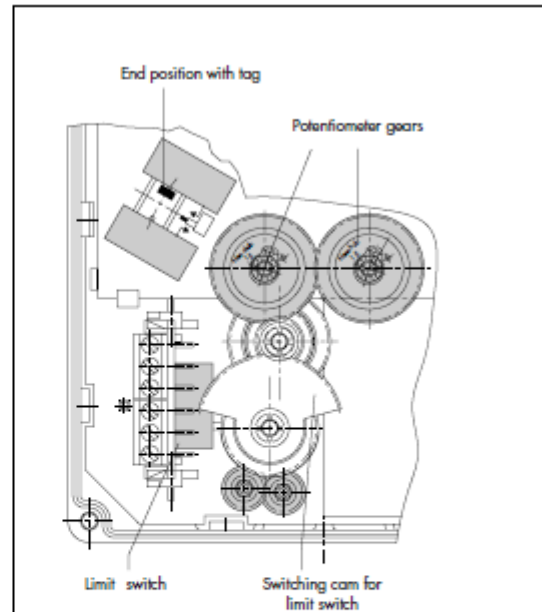
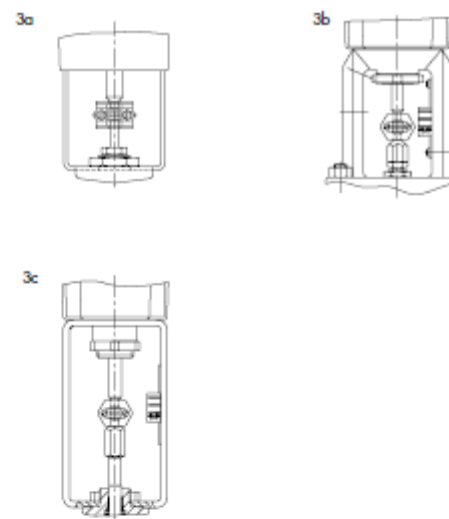


Fig. 2 - Partial view with opened cover



With integrated yoke for  
3a - V2001 Series, Type 3260 (DN 65 to DN 150)  
Type 3214 (DN 65 to DN 100)

With central attachment for  
3b - Series 240  
3c - Type 3214 (DN 125 to DN 250)  
Series 240 (Type 3241 and Type 3244)

Fig. 3 - Attachment to various valves



Postboks 166 Bragernes, 3001 Drammen  
Tlf. 32 21 21 21, Fax 32 21 21 99, www.pettersen.no

## PTFE insulated heating tape series MIL-HT-CN

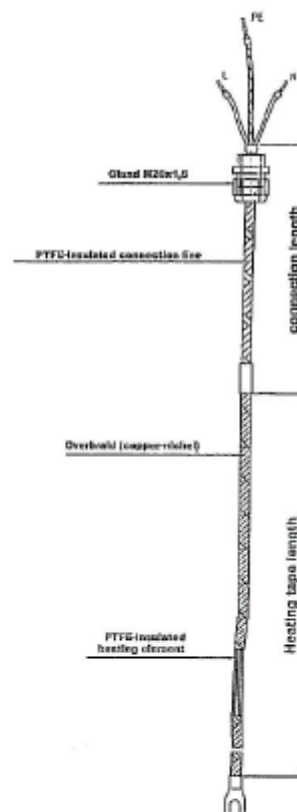
Max. surface temperature 250 °C

For application in : **Industrial plants**  
**Chemical industries**  
**Research and Development**  
**Process engineering**

**Product description:** This PTFE-insulated and factory ready-to-use heating tape has an overbraid copper-nickel wire for application temperature up to 250 °C.

### Important characteristics:

- very flexible
- easy to install
- inexpensive
- single-sided connection



### Application examples:

This tape is suitable for heating pipes, pumps, and process heating at laboratory plants to a maximum temperature of 250 °C.

This product is also suitable to hold chemical and oil liquids at a constant temperature.

## Technical data

Nominal Voltage	230	V AC
Nominal Wattage	35-50	W /m
Dimensions	ca. 4x8	mm
Protection class	I	
System of protection	IP 65	
Max. temperature	250	°C
Connection length	1,5	m
Gland	M20x1,5	Skintop

## Standard lengths and loadings table

Nominal power output  
approx. 35 W / m

Length (m)	W	V	Part No.
1,9	67	230	11000019
2,7	95	230	11000027
3,9	137	230	11000039
5,0	175	230	11000050
6,0	210	230	11000060
7,0	245	230	11000070
8,1	284	230	11000081
9,1	319	230	11000091
10,3	361	230	11000103
12,6	441	230	11000126
13,8	483	230	11000138
17,4	609	230	11000174
20,8	728	230	11000208
24,5	858	230	11000245
28,0	980	230	11000280
33,5	1173	230	11000335
42,0	1470	230	11000420

Nominal power output  
approx. 50 W / m

Length (m)	W	V	Part No.
2,3	115	230	11100020
4,2	210	230	11100040
7,6	380	230	11100080
9,6	480	230	11100100
12,5	625	230	11100120
16,0	800	230	11100150
20,5	1025	230	11100200
23,0	1150	230	11100250
28,0	1400	230	11100300
35,0	1750	230	11100350

Other lengths and power specifications available upon request.



Application type	Thermal, acoustic
Construction type	Roofs and ceilings

**ROCKWOOL**

## Roll

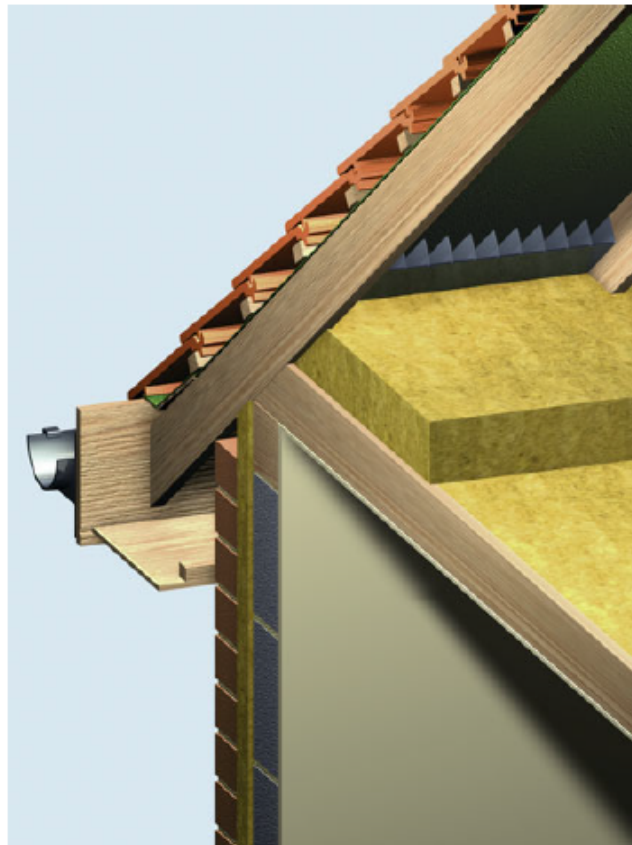
Thermal insulation for lofts. Acoustic insulation for suspended ceilings

Rockwool Roll is a medium density multi-application insulation mat.

This versatile Roll is suitable for thermal insulation of roof spaces in domestic, commercial and industrial buildings. It is also useful for improving the acoustic performance of suspended ceilings.

Roll is produced in 1200mm width. The packaging provides cutting guidelines should the product be required in 400mm or 600mm widths. By cutting through the product with a long serrated blade, this will ensure the material can be cut to the desired widths.

Alternatively, Rollbatt is supplied pre-cut to 400mm (x3) or 600mm (x2) widths.



Double layer insulation in a loft space using Rockwool Roll

### Advantages

- Multi-application product
- Fire, thermal and acoustic properties
- Easy to cut and use for 400 and 600 mm centres
- Higher density provides superb fit



The following NBS Plus clauses include Rockwool Roll: K10:215, K10:225, K10:235, K11:115, K11:125, K11:135, K11:145, K20:150, K20:160, K21:120, K21:130, K40:105, K40:110, K40:130, K40:226, P10:140, P10:250



## Description, performance and properties

### Description

#### Dimensions

Rockwool Roll is manufactured at 1200 mm width. Rollbatt is manufactured at 400 mm (x3) or 600 mm (x2) widths.

Thickness* (mm)	Roll length (mm)
100	4800
150	3200
170	2800

### Standards & approvals

Rockwool Roll conforms to BS EN 13162:2001 'Specification for factory-made mineral wool products'.

### Performance and properties

#### Fire Classification

Rockwool Roll achieves a reaction to fire classification of A1 as defined in BS EN 13501-1.

#### Acoustic

The incorporation of Rockwool Roll within suitably designed constructions can provide improved levels of sound reduction.

### Compatibility

Rockwool will not react with any metal components in the loft, nor will it cause loss of plasticiser from PVC cables and pipes (see also the note on electrical cables below).

### Watertanks

Insulation should not be placed directly under the cold water tank. Where access is required to water tanks etc, supports should be provided for a raised walkway.

### Loft hatches

To preserve continuity of insulation, covers to loft hatches should be insulated with a minimum 100 mm thickness of Rockwool Roll. Double-sided adhesive tape may be used to hold the insulation in place.

### Electrical cables

The IEE Wiring Regulations, 16th edition, British Standard BS 7671: 2001 and the Electricians' Handbook (latest edition) give guidance on the correction factors to be applied in down-rating cables according to situation, and each case should be separately calculated. Where possible, all cables should be lifted free of the insulation.

### Handling and storage

Rockwool Roll is very light and easy to handle. It is supplied palletised, protected by a waterproof covering which allows the product to be stored outside.

### Ordering

Rockwool Roll: Please quote area and thickness required.

### Environment

Relying on entrapped air for its thermal properties, Rockwool insulation does not contain (and has never contained) gases that have Ozone Depleting Potential (ODP) or Global Warming Potential (GWP). Rockwool therefore complies with the relatively modest threshold of GWP<5 included in documents such as the Code for Sustainable Homes.

Rockwool Ltd is increasingly involved in recycling waste Rockwool material that may be generated during installation or at end of life disposal. We are happy to discuss the individual requirements of contractors and users considering returning Rockwool materials to our factory for recycling.



## Thermal performance and U-values

### Thermal application

#### Thermal Performance

Rockwool Roll has a thermal conductivity (k value) of 0.044W/mK.

#### Installation

Part L: 2006 edition requires new pitched roofs with loft spaces to achieve U values between 0.16 and 0.11W/m<sup>2</sup>K. To meet this thermal performance and minimise heat loss through the timbers, Rockwool Roll should be cross-layered between and over the ceiling joists.

The first layer (generally of 100 mm thickness) is rolled between the ceiling joists, which are normally spaced at 400 mm or 600 mm centres. A second layer of Rockwool Roll (e.g. 170 mm thick) is then cross-layered to cover the first layer of insulation and the ceiling joists (see fig 1).

If upgrading loft insulation, check to see if existing insulation between joists is tightly butt jointed to sides of timber. If not, remove and replace as above. If the existing insulation is in good condition, cross-layer this with a minimum of 170 mm Rockwool Roll.

### U-values

100mm Rockwool Roll between joists (with the additional thickness of Rockwool Roll laid over joists shown in table below).

Ceiling joist joist spacing	38x100 mm		47x100 mm	
	400 mm	600 mm	400 mm	600 mm
RW Roll Thickness (mm)	U-values W/m <sup>2</sup> K		U-values W/m <sup>2</sup> K	
100	0.22	0.21	0.22	0.21
150	0.17	0.17	0.17	0.17
170	0.16	0.16	0.16	0.16
200 (100+100)	0.15	0.14	0.15	0.15
250 (100+150)	0.12	0.12	0.13	0.12
300 (150+150)	0.11	0.11	0.11	0.11

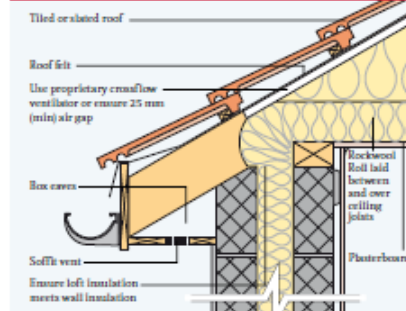


Figure 2

### Health and safety

Current HSE 'CHIP' Regulations and EU directive 97/69/EC confirm the safety of Rockwool mineral wool; Rockwool fibres are not classified as a possible human carcinogen.

The maximum exposure limit for mineral wool is 5mg/m<sup>3</sup>, 8 hour time-weighted average.

A Material Safety Data Sheet is available from Rockwool Customer Support (0871 222 1780) to assist in the preparation of risk assessments, as required by the Control of Substances Hazardous to Health Regulations (COSHH).

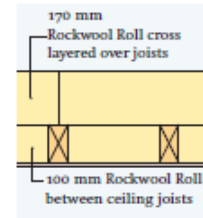


Figure 1 Cross layered roll U value 0.16W/m<sup>2</sup>

### Specification Clause

Thermal insulation to be Rockwool Roll 600 or 400 mm wide (delete whichever is not appropriate). The first layers fitted between ceiling joists ..... mm (insert 100, 150 or 170). The additional layer(s) .....mm (insert 100, 150 or 170) to be cross layered over ceiling joists, with all joists to be closely butted.

### More information

For further details visit our website at [www.rockwool.co.uk](http://www.rockwool.co.uk).

Rockwool Limited reserves the right to alter or amend the specification of products without notice as our policy is one of constant improvement.

The information contained in this data sheet is believed to be correct at the date of publication. Whilst Rockwool will endeavour to keep its publications up to date, readers will appreciate that between publications there may be pertinent changes in the law, or other developments affecting the accuracy of the information contained in this data sheet.

The applications shown do not necessarily represent an exhaustive list of applications for Roll. Rockwool Limited does not accept responsibility for the consequences of using Roll in applications different from those described above. Expert advice should be sought where such different applications are contemplated, or where the extent of any listed application is in doubt.

## ROCKWOOL

Rockwool Limited  
Pencoed, Bridgend, CF35 6NW  
26/28 Hammersmith Grove  
Hammersmith  
London  
W6 7HA

info@rockwool.co.uk  
[www.rockwool.co.uk](http://www.rockwool.co.uk)

Printed on recycled paper using environmentally friendly processes





**SIERRA**  
EXPERIENCE OUR PASSION FOR FLOW!

5 Harris Court, Building L / Monterey, CA 93944  
800.966.0200 / 831.373.0200  
fax: 831.373.4402  
www.sierrainstruments.com

# CALIBRATION CERTIFICATE

CERTIFICATE NUMBER **5532872115**

PAGE 1 OF 1

<b>Applicant/Customer</b>	<b>Name</b>	
	<b>Customer Address</b>	
	<b>City, State, Zip Code</b>	
	<b>Country</b>	
	<b>Sales Order</b>	120253
	<b>Purchase Order</b>	
<b>Instrument</b>	<b>Model</b>	620S-L04-M1-EN2-V4-NR-10
	<b>Serial number</b>	136685
	<b>Tag #:</b>	N/A
	<b>Input Power</b>	18-30 Volt DC
	<b>Factory F/S</b>	29.3125
	<b>User Full Scale</b>	23.45
	<b>Output signal</b>	4 20
	<b>Display</b>	N/A
	<b>Totalizer</b>	N/A
	<b>Alarm settings</b>	Low
	<b>Customer line size</b>	40.5mm
	<b>Accuracy DUT (+/-)</b>	1.0% F/S
<b>Calibration method</b>	<b>Calibration Station/Cal Due Date</b>	Flobot Asset # 0479 January 17, 2011
	<b>Calibration Procedure</b>	6440 Rev. D
	<b>Software release</b>	Flobot Calibration System, Rev. 1.01.13
	<b>Repeatability</b>	+/- 0.2% of full scale
	<b>Temperature coefficient</b>	+/- 0.02% of reading per °F within +/- 50°F of customer specified conditions
	<b>Pressure coefficient</b>	0.02% per psi for air, consult factory for other gases
	<b>System ERROR</b>	maximum systematic ERROR = 0.2%
	<b>DMM Asset / Cal Due Date</b>	1373 January 19, 2011
<b>Calibration details</b>	<b>Date of calibration</b>	October 28, 2010
	<b>Suggested recal date</b>	October 28, 2011
<b>Calibration data</b>	<b>Ambient pressure</b>	29.72 In Hg a.
	<b>Ambient temperature</b>	69.00 °F
	<b>Gas</b>	Nitrogen
	<b>Calibration gas</b>	Nitrogen
	<b>K-Factor</b>	1.000
	<b>Reference temperature</b>	15.0 °C
	<b>Reference pressure</b>	1 ATM
	<b>Calibration pressure</b>	1.20 Bar a.
	<b>Calibration temperature</b>	50.00 °C
	<b>Other</b>	
	<b>Special Calibration Information</b>	

**Calibration results**

Bridge	Output	Indicated Flow	Actual Flow	Difference	Difference
Voltage	4-20 mA	NM3/H	NM3/H	Allowable	Actual
3.383	4.000	0.000	0.0000	0.293	0.000
4.499	7.923	5.750	5.7120	0.293	0.038
4.895	12.000	11.725	11.6850	0.293	0.040
5.161	15.980	17.558	17.4910	0.293	0.067
5.367	19.980	23.421	23.3700	0.293	0.051

**Traceability**

Calibration of Sierra products is performed with equipment containing components which are tested and calibrated in accordance with ANSI/NCSL Z540 and/or ISO 17025 and are traceable to NIST. The results of this report relate only to the item calibrated or tested.

**Calibration technician**

*[Signature]*

**Q.C. Technician**

*[Signature]*

This calibration certificate shall not be reproduced, except in full, without the written approval of Sierra Instruments, Inc.

---

## Appendix D

This appendix includes the Risk Assessment Report for the heat pipe test rig done by the author and Ph.D. candidate Geir Hansen.

# Risk Assessment Report

## [Heat Pipe Testrigg]

<b>Prosjekttittel</b>	Heat Pipe
<b>Prosjektleder</b>	Erling Næss
<b>Enhet</b>	NTNU
<b>HMS-koordinator</b>	Erik Langørgen
<b>Linjeleder</b>	Olav Bolland
<b>Plassering</b>	
<b>Romnummer</b>	
<b>Riggansvarlig</b>	Geir Hansen
<b>Risikovurdering utført av</b>	Dan Adrian Odden / (Geir Hansen)



## TABLE OF CONTENTS

1	INTRODUCTION .....	2
2	ORGANISATION .....	2
3	RISK MANAGEMENT IN THE PROJECT .....	2
4	DRAWINGS, PHOTOS, DESCRIPTIONS OF TEST SETUP .....	3
5	EVACUATION FROM THE EXPERIMENT AREA.....	5
6	WARNING.....	6
6.1	Before experiments.....	6
6.2	Nonconformance.....	6
7	ASSESSMENT OF TECHNICAL SAFETY .....	7
7.1	HAZOP.....	7
7.2	Flammable, reactive and pressurized substances and gas .....	7
7.3	Pressurized equipment.....	7
7.4	Effects on the environment.....	7
7.5	Radiation .....	8
7.6	Usage and handling of chemicals. ....	8
7.7	EI safety (need to deviate from the current regulations and standards.) .....	8
8	ASSESSMENT OF OPERATIONAL SAFETY.....	8
8.1	Prosedure HAZOP .....	8
8.2	Operation and emergency shutdown procedure.....	8
8.3	Training of operators.....	8
8.4	Technical modifications.....	9
8.5	Personal protective equipment.....	9
	8.5.1 General Safety .....	9
8.6	Safety equipment .....	9
8.7	Special actions .....	9
9	QUANTIFYING OF RISK - RISK MATRIX .....	9
10	CONCLUSION .....	10
11	REGULATIONS AND GUIDELINES .....	11
12	DOCUMENTATION.....	12
•	VEDLEGG A HAZOP MAL.....	1
•	VEDLEGG F HAZOP MAL PROSEDYRE .....	1
•	VEDLEGG G FORSØKSPROSEDYRE .....	1
•	VEDLEGG H OPPLÆRINGSPLAN FOR OPPERATØRER .....	3
•	VEDLEGG I SKJEMA FOR SIKKER JOBBANALYSE SJA.....	
	APPARATURKORT UNITCARD .....	5

## 1 INTRODUCTION

The test rig facility consists of a heat pipe connected to a nitrogen cooling circuit. However, at present the rig will be run using a bypass tube instead of the actual Heat Pipe. What is to be tested is the cooling circuit for the Heat Pipe. The cooling circuit uses nitrogen, and the hot nitrogen flow is cooled with tap water in a plate heat exchanger. The cooling circuit is shown in Figure 1 and is described in chapter 4.

The purpose of the experiments is to study the dynamics and response time of the cooling circuit. Temperature effects due to regulating the rotational speed of the side channel blower and tracing, is also of interest.

## 2 ORGANISATION

Rolle	NTNU	Sintef
Lab Ansvarlig:	Morten Grønli	Harald Mæhlum
Linjeleder:	Olav Bolland	Lars Sørum
HMS ansvarlig: HMS koordinator HMS koordinator	Olav Bolland Erik Langørgen Bård Brandåstrø	Lars Sørum Harald Mæhlum
Romansvarlig:		
Prosjekt leder:	Erling Næss/Geir Hansen	
Ansvarlig riggoperatører:	Geir Hansen/Dan Adrian Odden	

## 3 RISK MANAGEMENT IN THE PROJECT

Hovedaktiviteter risikostyring	Nødvendige dokumentasjon	tiltak,	DATE
Prosjekt initiering	Prosjekt initiering mal		
Veiledningsmøte Guidance Meeting	Skjema for Veiledningsmøte med pre-risikovurdering		23.04.12
Innledende risikovurdering Initial Assessment	Fareidentifikasjon – HAZID Skjema grovanalyse		
Vurdering av teknisk sikkerhet Evaluation of technical security	Prosess-HAZOP Tekniske dokumentasjoner		24.04.2012
Vurdering av operasjonell sikkerhet Evaluation of operational safety	Prosedyre-HAZOP Opplæringsplan for operatører		24.04.2012
Sluttvurdering, kvalitetssikring Final assessment, quality assurance	Uavhengig kontroll Utstedelse av apparaturkort Utstedelse av forsøk pågår kort		

## 4 DRAWINGS, PHOTOS, DESCRIPTIONS OF TEST SETUP

The circulation of nitrogen in the cooling circuit is produced by a side channel blower type SAH. It can deliver a pressure of about 420 mBarg, see Figure 2.

The nitrogen gas passes through a pipe section with external heating using an electric heating band (tracing), it is heated to a temperature of 50 degrees Celsius at the inlet of the Heat Pipe, or in this case the inlet of the bypass tube.

The mass flow of nitrogen gas through the Heat Pipe condenser can be regulated with the control valve, speed control or with the bypass valve, see Figure 1. The mass flow of Nitrogen gas is measured with an Insertion Mass Flow Meter.

After the bypass tube the hot nitrogen gas is heat exchanged with tap water in a gasket free plate heat exchanger, and then enters the side channel blower again.

Figure 1 below shows the Process and Instrumentation Diagram (PID) for the Heat Pipe test rig. The safety chamber will not be in use during the experiments because the actual heat pipe is replaced with a bypass tube.

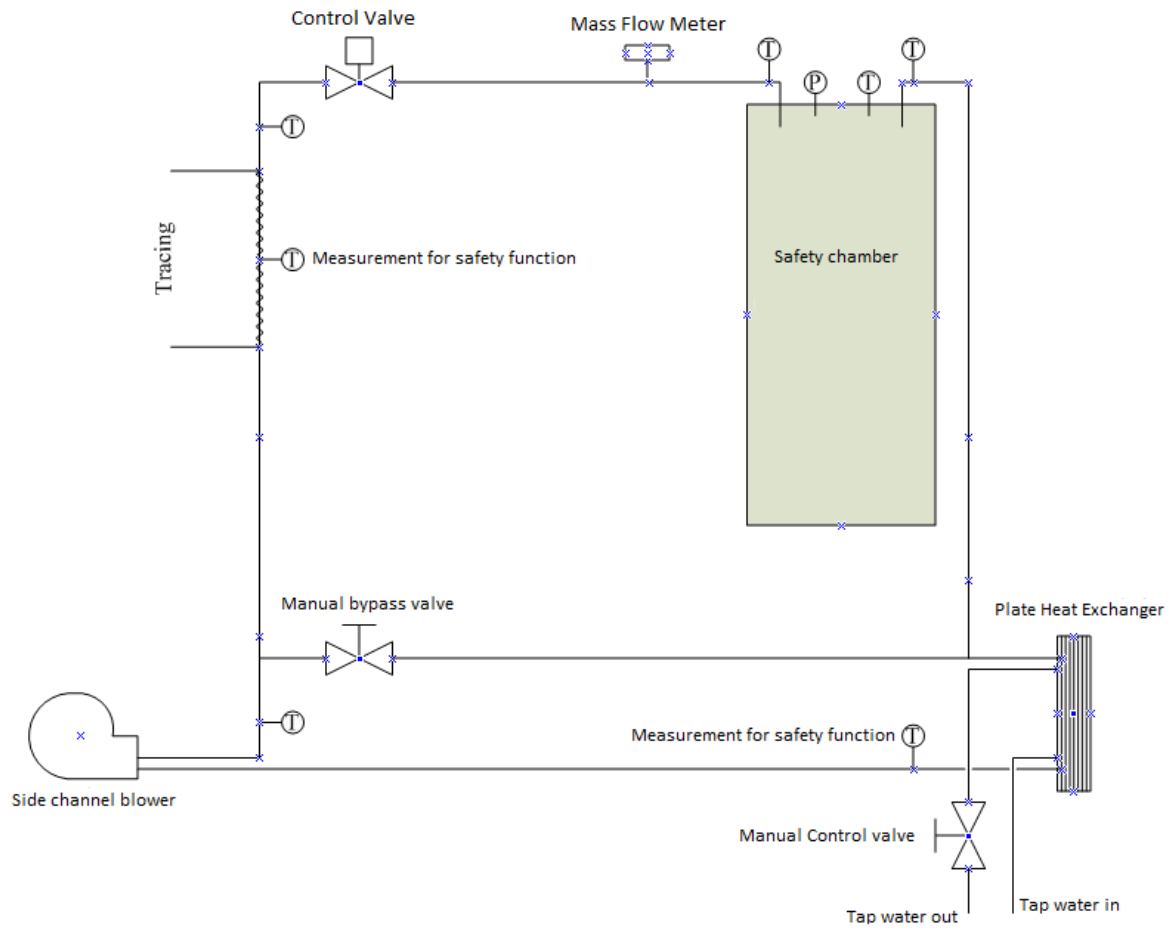


Figure 1

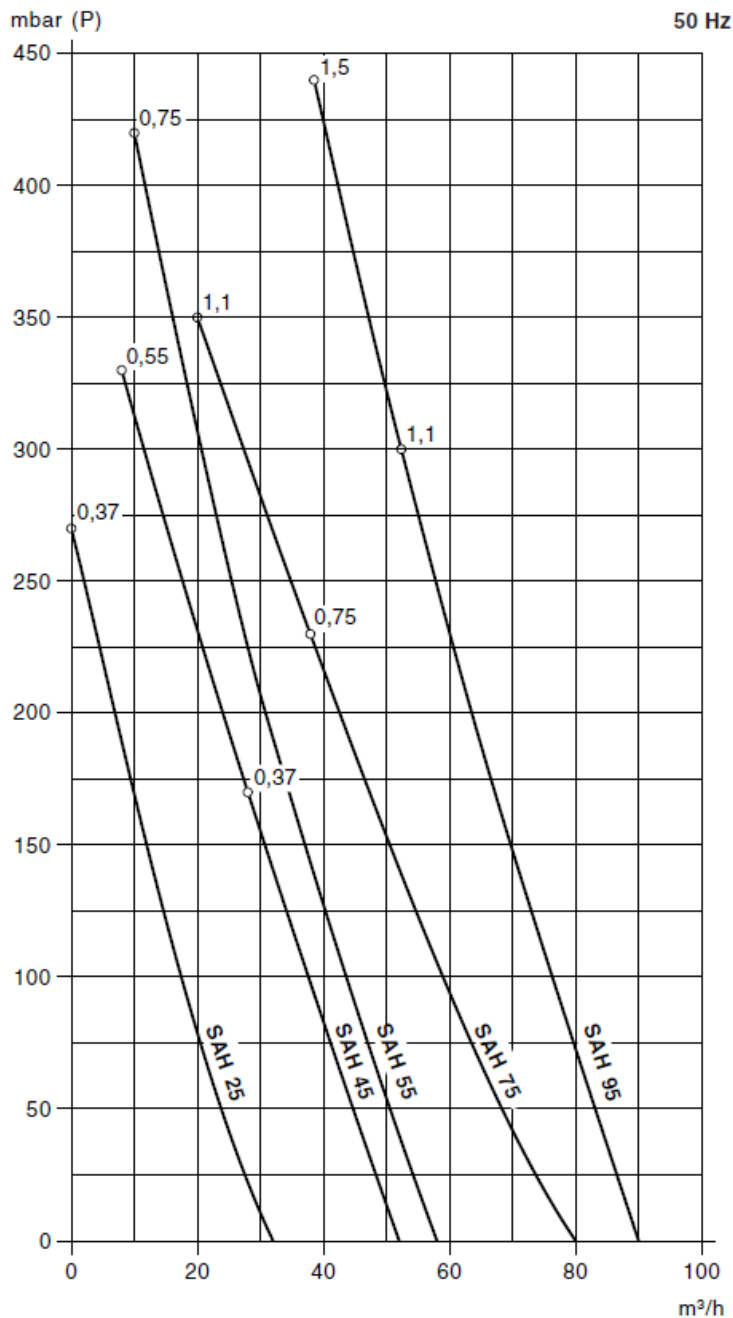


Figure 2

## 5 EVACUATION FROM THE EXPERIMENT AREA

Evacuate at signal from the alarm system or local gas alarms with its own local alert with sound and light outside the room in question, see 6.2

Evacuation from the rigging area takes place through the marked emergency exits to the assembly point, (corner of Old Chemistry Kjelhuset or parking 1a-b.)

**Action on rig before evacuation:**

Shut off the air and water supply. Power off the electrical supply.

## 6 WARNING

### 6.1 Before experiments

E-mail with information about the planned experiment to:

[iept-experiments@ivt.ntnu.no](mailto:iept-experiments@ivt.ntnu.no)

The e-mail should contain the following items:

- Name of responsible person:
- Experimental setup/rig:
- Start Experiments: (date and time)
- Stop Experiments: (date and time)

### 6.2 Nonconformance

#### FIRE

Fire you are not able to put out with locally available fire extinguishers, activate, the nearest fire alarm and evacuate area. Be then available for fire brigade and building caretaker to detect fire place.

If possible, notify:

NTNU	SINTEF
Labsjef Morten Grønli, tlf: 918 97 515	Labsjef Harald Mæhlum tlf 930 149 86
HMS: Erik Langørgen, tlf: 91897160	Forskningsjef Lars Sørnum tlf 928 049 25
HMS: Bård Brandåstrø, tlf918 97 257	
Instituttleder: Olav Bolland: 91897209	
NTNU Sintef Beredskapstelefon	800 80 388

#### GASALARM

At a gas alarm, close gas bottles immediately and ventilated the area. If the level of gas concentration does not decrease within a reasonable time, activate the fire alarm and evacuate the lab. Designated personnel or fire department checks the leak to determine whether it is possible to seal the leak and ventilate the area in a responsible manner.

Alert Order in the above paragraph.

#### PERSONAL INJURY

- First aid kit in the fire / first aid stations
- Shout for help
- Start life-saving first aid
- **CALL 113** if there is any doubt whether there is a serious injury

#### Other Nonconformance (AVVIK)

##### NTNU:

Reporting nonconformance, Innsida, avviksmelding:

[https://innsida.ntnu.no/lenkesamling\\_vis.php?katid=1398](https://innsida.ntnu.no/lenkesamling_vis.php?katid=1398)

##### SINTEF:

Synergi

## 7 ASSESSMENT OF TECHNICAL SAFETY

### 7.1 HAZOP

The experiment set up is divided into the following nodes:

Node 1	Nitrogen cooling circuit
--------	--------------------------

**Attachments: skjema: Hazop\_mal**

**Conclusion:**

### 7.2 Flammable, reactive and pressurized substances and gas

A leakage in the Heat Exchanger will lead to water entering the cooling circuit. This will result in water being dissolved in the nitrogen, and water droplets can be dragged with the nitrogen flow. The pressure in the circuit is then expected to increase. The main switch has to be turned off, and the water valve closed.

Experiment setup area should be reviewed with respect to the assessment of Ex zone:

- Zone 0: Always explosive atmosphere, such as inside the tank with gas, flammable liquid.
- Zone 1: Primary zone, sometimes explosive atmosphere such as a complete drain point
- Zone 2: secondary discharge could cause an explosive atmosphere by accident, such as flanges, valves and connection points

See Ex-zone map. Shall be made when ex-zones are present, with basis in P&ID.

**Conclusion:** Based on the above-mentioned zones, the plant is considered as a zone 2; secondary discharge site that can only get an explosive atmosphere by accident. It is not considered necessary to equip the plant with ex-proof equipment.

### 7.3 Pressurized equipment

No components should be under high pressure. The largest pressure at normal operating conditions is 1.3 bara in the cooling circuit (ref. Figure 1).

The side channel blower was leakage-tested at 1.5bara after being sealed (ref: Ph.D-candidate Geir Hansen). The low operating pressure of the cooling circuit will not present any dangers if a nitrogen leakage occurs.

**Conclusion: The test rig has been pressure tested and is ready for use.**

### 7.4 Effects on the environment

The experiments will not generate smoke, gas or special waste.

**Conclusion: No contamination to the environment**

### 7.5 Radiation

There is no danger of radiation in the test rig.

**Conclusion: No radiation**

### 7.6 Usage and handling of chemicals.

If a leak or error in the valves leads to nitrogen leakage, pure nitrogen gas has to be refilled in the cooling circuit. Nitrogen gas is in itself not dangerous (78% in air), but it can displace air, which can lead to lack of oxygen. Nitrogen is the only chemical that needs to be refilled. The volume of nitrogen to be used in the test is very small, so there is no danger with respect to suffocation.

**Attachments: MSDS**

**Conclusion: There is no use or production of hazardous chemicals at normal operating conditions.**

### 7.7 El safety (need to deviate from the current regulations and standards.)

NO

**Conclusion: All components are standard and are in accordance with current regulations.**

## 8 ASSESSMENT OF OPERATIONAL SAFETY

For ensuring that established procedures cover all identified risk factors that must be taken care of through procedures and ensure that the operators and technical performance have sufficient expertise.

### 8.1 Prosedure HAZOP

The method is a procedure to identify causes and sources of danger to operational problems.

**Attachments:** HAZOP\_MAL\_Proseedyre

**Conclusion:**

### 8.2 Operation and emergency shutdown procedure

The operating procedure is a checklist that must be filled out for each experiment. Emergency procedure should attempt to set the experiment set up in a harmless state by unforeseen events.

**Attachments:** Procedure for running experiments

**Emergency shutdown procedure:**

Shut off the air and water supply. Power off the electrical supply

### 8.3 Training of operators

All operators have to take the "HMS in laboratories"-course by TRAINOR in order to be allowed to perform experiments on the test rig.



**Attachments: “Opplæringsplan for operatører”**

#### 8.4 Technical modifications

No technical modifications are to be made without consulting the Technical staff. Replacements of components shall be made by Technical staff.

**Conclusion: Replacement of components and technical modifications should be made by Technical staff.**

#### 8.5 Personal protective equipment

- It is mandatory use of eye protection in the rig zone
- Use gloves when there is danger of contact with hot/cold surfaces.

##### 8.5.1 General Safety

- The area around the staging attempts shielded.
- Gantry crane and truck driving should not take place close to the experiment.
- Gas cylinders shall be placed in an approved carrier with shut-off valve within easy reach.

**Conclusion: The operator should be present when experiments are running.**

#### 8.6 Safety equipment

There is no need for portable gas detectors during test execution. However, a fire extinguisher shall be available during test execution.

#### 8.7 Special actions

During experiments the following special actions should be

- Monitoring.
- Safe Job Analysis of modifications, (SJA)

## 9 QUANTIFYING OF RISK - RISK MATRIX

The risk matrix will provide visualization and an overview of activity risks so that management and users get the most complete picture of risk factors.

IDnr	Aktivitet-hendelse	Frekv-Sans	Kons	RV
1	<i>Leakage of nitrogen could swirl dust on people operating the rig.</i>	1	B1	B1

**Conclusion :** *Participants will make a comprehensive assessment to determine whether the remaining risks of the activity / process is acceptable. Barriers and driving outside working hours e.g.*

## 10 CONCLUSION

The rig is built in good laboratory practice (GLP).

When the actual heat pipe is connected to the cooling circuit inside the safety chamber a new risk assessment has to be done. The heat pipe will present more possible dangers that need to be addressed.

Experiment unit card get a period of **XX months**

Experiment in progress card get a period of **XX months**

## 11 REGULATIONS AND GUIDELINES

Se <http://www.arbeidstilsynet.no/regelverk/index.html>

- Lov om tilsyn med elektriske anlegg og elektrisk utstyr (1929)
- Arbeidsmiljøloven
- Forskrift om systematisk helse-, miljø- og sikkerhetsarbeid (HMS Internkontrollforskrift)
- Forskrift om sikkerhet ved arbeid og drift av elektriske anlegg (FSE 2006)
- Forskrift om elektriske forsyningsanlegg (FEF 2006)
- Forskrift om utstyr og sikkerhetssystem til bruk i eksplosjonsfarlig område NEK 420
- Forskrift om håndtering av brannfarlig, reaksjonsfarlig og trykksatt stoff samt utstyr og anlegg som benyttes ved håndteringen
- Forskrift om Håndtering av eksplosjonsfarlig stoff
- Forskrift om bruk av arbeidsutstyr.
- Forskrift om Arbeidsplasser og arbeidslokaler
- Forskrift om Bruk av personlig verneutstyr på arbeidsplassen
- Forskrift om Helse og sikkerhet i eksplosjonsfarlige atmosfærer
- Forskrift om Høytrykksspyling
- Forskrift om Maskiner
- Forskrift om Sikkerhetsskilting og signalgivning på arbeidsplassen
- Forskrift om Stillaser, stiger og arbeid på tak m.m.
- Forskrift om Sveising, termisk skjæring, termisk sprøyting, kullbuemeisling, lodding og sliping (varmt arbeid)
- Forskrift om Tekniske innretninger
- Forskrift om Tungt og ensformig arbeid
- Forskrift om Vern mot eksponering for kjemikalier på arbeidsplassen (Kjemikalieforskriften)
- Forskrift om Vern mot kunstig optisk stråling på arbeidsplassen
- Forskrift om Vern mot mekaniske vibrasjoner
- Forskrift om Vern mot støy på arbeidsplassen

Veiledninger fra arbeidstilsynet

Se: <http://www.arbeidstilsynet.no/regelverk/veiledninger.html>

## 12 DOCUMENTATION

- Hazop\_mal
- HAZOP\_MAL\_Prosedeyre
- Forsøksprosedyre
- Opplæringsplan for operatører
- Skjema for sikker jobb analyse, (SJA)
- Apparatorkortet
- Forsøk pågår kort

# Vedlegg til Risikovurderingsrapport

[Heat Pipe Testrigg]

<b>Prosjekttittel</b>	Heat Pipe
<b>Prosjektleder</b>	Erling Næss
<b>Enhet</b>	NTNU
<b>HMS-koordinator</b>	Erik Langørgen
<b>Linjeleder</b>	Olav Bolland
<b>Riggnavn</b>	
<b>Plassering</b>	VATL Termisk lab
<b>Romnummer</b>	
<b>Riggansvarlig</b>	Erling Næss og Geir Hansen

---

## INNHOLDSFORTEGNELSE

- VEDLEGG A HAZOP MAL..... 1
- VEDLEGG F HAZOP MAL PROSEDYRE ..... 1
- VEDLEGG G FORSØKSPROSEDYRE ..... 1
- VEDLEGG H OPPLÆRINGSPLAN FOR OPERATØRER ..... 3
- VEDLEGG I SKJEMA FOR SIKKER JOBB ANALYSE..... 6
- VEDLEGG J APPARATURKORT UNITCARD..... 5

• VEDLEGG A HAZOP MAL

Project: Node: 1							Page
Ref #	Guideword	Causes	Consequences	Safeguards	Recommendations	Action	Date Sign
1	Malfunctioning temperature measurement in cooling circuit.	Electrical error, installation error, component error.	Possible overheating of heat exchanger and pump. Will lead to incorrect results and measurements.	-Multiple measurements and redundancy in heat measurements.	-Proper installation and redundant systems.		
2	No flow of cooling water.	Human error, loss of delivery pressure.	No cooling of the nitrogen gas in the cooling circuit. Can lead to overheating of the system.	-Temperature measurements in cooling circuit.	-Multiple temperature measurements.		
3	Leakage of water	Hole in the water/N2 heat exchanger. Hole in tubing.	Increased pressure in the nitrogen gas cooling circuit. Water spill on the floor.	Pressure measurement in the nitrogen circuit. Operator observations.	Water valve.		
4	More flow(N2)	Too low pressure drop for the system.	Too much cooling. Have to increase heat	Temperature measurement in the nitrogen			

Project: Node: 1							Page
Ref #	Guideword	Causes	Consequences	Safeguards	Recommendations	Action	Date Sign
5	Less flow(N2)	Too high pressure drop for the system.	load (tracing) to compensate for increased cooling.  Too little cooling. Inlet temperature of nitrogen on bypass tube too high. Have to reduce heat load (tracing).	circuit.  Temperature measurements before and in flow meter.			
	Malfunctioning flow-meter	Incorrect installation	Ref: 4 and 5				
	More viscosity	Not applicable					
	Less viscosity	Not applicable					
	Composition Change	Not applicable					
	Contamination	Not applicable					
	Relief	Not applicable					
	Instrumentation	Electrical error.	Shut down of the experiment.	Electrical emergency stop.			



Project: Node: 1								Page
Ref #	Guideword	Causes	Consequences	Safeguards	Recommendations	Action	Date Sign	
			Danger of contact with instruments.					
	Sampling	Not applicable						
	Corrosion/erosion	Not applicable						
	Service failure	Not applicable						
	Abnormal operation	Human error.	System failure. Failed experiment, shut down of experiment.	Training of operators.				
	Maintenance	Not applicable						
	Ignition	Not applicable						
	Spare equipment	Not applicable						

- VEDLEGG F HAZOP MAL PROSEDYRE

Project: Node: 1		Page					
Ref #	Guideword	Causes	Consequences	Safeguards	Rec#	Recommendations	Action
	Unclear	Procedure is made to ambitious or is characterized by confusion.	System failure. Breakdown.	Stepwise progress.			
	Step on wrong place	The procedure will lead to actions being performed in incorrect sequence.	System failure. Breakdown.	An operational start up procedure is made.			
	Wrong action	The procedures action is incorrect specified.	System failure. Breakdown.	Proper training of operator			
	Incorrect information	The information given in advance is not specified correct.	System failure. Breakdown.				
	Step skipped	Missing step, or step requires too much of operator.	System failure. Breakdown.				
	Step unsuccessful	Step has a large probability of malfunctioning.	System failure. Breakdown.				
	Influence from others	The procedures performance will most likely be affected by other sources.	Endangering of operator.	System of signs.			

Ref #	Guideword	Causes	Consequences	Safeguards	Rec#	Recommendations	Action

- **VEDLEGG G FORSØKSPROSEDYRE**

<b>Experiment, name, number:</b> Heat Pipe test rig experiment	<b>Date/ Sign</b>
<b>Project Leader:</b> Erling Næss / Geir Hansen	
<b>Experiment Leader:</b> Geir Hansen	
<b>Operator, Duties:</b> Dan Adrian Odden / Geir Hansen	

	<b>Conditions for the experiment:</b>	<b>Completed</b>
	Experiments should be run in normal working hours, 08:00-16:00 during winter time and 08.00-15.00 during summer time. Experiments outside normal working hours shall be approved.	
	One person must always be present while running experiments, and should be approved as an experimental leader.	
	An early warning is given according to the lab rules, and accepted by authorized personnel.	
	Be sure that everyone taking part of the experiment is wearing the necessary protecting equipment and is aware of the shutdown procedure and escape routes.	
	<b>Preparations</b>	<b>Carried out</b>
	<i>Post the "Experiment in progress" sign.</i>	
	<i>Start-up procedure</i>	
	<i>Make sure that control valve is fully open</i>	
	<i>Fully open water valve</i>	
	<i>Adjust the nitrogen pressure in the circuit stepwise to maximum 0.4barg</i>	
	<b>During the experiment</b>	
	<i>Control of temperature by monitoring the computer screen which uses labVIEW</i>	
	<i>Control of pressure using manometers</i>	
	<b>End of experiment</b>	
	<i>Shut down procedure</i>	
	<i>Close nitrogen valve</i>	
	<i>Close water valve</i>	
	<i>Remove all obstructions/barriers/signs around the experiment.</i>	
	<i>Tidy up and return all tools and equipment.</i>	
	<i>Tidy and cleanup work areas.</i>	
	<i>Return equipment and systems back to their normal operation settings (fire alarm)</i>	
	<b>To reflect on before the next experiment and experience useful for others</b>	
	Was the experiment completed as planned and on scheduled in professional terms?	
	Was the competence which was needed for security and completion of the	

---

	experiment available to you?	
	Do you have any information/ knowledge from the experiment that you should document and share with fellow colleagues?	

• **VEDLEGG H OPPLÆRINGSPLAN FOR OPERATØRER**

<b>Experiment, name, number:</b> Heat Pipe test rig experiment	<b>Date/ Sign</b>
<b>Project Leader:</b> Erling Næss / Geir Hansen	
<b>Experiment Leader:</b> Geir Hansen	
<b>Operator:</b> Dan Adrian Odden / Geir Hansen	

	<b>Kjennskap til EPT LAB generelt</b>	
	Lab - adgang -rutiner/regler -arbeidstid	
	Kjenner til evakueringsprosedyrer	
	Aktivitetskalender	
	<b>Kjennskap til forsøkene</b>	
	Prosedyrer for forsøkene	
	Nødstop	
	Nærmeste brann/førstehjelpsstasjon	

## Forsøk pågår! Experiment in progress!

Dette kort skal settes opp før forsøk kan påbegynnes This card has to be posted before an experiment can start

<b>Ansvarlig / Responsible</b> Erling Næss og Geir Hansen	<b>Telefon jobb/mobil/hjemme</b> 91897970 (Erling) 47666881 (Geir)
<b>Operatører/Operators</b> Dan Adrian Odden	<b>Forsøksperiode/Experiment time(start – slutt)</b> 23.04.2012-21.05.2012
<b>Prosjektleder</b> Erling Næss og Geir Hansen	<b>Prosjekt</b> Heat Pipe

**Kort beskrivelse av forsøket og relaterte farer**  
**Short description of the experiment and related hazards**

Det skal utføres varmetekniske eksperimenter på vår "Heat Pipe Testrigg", som er en kjølekrets med nitrogen som arbeidsmedium. Riggen vil i første omgang bli kjørt uten heat pipe montert. Temperaturene i kretsen når man varierer turtallet til sidekanalsblåseren, effektpådraget til tracingen og åpningen på reguleringsventilen vil bli målt.

Risiko forbundet med arbeidet:

Trykket i kretsen er relativt lavt, maks ca. 0,5 barg, men man kan få virvlet opp støv ved en eventuell lekkasje og vernebriller skal derfor brukes.

Vannlekkasje (steng vannventil).

Elektrisk feil (bruk nødstop på el-skap).

**NTNU**  
**Institutt for energi og prosessteknikk**

**Dato**

---

**Signert**

---



---



---

# APPARATURKORT UNITCARD

## Apparatur/unit

Dette kortet SKAL henges godt synlig på apparaturen! *This card MUST be posted on a visible place on the unit!*

<b>Faglig Ansvarlig</b> (Scientific Responsible) Erling Næss	<b>Telefon mobil/privat</b> (Phone no. mobile/private) 91897970
<b>Apparaturansvarlig</b> (Unit Responsible) Geir Hansen	<b>Telefon mobil/privat</b> (Phone no. mobile/private) 47666881
<b>Sikkerhetsrisikoer</b> (Safety hazards) Trykket i nitrogenkretsen er relativt lavt, maks ca. 0,5 barg, men man kan få virvlet opp støv ved en eventuell lekkasje og vernebriller skal derfor brukes. Vannlekkasje. Elektrisk feil.	
<b>Sikkerhetsregler</b> (Safety rules) Vernebriller. Steng vannventil. Nødstopp på el-skap.	
<b>Nødstopp prosedyre</b> (Emergency shutdown) Steng vannventil hvis vannlekkasje. Nødstopp på el-skap.	

Her finner du (Here you will find):

<b>Prosedyrer</b> (Procedures)
<b>Bruksanvisning</b> (Users manual)

Nærmeste (nearest)

<b>Brannslukningsapparat</b> (fire extinguisher)	<b>Ved heis.</b>
<b>Førstehjelpsskap</b> (first aid cabinet)	<b>Ved heis.</b>

NTNU  
Institutt for energi og prosessteknikk

Dato

Signert



## VEDLEGG I SKJEMA FOR SIKKER JOBB ANALYSE

<b>SJA tittel: Uttesting av Heat Pipe Testrigg</b>	
Dato: 19.04.2012	Sted: NTNU, EPT
Kryss av for utfylt sjekklister: <input checked="" type="checkbox"/>	

Deltakere: Dan Adrian Odden, Geir Hansen		
SJA-ansvarlig: Geir Hansen		

<p>Arbeidsbeskrivelse: (Hva og hvordan?)</p> <p>Det skal utføres varmetekniske eksperimenter på vår "Heat Pipe Testrigg", som er en kjølekrets med nitrogen som arbeidsmedium. Riggeren vil i første omgang bli kjørt uten heat pipe montert. Temperaturene i kretsen når man varierer turtallet til sidekanalsblåseren, effektpådraget til tracingen og åpningen på reguleringsventilen vil bli målt.</p>
<p>Risiko forbundet med arbeidet:</p> <p>Trykket i kretsen er relativt lavt, maks ca. 0,5 barg, men man kan få virvlet opp støv ved en eventuell lekkasje og vernebriller skal derfor brukes.</p> <p>Vannlekkasje.</p> <p>Elektrisk feil.</p>
<p>Beskyttelse/sikring: (tiltaksplan, se neste side)</p> <p>Vernebriller.</p> <p>Steng vannventil.</p> <p>Nødstopp på el-skap.</p>
<p>Konklusjon/kommentar:</p>

Anbefaling/godkjenning:	Dato/Signatur:	Anbefaling/godkjenning:	Dato/Signatur:
SJA-ansvarlig:		Områdeansvarlig:	
Ansvarlig for utføring:		Annen (stilling):	

HMS aspekt	Ja	Nei	Ikke aktuelt	Kommentar / tiltak	Ansv.
<b>Dokumentasjon, erfaring, kompetanse</b>					
Kjent arbeidsoperasjon?		X		Det har ikke vært kjørt eksperimenter på riggen tidligere.	
Kjennskap til erfaringer/uønskede hendelser fra tilsvarende operasjoner?		X			
Nødvendig personell?	X				
<b>Kommunikasjon og koordinering</b>					
Mulig konflikt med andre operasjoner?		X			
Håndtering av en evt. hendelse (alarm, evakuering)?	X				
Behov for ekstra vakt?		X			
<b>Arbeidsstedet</b>					
Uvante arbeidsstillinger?			X		
Arbeid i tanker, kummer el.lignende?			X		
Arbeid i grøfter eller sjakter?			X		
Rent og ryddig?	X				
Verneutstyr ut over det personlige?		X			
Vær, vind, sikt, belysning, ventilasjon?			X		
Bruk av stillaser/lift/seler/stropper?			X		
Arbeid i høyden?			X		
Ioniserende stråling?			X		
Rømningsveier OK?	X				
<b>Kjemiske farer</b>					
Bruk av helseskadelige/giftige/etsende kjemikalier?		X			
Bruk av brannfarlige eller eksplosjonsfarlige kjemikalier?		X			
Må kjemikaliene godkjennes?		X			
Biologisk materiale?		X			
Støv/asbest?		X			
<b>Mekaniske farer</b>					
Stabilitet/styrke/spenning?		X			
Klem/kutt/slag?		X			
Støy/trykk/temperatur?	X			Veldig moderat risiko.	
Behandling av avfall?			X		
Behov for spesialverktøy?			X		
<b>Elektriske farer</b>					
Strøm/spenning/over 1000V?			X		
Støt/krypstrøm?		X			
Tap av strømtilførsel?		X			
<b>Området</b>					
Behov for befaring?		X			
Merking/skilting/avsperring?	X				
Miljømessige konsekvenser?		X			
<b>Sentrale fysiske sikkerhetssystemer</b>					
Arbeid på sikkerhetssystemer?		X			
Frakobling av sikkerhetssystemer?		X			

---

Annet					
-------	--	--	--	--	--